ADAPTIVE URBAN MODELLING FOR SOLAR ENERGY SIMULATIONS

David Muñoz Novoa

DOCTORAL THESIS

ADAPTIVE URBAN MODELLING FOR SOLAR ENERGY SIMULATIONS

David Muñoz Novoa

2019

DOCTORAL THESIS

ADAPTIVE URBAN MODELLING FOR SOLAR ENERGY SIMULATIONS

David Muñoz Novoa

2019

DOCTORAL PROGRAMME IN TECHNOLOGY

Advisors: Dr. Gustavo Patow and Dr. Gonzalo Besuievsky

Memory presented to opt for the Doctor in Technology degree
from the University of Girona

List of Publications

Muñoz, D., Beckers, B., Besuievsky, G., & Patow, G. (2015, November). Far-LoD: Level of detail for massive sky view factor calculations in large cities. In Proceedings of the Eurographics Workshop on Urban Data Modelling and Visualisation (pp. 1-6). Eurographics Association.

Muñoz, D., Besuievsky, G., & Patow, G. (2017, August). A rule-based approach for thermal model analysis on buildings. Ref. IMAE17-01-RR

Muñoz, D., Beckers, B., Besuievsky, G., & Patow, G. (2018, March). A technique for massive sky view factor calculations in large cities. International Journal of Remote Sensing, 39(12), 4040-4058.

Muñoz, D., Besuievsky, G., & Patow, G. (2018, June). A procedural approach for thermal visualization on buildings. In Proceedings of the XXVIII Spanish Computer Graphics Conference (pp. 109-117). Eurographics Association.

Muñoz, D., Besuievsky, G., & Patow, G. (2019). A procedural technique for thermal simulation and visualization in urban environments. Accepted in Building Simulation.

Muñoz, D., Besuievsky, G., & Patow, G. (2019). A Level-of-Detail Technique for Urban Physics Calculations in Large Urban Environments. Accepted in the XXIX Spanish Computer Graphics Conference. Eurographics Association.

List of Abbreviations

BEMP	**B**uilding **E**nergy **M**odelling **P**rogram
DSM	**D**igital **S**urface **M**odels
FF	**F**orm **F**actor
IR	**I**nfra-red **R**adiation
LIDAR	**L**aser **I**maging **D**etection **A**nd **R**anging
LoD	**L**evel **o**f **D**etail
LW	**L**ong **W**ave
SVF	**S**ky **V**iew **F**actor
SW	**S**hort **W**ave
UHI	**U**rban **H**eat **I**sland

List of Figures

List of Tables

Dedicated to my girlfriend, for holding my hand firmly and getting me back on the road every time a rail line went off the train track, and my family, for never ceasing to believe in me since I have a memory.

Acknowledgements

I want to thank in the first place Gustavo Patow, who gave me the opportunity to work with him and under his baton in what has been the most interesting adventure of my entire career. You were the first to believe in me, to encourage me and to serve as an example and model at every step of the investigation. Thank you for your invaluable direction and teaching.

I want to thank Gonzalo Besuievsky for having co-directed my thesis, always keeping our feet on the ground and contributing his reasoning and critical opinion so that we never stray from the path. I think that by forming a team with Gustavo, you are the perfect machine and you can make any project come to fruition.

I want to especially thank Benoit Beckers, who guided my steps to get away from engineering and immerse myself in architecture and physics, making me grow professionally and expanding my vision about many topics. You literally opened the doors to a new world for me and gave me another perspective on it. Without your help and without my pleasant stay at the Université de Technologie de Compiègne, without a doubt a large part of this work would not have been possible.

I also thank Raphaël Nahon for his help, his company and above all his patience to share some of his knowledge on thermal and energy while he worked on his own thesis.

Thanks to Albert Juncà i Sabrià for his company in our office of the University of Girona and for helping me to understand the problem of conductive heat exchange. Thanks also to Fabien Dobigny, who through his thesis using finite elements, guided me in the construction of an equation that had me blocked for weeks.

Thanks to Elena García Nevado from the Universitat Politècnica de Catalunya who did the thermographies of a street in Petit Bayonne which illustrates the fourth chapter of this thesis.

Thanks to the University of Girona for hosting me and giving me an environment to develop my thesis, surrounded by real professionals. The FiUdG research aid grant that was so generously granted to me, gave me the resources and support necessary to complete this doctoral thesis.

Thanks to my family and my colleagues for having endured my humour during the last years, for not giving up with me and for always giving me the support I needed.

Finally, to those I have forgotten and to you who take the trouble to read me, thank you.

"Each problem that I solved became a rule, which served afterwards to solve other problems."

René Descartes

"Mathematics compares the most diverse phenomena and discovers the secret analogies that unite them."

Joseph Fourier

"It's in humanity's nature to want to rise above our limits. Think about it: we were cold, so we harnessed fire; we were weak, so we invented tools. Every time we met an obstacle, we used creativity and ingenuity to overcome it. The cycle is inevitable."

Adam Jensen

Contents

List of Symbols

Symbol	Description	Magnitude
A_i	area of surface i	m^2
C	thermal capacitance	$J \cdot K^{-1}$
c_p	thermal capacity	$J \cdot kg^{-1} \cdot K^{-1}$
e	thickness	m
G_{cb}	beam solar radiation	$W \cdot m^{-2}$
G_{cd}	diffuse solar radiation	$W \cdot m^{-2}$
G_{sc}	solar constant	1,367 $W \cdot m^{-2}$
H	altitude	m
h_e	exterior convective heat transfer coefficient	$W \cdot m^{-2} \cdot K^{-1}$
h_i	interior convective heat transfer coefficient	$W \cdot m^{-2} \cdot K^{-1}$
k	thermal resistance	$W \cdot m^{-1} \cdot K^{-1}$
m	mass	kg
Q_{cond}	heat flow	$W \cdot m^{-2}$
r_i	albedo surface coefficient i	%
T_{gr}	ground temperature	K
T_{ext}	external air temperature	K
$Tint_f$	internal temperature at floor f	K
$T_{w\,l}$	temperature at the material layer l of the wall w	K
UA	glazing transmittance by translucent surfaces	$W \cdot K^{-1}$
α	absorbency coefficient	%
α_{sun}	sun's altitude angle	rad
γ_{sun}	sun's azimuth angle	rad
δ	earth's declination angle	rad
ϵ	emissivity coefficient	%
θ	zenith angle	rad
λ	thermal conductivity	$W \cdot m^{-1} \cdot K^{-1}$
ρ	material density	$kg \cdot m^{-3}$
σ	Stefan-Boltzmann's constant	$5.67 \cdot 10^{-8}$ $W \cdot m^{-2} \cdot K^{-4}$
τ_b	beam solar radiation coefficient	
τ_d	diffuse solar radiation coefficient	
φ	latitude angle	rad
ω	hour angle	rad
Ω	solid angle	rad

UNIVERSITAT DE GIRONA

Resum

Escola Politècnica Superior
Universitat de Girona

Programa de Doctorat en Tecnologia

Adaptive Urban Modelling for Solar Energy Simulations

by David Muñoz Novoa

Els problemes als quals s'enfronten les ciutats són molt complexes, ja que qualsevol decisió pot afectar no només a la comoditat, a la salut i a la qualitat de vida de les persones que hi viuen, sinó que també pot afectar a tot l'ecosistema que envolta les ciutats, fins a distàncies respecte al seu nucli urbà que han sorprès als investigadors en els darrers anys.

Un clar exemple és l'illa de calor, un fenomen que provoca que les ciutats tinguin temperatures més altes que els seus voltants. Fa uns anys, es va descobrir que aquest fenomen té conseqüències impensables per al seu entorn natural: per exemple, es va observar empíricament que la calor que es genera a les ciutats de la costa oest dels Estats Units provoca un escalfament que les corrents de vent arrosseguen i escampen. A causa de les condicions climàtiques, aquest escalfament acaba "caient" sobre la tundra canadenca, on el seu efecte està reduint les capes de gel del nord del Canadà, el que s'espera que sigui un problema greu en els propers anys.

A causa de la seva joventut, l'estudi de la física urbana amb prou feines ha explicat el comportament dels elements constituents (humitat, calor, vent, contaminació, llum, etc.) en carrers o veïnats molt petits, però la gran quantitat de dades que involucra la geometria de tota una ciutat ha dificultat que aquests estudis s'expandeixin a àrees més grans.

En aquesta tesi, proposem trobar solucions que permetin que aquestes simulacions s'estenguin a tota una ciutat, intentant donar un pas decisiu per abordar el tractament d'aquesta gran quantitat de dades i la seva resolució. Per aquesta raó, es proposa estudiar sistemes jeràrquics i desacoblar una ciutat en àrees més petites, així com la incorporació de tècniques de nivell de detall i el seu ús combinat junt amb tècniques procedimentals com a clau per resoldre aquest problema tan important i alhora tan extremadament complex al qual s'enfronten les ciutats modernes.

Mitjançant l'ús d'una analogia elèctrica i el càlcul dels factors de vista del cel i de forma, les nostres tècniques permeten simular i estudiar el comportament tèrmic d'un entorn urbà, tenint en compte la radiació solar i del cel, les temperatures de l'aire i del cel, i fins i tot la interacció tèrmica entre edificis propers entre sí. També mostrem que és possible, des d'una recreació en 3D d'un gran entorn urbà, simular els intercanvis de calor que tenen lloc entre els edificis d'una ciutat i els seus voltants immediats. De la mateixa manera, tenint en compte la zona terrestre, l'altitud i el tipus de clima amb el qual es realitzen les simulacions, és possible comparar el comportament tèrmic d'un gran entorn urbà d'acord amb les condicions triades.

En resum, aquesta tesi proposa abordar el problema de simular els efectes físics en grans entorns urbans mitjançant l'ús de regles procedimentals i tècniques de nivell de detall, per tal de reduir la complexitat computacional d'aquestes simulacions, però tractant alhora de mantenir una precisió acceptable en els resultats per a la presa de decisions. Els resultats finals mostren que és possible obtenir resultats creïbles en diferents casos d'estudi, tots amb temps de càlcul raonables, amb l'usuari ajustant els paràmetres per obtenir l'equilibri desitjat entre precisió i temps de càlcul.

UNIVERSITAT DE GIRONA

Resumen

Escuela Politécnica Superior
Universitat de Girona

Programa de Doctorado en Tecnología

Adaptive Urban Modelling for Solar Energy Simulations

by David Muñoz Novoa

Los problemas a los que se enfrentan las ciudades son muy complejos, ya que cualquier decisión puede afectar no sólo a la comodidad, a la salud y a la calidad de vida de las personas que viven en ellas, sino que también puede afectar a todo el ecosistema que rodea las ciudades, hasta distancias respecto a su núcleo urbano que han sorprendido a los investigadores en los últimos años.

Un claro ejemplo es la isla de calor, un fenómeno que provoca que las ciudades tengan temperaturas más altas que sus alrededores. Hace unos años, se descubrió que este fenómeno tiene consecuencias impensables para su entorno natural: por ejemplo, se observó empíricamente que el calor que se genera en las ciudades de la costa oeste de los Estados Unidos provoca un calentamiento que las corrientes de viento arrastran y esparcen. Debido a las condiciones climáticas, este calentamiento termina "cayendo" sobre la tundra canadiense, donde su efecto está reduciendo las capas de hielo del norte de Canadá, lo que se espera que sea un problema grave en los próximos años.

Debido a su juventud, el estudio de la física urbana apenas ha explicado el comportamiento de los elementos constituyentes (humedad, calor, viento, contaminación, luz, etc.) en calles o vecindarios muy pequeños, pero la gran cantidad de datos que involucra la geometría de toda una ciudad ha dificultado que estos estudios se expandan a áreas más grandes.

En esta tesis, proponemos encontrar soluciones que permitan que estas simulaciones se extiendan a toda una ciudad, intentando dar un paso decisivo para abordar el tratamiento de esta gran cantidad de datos y su resolución. Por esta razón, se propone estudiar sistemas jerárquicos y desacoplar una ciudad en áreas más pequeñas, así como la incorporación de técnicas de nivel de detalle y su uso combinado junto a técnicas procedimentales como clave para resolver este problema tan importante y a la vez tan extremadamente complejo al cual se enfrentan las ciudades modernas.

Mediante el uso de una analogía eléctrica y el cálculo de los factores de vista del cielo y de forma, nuestras técnicas permiten simular y estudiar el comportamiento térmico de un entorno urbano, teniendo en cuenta la radiación solar y del cielo, las temperaturas del aire y del cielo, e incluso la interacción térmica entre edificios cercanos entre sí. También mostramos que es posible, desde una recreación en 3D de un gran entorno urbano, simular los intercambios de calor que tienen lugar entre los edificios de una ciudad y sus alrededores inmediatos. Del mismo modo, teniendo en cuenta la zona terrestre, la altitud y el tipo de clima con el que se realizan las simulaciones, es posible comparar el comportamiento térmico de un gran entorno urbano de acuerdo con las condiciones elegidas.

En resumen, esta tesis propone abordar el problema de simular los efectos físicos en grandes entornos urbanos mediante el uso de reglas procedimentales y técnicas de nivel de detalle, a fin de reducir la complejidad computacional de estas simulaciones, pero tratando a la vez de mantener una precisión aceptable en los resultados para la toma de decisiones. Los resultados finales muestran que es posible obtener resultados creíbles en diferentes casos de estudio, todos con tiempos de cálculo razonables, con el usuario ajustando los parámetros para obtener el equilibrio deseado entre precisión y tiempo de cálculo.

UNIVERSITAT DE GIRONA

Abstract

Polytechnic School
Universitat de Girona

Doctoral Programme in Technology

Adaptive Urban Modelling for Solar Energy Simulations

by David Muñoz Novoa

Cities face complex problems, where any decision can affect not only the comfort, health and life quality of the people who live there, but also the entire ecosystem that surrounds them, reaching distances from the urban nucleus that surprised the researchers in recent years.

A clear example is the heat island, which is a phenomenon where cities have higher temperatures than their surroundings. It was discovered a few years ago that the heat island has previously unthinkable consequences for its natural environment: for example, it was empirically observed that the heat generated in cities on the west coast of the United States causes a warming that wind currents sweep away and, due to weather conditions, ends up "falling" on the Canadian tundra. As a consequence, this is reducing the ice sheets of northern Canada, which is expected to be a serious problem in the coming years.

Due to its youth, the study of urban physics has barely being able to explain the behaviour of constituent elements (humidity, heat, wind, pollution, light, etc.) for very small streets or neighbourhoods. However, the large amount of data that involves the geometry of an entire city has made it difficult for these studies to make solid predictions for larger areas.

In this thesis we propose to find solutions that allow extending these simulations to a whole city, trying to take a decisive step to address the treatment and resolution of the massive amount of data involved. For this reason, we propose to study hierarchical systems and to decouple the city into smaller areas, as well as the use of Level-of-Detail techniques and the combined use of procedural techniques as a key to solving this very important but extremely complex problem for modern cities.

The techniques we have developed in this thesis, based on the use of an electrical analogy and the efficient calculation of sky view factors and form factors, make it possible to simulate and study the thermal behaviour of an urban environment taking into account the solar and sky radiation, the air and sky temperatures, and even the thermal interaction between nearby buildings. We also show that it is possible, from a 3D recreation of a large urban environment, to simulate the heat exchanges that take place between the buildings of a city and its immediate surroundings. In the same way, taking into account the terrestrial zone, the altitude and the type of climate with which the simulations are carried out, it is possible to analyse the thermal behaviour of a large urban environment.

In summary, this thesis proposes to address the problem of simulating physical effects in large urban environments through the use of procedural rules and Level-of-Detail techniques, in order to reduce the computational complexity of these simulations, but at the same time trying to maintain an acceptable accuracy in the results for decision-making. The final results show that it is possible to obtain credible results in different study cases, all with reasonable calculation times, with the user being able to adjust the parameters to obtain the desired balance between accuracy and calculation time.

Chapter 1

Introduction

1.1 Urbanisation trends

Around the world, people are moving to urban centres in unprecedented numbers (Cohen, 2015). The global population is expected to increase by 1.1 billion during the period between 2015 and 2030, with nearly all of this growth concentrated in cities. Current projections by the United Nations assume that this growth continues (UN, 2014). By 2050, every two out of three persons are expected to live in urbanised areas, corresponding to 6.3 billion people. Over the past decades, urbanisation mainly took place in Europe and the US, while nowadays, the centre of urbanisation moved to Asia and Africa as consequence of their rapid economic growth, see Figure 1.1.

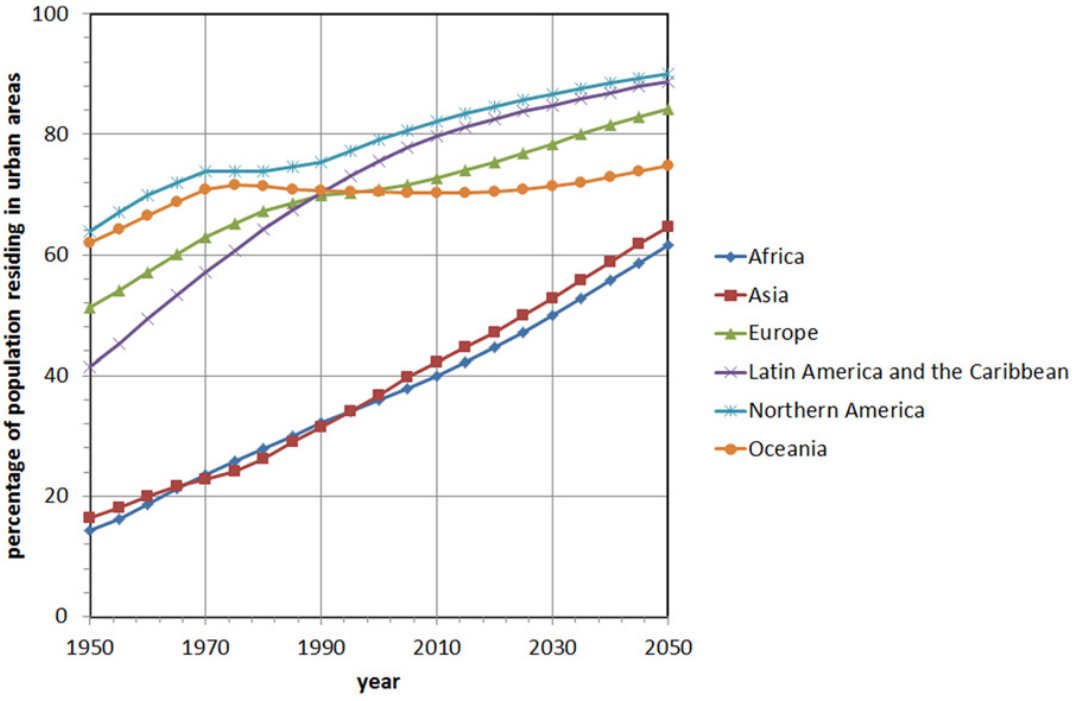

Figure 1.1. Percentage of population residing in urban areas by continent 1950–2050 (based on data from United Nations (2014)).

1.1.1 Urban heat island

Urbanisation needs an expansion of the city boundaries, as well as an increase in density of the urban issue. The latter often results in the construction of tall building

structures along relatively narrow streets. As a consequence of the altered heat balance, the air temperatures in densely built urban areas are generally higher than in the surrounding rural hinterland, a phenomenon known as the "urban heat island" (UHI), see Figure 1.2. The heat island is the most obvious climatic manifestation of urbanisation (Landsberg, 1981).

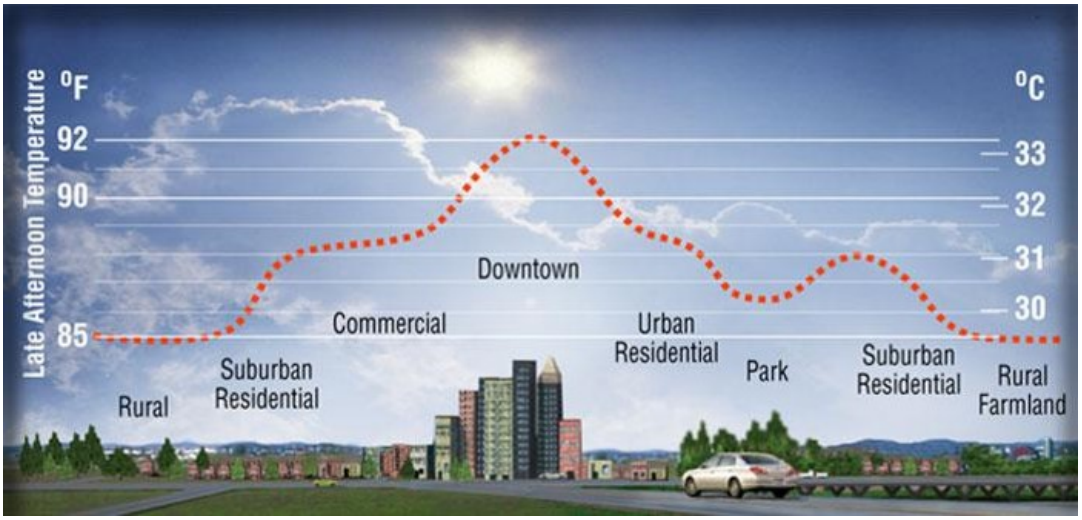

Figure 1.2. An urban heat island is a metropolitan area that is significantly warmer than its surrounding areas due to human activities (Image from Lawrence Berkeley Labs).

Possible causes for the urban heat island were suggested (Oke, 1995; Moonen et al., 2012; Nuruzzaman, 2015) and their relative importance was determined in numerous follow-up studies (Busato, Lazzarin, and Noro, 2014; Santamouris, 2014; Mohajerani, Bakaric, and Jeffrey-Bailey, 2017). Some of these causes seem to be:

- Trapping of short and long-wave radiation in between buildings.
- Decreased long-wave radiative heat losses due to reduced sky view factors.
- Increased storage of sensible heat in the construction materials.
- Anthropogenic heat released from combustion of fuels (domestic heating, traffic).
- Reduced convective heat removal due to the reduction of wind speed.

Studies of the urban heat island usually refer to the heat island intensity, which is the maximum temperature difference between the city and the surrounding area. The intensity is mainly determined by the thermal balance of the region, and is consequently subject to diurnal variations and short-term weather conditions, as can be observed through the information gathered from a large number of heat island studies worldwide (Santamouris, 2013).

A significant amount of research is directed towards the mitigation of the undesired consequences of the urban heat island. One way to mitigate the excess heat is to make use of evaporative cooling (Krüger and Pearlmutter, 2008). Alternatively one can try to control the amount of solar gains, e.g. by applying high-albedo materials, especially at horizontal surfaces (Evyatar, Pearlmutter, and Williamson, 2011). For novel urban developments, the shape and location of building volumes can be designed in order to control and optimise solar access.

1.1.2 Climate change

Despite being extremely important, the urban heat island is a localised phenomenon and does not significantly contribute to the observed large-scale trends of climate change (Solomon et al., 2007). The inverse statement is however not true: global climate change will add an additional thermal burden to urban areas, accentuating urban heat island impacts (Douglas and Munn, 2002). According to the most recent Intergovernmental Panel on Climate Change (IPPC) report (Stocker, 2014), warming of the climate system is unequivocal. It can be observed by the increase in global average air and ocean temperatures, the widespread melting of snow and ice and the rise of the global average sea level. They state that the observed increase in global average temperatures since the mid-20th century can most likely be attributed to the increase in anthropogenic greenhouse gas concentrations. As global greenhouse gas emissions are expected to continue to grow, a warming of about 0.2° C per decade is projected for the next two decades, after which temperature projections increasingly depend on specific emission scenarios. The report also discusses the potential impacts of the continuing temperature rise. They include amongst others increases in frequency of hot extremes, heat waves and heavy precipitation, increases in precipitation in high latitudes and precipitation decreases in most subtropical land regions, and contraction of snow cover area and corresponding sea level rise. Asian and African mega-deltas, as well as the African continent, are expected to suffer the most from these consequences. Nevertheless, also within other areas, even those with high incomes, some people (such as the poor, young children and the elderly) can be particularly at risk.

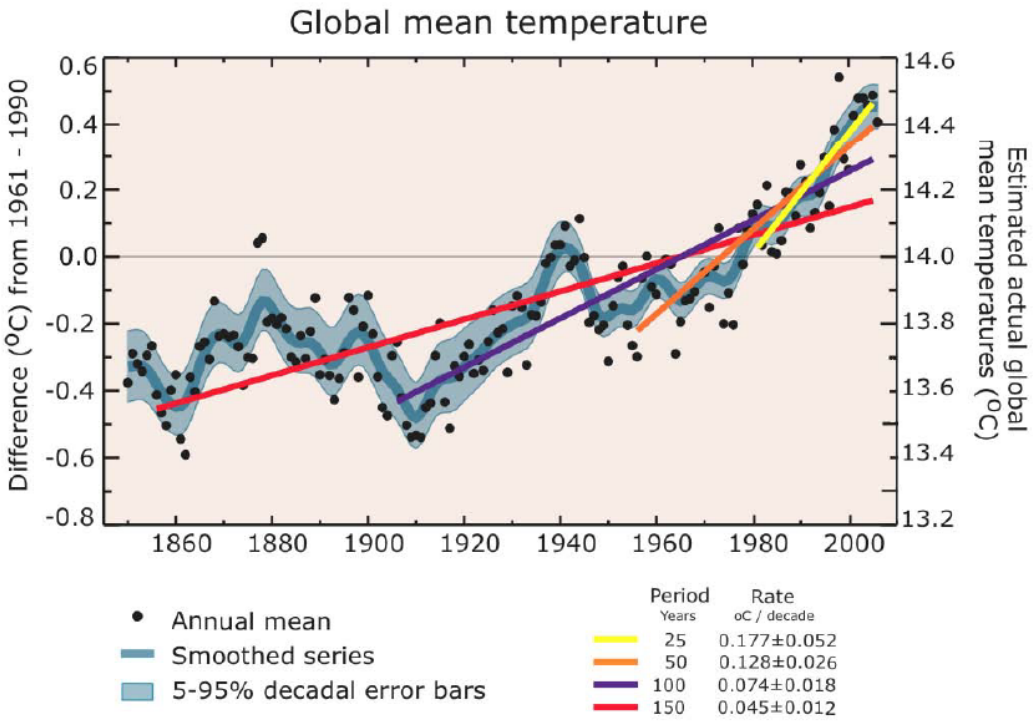

Figure 1.3. Annual global mean temperatures with linear fits to the data. The temperature change from the first 70 years of the instrumental record (1850–1919) to the last 5 years (2001–2005) is 0.78 ± 0.18° C (Solomon et al., 2007).

1.1.3 Major urban problems and challenges

From the preceding, it is clear that the combined effects of urbanisation and global climate warming can give rise to a decrease in urban air quality and an increase in urban heat island intensity, amplifying the risk to expose the citizens to discomfort and health-related problems, and leading to higher energy demands for cooling. In assessing these aspects, it is needed to consider a wide scope of phenomena, occurring over a wide range of spatial scales. The individual building with its technical installation marks one end of the spectrum. At increasingly larger scales we have the effect of the urban morphology at the neighbourhood scale, the urban heat island effect at the city scale, the effect of topography at the regional scale and finally the global effects of climate and climate change.

1.2 Urban physics

Urban physics is a discipline that incorporates relevant branches of physics, environmental chemistry, aero-dynamics, meteorology and statistics. Therefore, Urban physics is well positioned to provide key-contributions to the existing urban problems and challenges (Moonen et al., 2012). Urban physics studies a lot of problems related to urban environments. Some of them are the study of wind and thermal comfort, energy demand, pollutant dispersion or wind-driven rain. All the problems studied are addressed by one of the three main research methods applied to Urban physics, namely, field experiments, experiments with wind tunnels and numerical simulations. It is precisely the last method, the numerical simulation, which was used in this thesis.

1.2.1 Urban simulations

Among the many problems that Urban Physics deals with, the main issue of this research is the simulation and study of thermal behaviour in large cities. This thesis proposes techniques to perform calculations and physical simulations in large urban environments efficiently. The objective is, concretely, to simulate in a realistic way the thermal behaviour of the buildings that make up a large urban environment, in order to be able to study the temperature trends and experiment with multiple case studies. We believe that through these study cases, which simulate the morphology, topography and climate of different real world areas, it is possible to support decision making regarding the design and layout of buildings in real urban environments so that their construction and location do not adversely affect the thermal behaviour of their immediate environment.

One of the most important concerns in construction is the energy efficiency. In the current ecological context it is very important to study the heat loss in buildings and the thermal efficiency of materials. Every objects loses heat by emission of electromagnetic radiation. It is possible to detect these radiations in the infra-red range with thermographic cameras that produce thermographies. This method is used in renovation to find the most important energy leaks. Another important point in heat analysis is the external contributions of the sun. The study of these contributions is important to tend toward zero-energy buildings. As a consequence, the interest and the benefits of the simulation are very important to design buildings.

1.2.2 Problem statement

When carrying out simulations in urban environments, the first problem that appears is the morphology. A large 3D urban model contains a considerable amount of geometry and, having to render and take each primitive into account in each calculation that affects the urban environment under study, increases the computational cost. The solutions presented in this thesis address this complexity through the use of procedural and Level-of-Detail techniques, to avoid having to use the totality of the geometry present in the urban environment to be simulated, drastically reducing the calculation time and therefore the computational cost.

In particular, we present two main techniques, which use Level-of-Detail and procedural technology to reduce the computational cost when performing physical calculations on urban 3D models, simplifying both the 3D model itself and the data structures necessary to perform the desired calculations and simulations. Being able to simulate physical phenomena in an urban environment, it is then possible to determine which properties of buildings can be improved to optimize the thermal behaviour.

1.3 Thesis structure

The rest of this thesis is divided into main chapters. The chapters present the following contents:

- The second chapter presents the sources and references studied throughout the thesis. All the material is grouped by topic, so that it is clear in which of the many aspects and problems of the thesis they served as support.
- The third chapter presents a technique for massive sky view factor calculations in large cities. This technique allows to perform a massive amount of calculations of the sky view factor over a large and complex urban environment, in an efficient way and maintaining a proper level of accuracy.
- The fourth chapter presents a procedural technique for thermal simulation and visualization in urban environments. This technique allows, from a large 3D urban model and a set of climatic data, to simulate and visualize the thermal behaviour of an urban environment in a realistic way and in a reasonable time by the use of procedural methods to speed up the calculations.
- The fifth chapter proposes the union of the two techniques previously presented with the objective of implementing a unique technique capable of simulating and visualizing the thermal behaviour of a large urban environment in a more efficient way by the combination of a procedural method and a Level-of-Detail method.
- The sixth and final chapter exposes the conclusions of the thesis, as well as a discussion and a section of future work that presents some of the paths that this thesis leaves open for future research in the field of Urban Physics.

Chapter 2

State of the art

2.1 Sky View Factor

Sky View Factor (SVF) is widely used as an important parameter in modelling thermal phenomena, such as the urban heat island (Unger, 2004). In addition to the important use in all aspects of urban climatology, it also plays a crucial role in forest climatology (Holmer, Postgård, and Eriksson, 2001) and human biometeorology (Lin, Matzarakis, and Hwang, 2010). Further, it can be used in a variety of new fields, such as renewable energy sources and urban planning (Lin, Matzarakis, and Hwang, 2010).

The formula to calculate the SVF derives from the equation of the solid angle (Ω), a measure of how large an object appears to an observer (Zakšek, Oštir, and Kokalj, 2011). Equation 2.1 expresses the solid angle (Ω), where ϕ stands for the latitude angle of the hemisphere and y_i stands for the elevation angles of the relief horizon, assuming the horizon is not of equal height in all directions.

$$\Omega = \sum_{i=1}^{n} \int_{y_i}^{\pi/2} \cos\phi \cdot d\phi = 2\pi \cdot \left(1 - \frac{\sum_{i=1}^{n} \sin y_i}{n}\right) \tag{2.1}$$

The SVF is expressed by Equation 2.2, where n stands for the number of directions used to estimate the vertical elevation angle of the relief horizon and y_i is the horizon vertical elevation angle. SVF ranges between 0 and 1. Values close to 1 mean that almost the entire hemisphere is visible, which is the case in exposed features (planes and peaks), while values close to 0 are present in areas with high concentration of large buildings, especially with narrow streets, from where almost no sky is visible. See Figure 2.1.

$$\mathrm{SVF} = 1 - \frac{\sum_{i=1}^{n} \sin y_i}{n} \tag{2.2}$$

There are several methodologies to compute the SVF (Brown, Grimmond, and Ratti, 2001), the two main families being photographic and simulation methods. Photographic methods compute the value by estimating the sky area of an acquired fish-eye image (Grimmond et al., 2001; Svensson, 2004; Pardo-García and Mérida-Rodríguez, 2017) or measuring it from Laser Imaging Detection and Ranging (LiDAR) data (Kidd and Chapman, 2012). Although they could be very accurate because they capture a real environment, they require *in situ* measurements and manual procedures that can be cost and time-consuming. This limits the study to be used only for small areas.

The increasing availability of 3D city models and raster Digital Surface Models (DSM) allows to compute the SVF on large scale using simulating methods. The main idea of these approaches is to estimate the building blocks of any surface by

simulating light radiation for samples taken on the surfaces of interest. For DSM-based methodologies (Ratti and Richens, 2004; Gál, Lindberg, and Unger, 2009; Zakšek, Oštir, and Kokalj, 2011), high-spatial resolution can be used to estimate SVFs along urban areas combining raster and vector data. A more accurate alternative can work directly on the geometric 3D model. In this case, for the computation of the SVF, the technique presented by Beckers and Beckers (Beckers and Beckers, 2014) can be used to generate a distribution of samples. Then, for each sample, a ray is traced from the current centre of projection to compute the proportion of unblocked sky. See Figure 2.1.

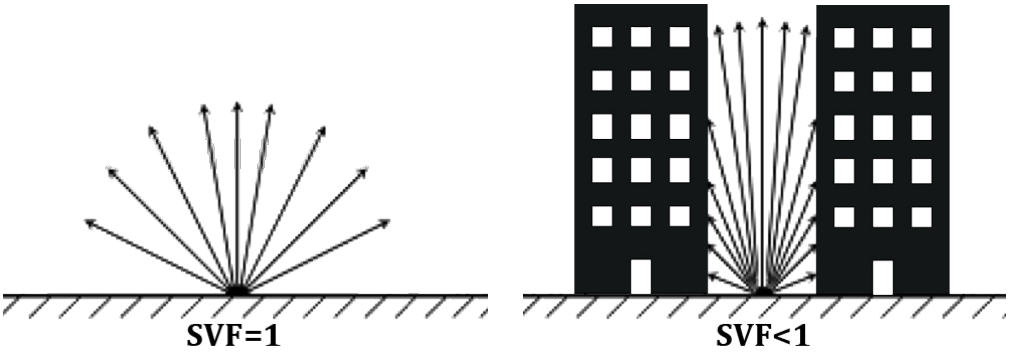

(*a*) SVF without occluders. (*b*) SVF in an urban environment.

Figure 2.1. The SVF is computed by tracing rays from a centre of projection.

2.2 Model Simplification

A standard solution when dealing with calculations like SVF in complex models is to simplify the geometry, which includes not only buildings, but also any urban element that can occlude visible parts of the sky from the point of view where the SVF is measured, such as vegetation, streetlights or even cars. There exist methods to incorporate trees and bushes in the SVF calculation (Gál, Lindberg, and Unger, 2009; Lindberg and Grimmond, 2010; Lindberg and Grimmond, 2011; Gál and Unger, 2014). The presented technique that we show in Section 3.3.3 does not discriminate between the type of urban elements and considers them all as geometry. Therefore, the simplification of urban 3D models can be done through the application of Level-of-Detail (LoD) techniques that reduce the complexity of the geometry.

In computer graphics, accounting for LoD involves decreasing the complexity of a 3D model representation as it moves away from the viewer or according to other metrics such as object importance, viewpoint-relative speed or position (Besuievsky and Patow, 2013a). LoD techniques increase the efficiency of rendering by decreasing the workload on graphics pipeline stages, usually vertex transformations. The reduced visual quality of the model is often unnoticed because of the small effect on object appearance when distant or moving fast. Although most of the time LoD is applied to geometry detail only, the basic concept can be generalized. A form of level of detail management has been applied to texture maps for years, under the name of mipmapping, also providing higher rendering quality.

Previous work on LoD for urban models can be found in the area of urban generalization, such as the cartographic generalization proposed by Anders (Anders, 2005), or the face collapse from known constructive structures as walls and roofs

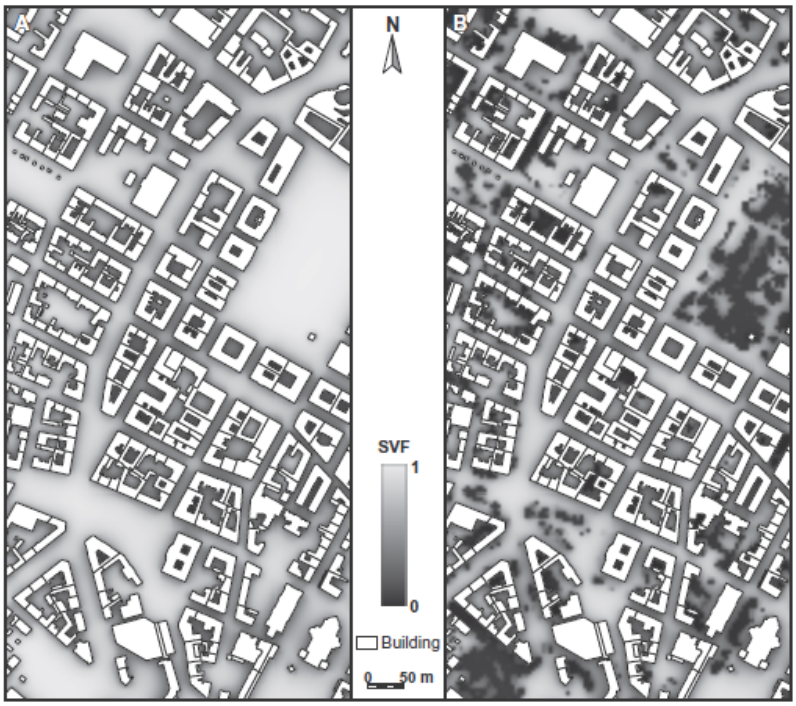

Figure 2.2. Spatial distribution of the calculated SVF without trees (A) and with trees (B) from (Gál and Unger, 2014).

(Rau et al., 2006). Simplification techniques were proposed also within the generation of the city models, using procedural modelling techniques (Besuievsky and Patow, 2013b; Besuievsky and Patow, 2013c). By integrating the LoD mechanism into the procedural processing, the right LoD for each asset can be controlled according to a user-defined criteria. However, these works focus more on solving rendering problems, whereas in our approach we target on the model preparation for simulation analysis.

The techniques presented in this thesis present simplification techniques that are deeply related to the efforts done in the Computer Graphics field with environment maps, based on the early works by Greene (Greene, 1986). One of the first extensions was presented by Shade et al. (Shade et al., 1996), where a hierarchical image caching technique was used for accelerated walkthroughs of complex environments. Later, Décoret et al. (Décoret et al., 1999) accelerated rendering computations by the use of multi-layered impostors. Then, Jeschke et al. (Jeschke and Wimmer, 2002; Jeschke, Wimmer, and Schumann, 2002) introduced the use of layered environment map impostors, used for navigating arbitrary scenes, and Eisemann and Décoret (Eisemann and Décoret, 2007) presented an accurate analysis on exact error bounds for view-dependent simplification while interactively navigating arbitrary scenes.

2.3 Building energy models

A large number of methods have been developed to construct energy consumption models that simulate a building system with different goals (Zhu et al., 2013; Harish and Kumar, 2016). Such models vary in magnitude from modelling a single slab (or a wall) to modelling a complete building through rooms subjected to temperature variations. The energy model we are going to present requires simulating the behaviour of entire buildings, composed of multiple floors. To do this, the model

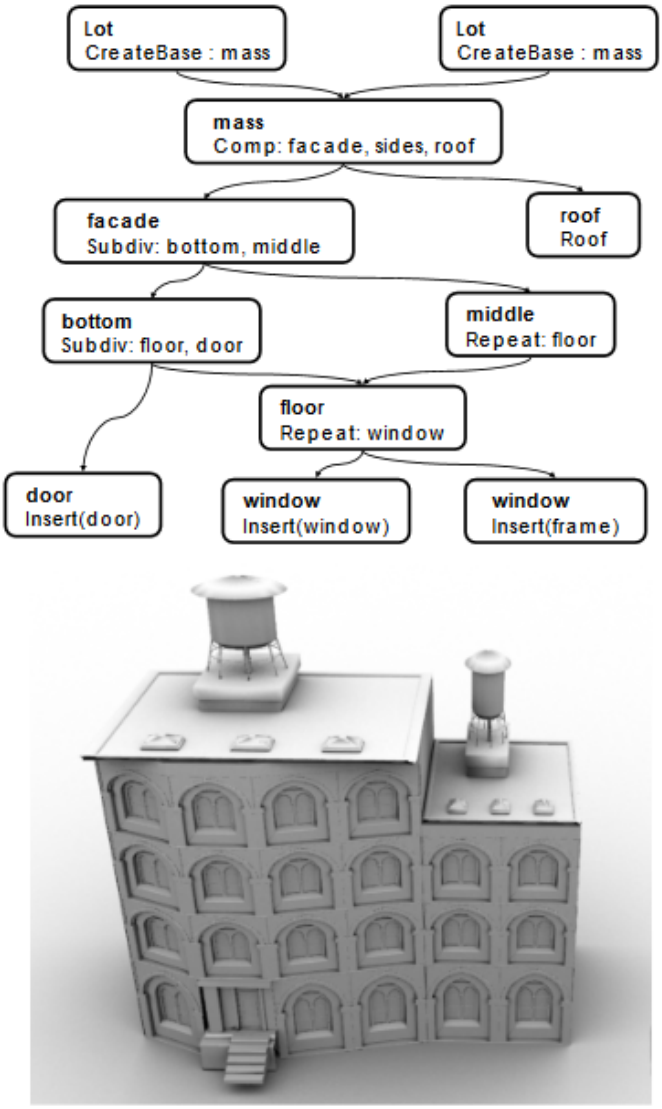

Figure 2.3. A graph-based set of rules (top) is used to obtain a building model (bottom) from (Besuievsky and Patow, 2013b).

uses both a radiative and conductive calculation, using climatic data and procedural rules.

2.3.1 Radiosity

Radiative exchange transfer was the starting point for global illumination computations in computer graphics (Sillion and Puech, 1994). Radiosity was introduced early on as a method for computing radiant heat exchanges between surfaces (Sparrow, 2018). At the heart of radiosity is the idea of breaking the surfaces in an environment down into a finite number of patches and solving the heat transfer for these patches. Attempts to obtain the best from radiosity and Monte Carlo techniques have been made through a series of steps using progressive refinement radiosity and Monte Carlo path tracing (Chen et al., 1991). First, approximate images are quickly produced, and then more accurate images are systematically created. Here, we also deal with related concepts such as the computation of the Sky View Factor (SVF)

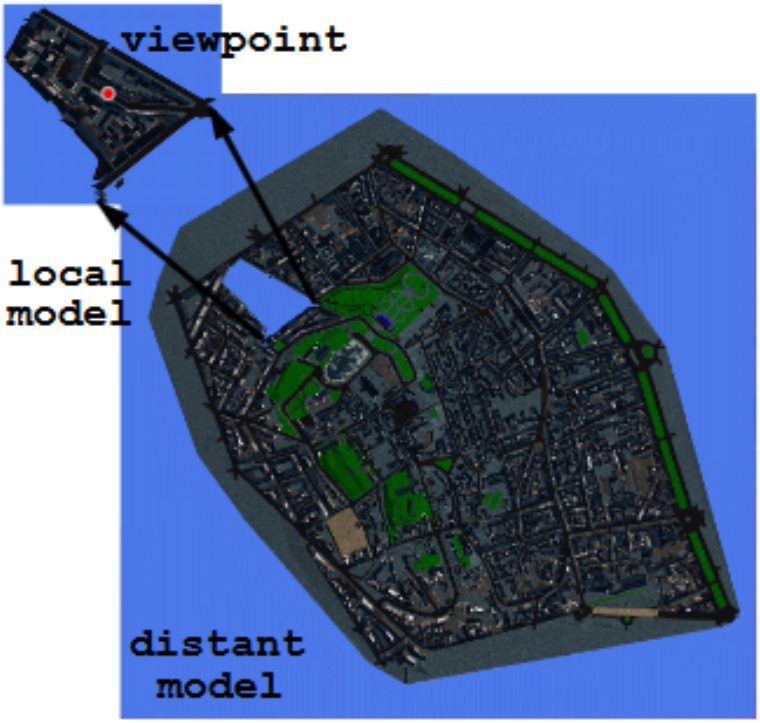

Figure 2.4. Schematic overview of the scene partitioning. A zone of near geometry rendered as polygons surrounds the user. More distant sections are replaced by image-based representations (Décoret et al., 1999).

and the Form Factor (FF) of the exterior surfaces of the buildings. The technique presented by Beckers and Beckers (Beckers and Beckers, 2014) can be used to to generate a distribution of samples that are projected from these surfaces to check for the visibility of the sky and other nearby urban surfaces. Also, the same technique can be used to project the distribution of samples from the sun onto the urban environment and check how many surfaces receive direct solar radiation, calculating solar energy with the equation for extraterrestrial solar radiation (Kaushika, Mishra, and Rai, 2018).

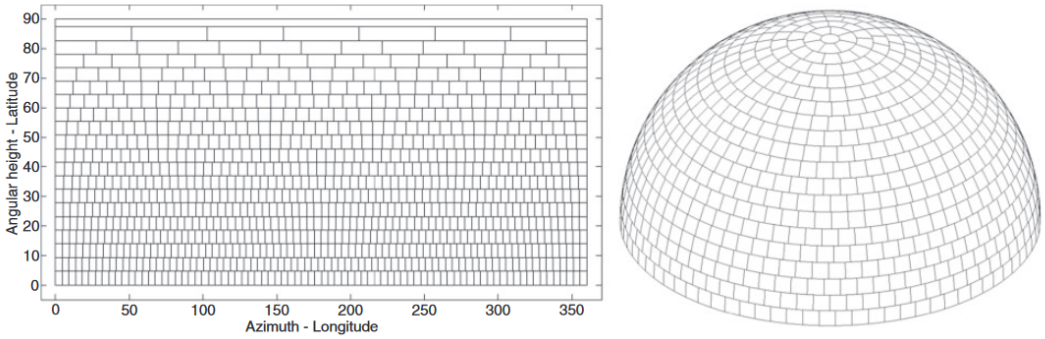

Figure 2.5. Equirectangular (left) and axonometric projections (right) of a 984 cells dome (Beckers and Beckers, 2014).

2.3.2 The electrical analogy

Methods for computing transient heat transfer in buildings can be classified into two categories: explicit solutions of the heat diffusion equation (Clarke, 2001; Kong, He, and Jiang, 2017) or model simplification techniques (Kampf and Robinson, 2007). In the first case, finite difference numerical methods can be used. The main drawback to this is that the computational effort is prohibitive for the early stage simulation of project goals (Lewis, Nithiarasu, and Seetharamu, 2004). On the other hand, the simplified models offer a good compromise between simplicity, data requirement and computational effort. Electrical analogy simplification is one of the methodologies most commonly used to represent heat transfer (Kampf and Robinson, 2007) and has even been used in urban-scale works (Hénon et al., 2011). The main idea behind electrical analogy is to connect the rooms (or floors) in a building by nodes that represent wall conductivity and capacitance (Nahon, 2017). The walls and roofs may be represented by many layers and could also be linked to the outside temperature. By solving the equivalent circuit network that has been composed, dynamic temperatures over time can be obtained. One of the drawbacks to this approach is that the nodes are mostly manually set (Levine, 2015). That is, the nodes are established by defining convenient zones. Furthermore, as it is a simplified model, it is difficult to know in advance how many nodes may be required and where to put them before testing the system with the corresponding building parameters. To overcome this difficulty, in this paper we propose a rule-based methodology that automatically generates the circuit system. However, when using electrical analogy the type of model employed for the walls is also important (Fraisse et al., 2002), because there are many types and selecting one or other may affect both the complexity of the circuit and the accuracy of its results. Taking this into account, the procedural method proposed in Chapter 4 allows multiple simulations to be carried out in a simple manner by changing the wall rule used, thus being able to compare efficiency and precision.

2.4 Sky simulation and climatic data

There are many methods to calculate the emissivity and temperature of the sky (Alados, Foyo-Moreno, and Alados-Arboledas, 2012; Evangelisti, Guattari, and Asdrubali, 2018). In this work, we use the sky radiation model developed by Clark and Allen (Clark and Allen, 1978) as it is frequently used in energy simulation applications; for instance, in EnergyPlus (Crawley et al., 2001). Our simulator assumes that the sky is always clear and without the presence of clouds, which this model admits.

The potential impact of climate change on buildings was investigated through transient building energy simulations and hourly weather data, which are typically used to calculate the demand for heating and cooling (Ahmad and Chen, 2018). Weather stations allow access to climatic data collected over decades, in order to use that reliable source as input to recreate simulations of the thermal behaviour of buildings and other studies (Remund et al., 2010).

2.5 Software tools

Computer simulation is an important and proven method to help understand and analyse the thermal performance of buildings, and predict their operational energy

consumption (Zhu et al., 2013). Since the 1960s, many Building Energy Modelling Programs (BEMPs) have been developed to perform building energy simulations, including the widely-used DOE-2 (DOE, 1982), EnergyPlus (Crawley et al., 2001), ESP (Clarke et al., 1991), and DeST (Yan et al., 2008). DOE-2 was developed at the Lawrence Berkeley National Laboratory with funding from the U.S. Department of Energy (USDOE) following the energy crisis in late 1970s and is still the most widely-used BEMP in the U.S. today. This includes its use both as a stand-alone calculation engine as well as with graphical user interfaces (GUI) such as VisualDOE (Green Design Tools, 2001), EnergyPro (EnergySoft, 2016), eQuest (Hirsch, 2010), and EnergyGauge (Fairey et al., 2002). EnergyPlus is a next-generation BEMP developed, supported and maintained by a team that has been led and funded by the USDOE since 1996. EnergyPlus is based on the loads algorithms of BLAST and the systems algorithms of DOE-2. New features and enhancements were added to support innovative, low-energy building designs and operational controls. The development of ESP-r started in 1974 at the University of Strathclyde and it is primarily used in Europe. DeST (Designer's Simulation Toolkits) is a BEMP that has been developed at Tsinghua University since the late 1980s to aid teaching, research and the practical use of building energy analysis and simulations in China. BEMPs play a significant role in the design of energy efficient envelopes and HVAC systems for new buildings, retrofitting existing buildings, developing building energy codes and standards, and defining and implementing building energy rating/labelling programs. However, the issue of large discrepancies existing between the simulation results of the different BEMPs, even for the same building modelled by the same person, has led many users and stakeholders to lose confidence in building simulation methods and their results. This is a major barrier to the wider adoption and effective application of building energy simulation and represents a challenge the industry must address.

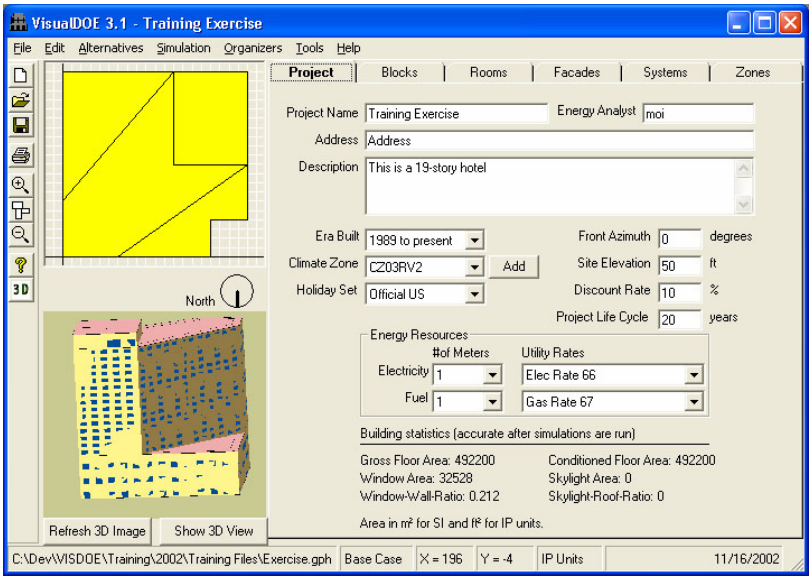

Figure 2.6. VisualDOE, a building energy simulation program.

Part of the complexity of the problem could be that, in a city, there are multiple environmental conditions to simulate. One of the most well-known and widely-used tools is Envi-Met (Elwy et al., 2018), which is a tool that simulates the elements of an urban micro-climate. This application allows elements of the environment such as

air pollution, wind flows, solar radiation and the presence of vegetation, to be introduced. SOLWEIG (Lindberg and Grimmond, 2018), on the other hand, is a software package that presents a model with which to estimate spatial variations of 3D radiation fluxes and mean radiant temperature in complex urban settings. Other tools, despite not having been designed for that specific purpose, have been extended by means of plug-ins to allow them to also build simulation models of outdoor environmental conditions, as is the case of PALM (Khan et al., 2018), whose PALM-4U extension has been developed to suit the needs of modern academic urban boundary layer research and practical city planning related to the urban micro-climate and climate change. There are also lighter applications, such as SkyHelios (Matzarakis and Matuschek, 2010) or RayMan (Matzarakis and Matuschek, 2017), which have been designed for more specific purposes and can be combined to conduct studies that help decision-making in urban planning (Matzarakis et al., 2015).

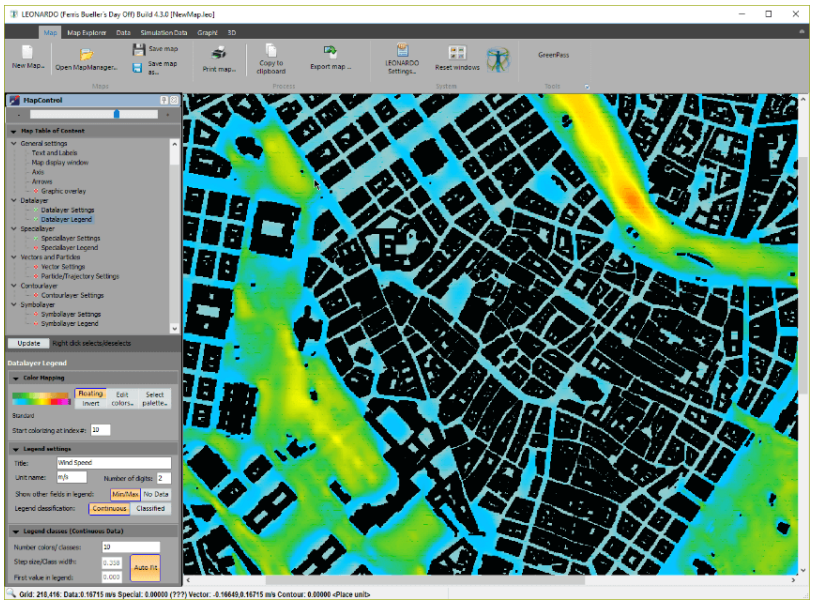

Figure 2.7. Envi-Met, an application to simulate urban microclimate.

Chapter 3

A Level-of-Detail Technique for Massive Sky View Factor Calculations in Large Cities

3.1 Introduction

The Sky View Factor (SVF) is of crucial importance in urban planning, architecture and related fields (Svensson, 2004; Gál, Lindberg, and Unger, 2009; Gál and Unger, 2014), because it is widely used as a basic parameter in modelling thermal phenomena in urban environments, such as the urban heat island effect (Unger, 2008). Traditional calculation techniques involve projecting the surrounding building geometries onto a hemisphere located at the measuring point, and computing the ratio of blocked versus unblocked parts of the sky (Brown, Grimmond, and Ratti, 2001).

However, these computations are particularly challenging when evaluated inside a complex urban landscape, where distant skyscrapers can block substantial part of the incoming daylight illumination (see Figure 3.1). Including this geometry, however important it is, may result in an explosion of complex evaluations that will result in a costly computational task if several evaluations are requested (e.g., for averages over whole streets or façades).

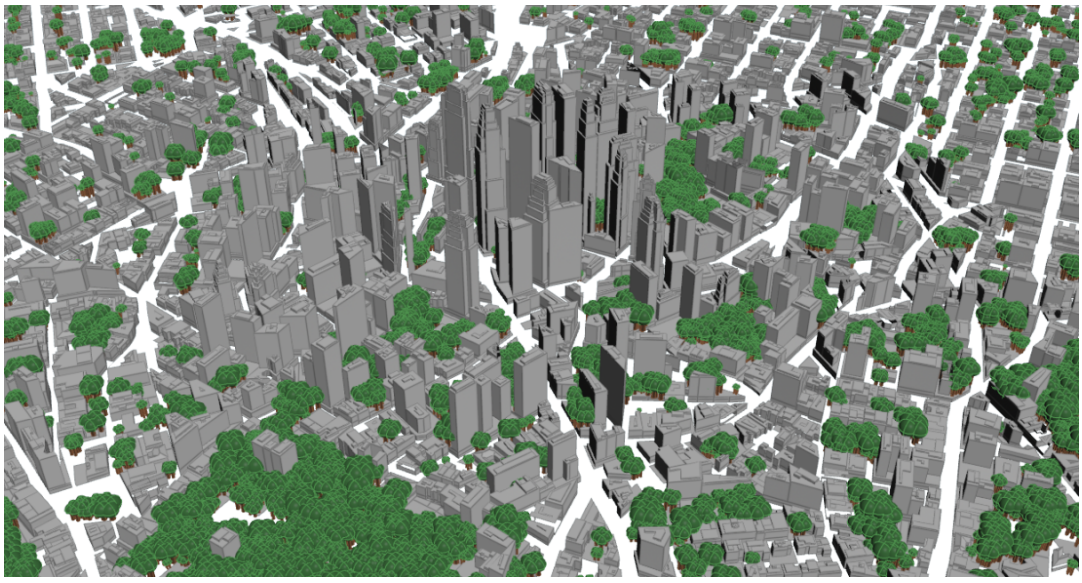

Figure 3.1. An example of a complex urban landscape where computations of the SVF can be time consuming.

In this chapter we introduce a technique for simplifying the computations of the SVF in large cities by simplifying the evaluation of distant geometry. For this, the city is partitioned using a regular grid and a set of localized *environment maps*, each one associated to one grid cell. In consequence, the evaluation of a SVF inside a grid cell simply amounts to the union of the evaluations of the occlusions by the geometric part inside the cell and by the buildings represented in the environment map, thus considerably reducing computational evaluation costs. The objective of this technique is to provide a precise and robust decision-making tool while working with large urban environments.

3.2 Material and Methods

Figure 3.2 provides an overview of the proposed method. Basically, it consists of partitioning the city into a grid and, for each grid cell, selecting an associated subset of the urban geometry. For the further SVF calculations, we also compute a cubical panoramic image (i.e., an environment map) of the geometry of the city, after removing the geometry associated with the cell, as previously selected. These cells are called *viewcells*, and are highlighted in red in Figure 3.2(*a*).

To further improve the final quality of the results, for each cell, the geometry of a subset of $N \times N$ cells centred in the selected cell is kept (N is odd in our implementation, to guarantee symmetry). They are shown as a yellow area in Figure 3.2(*a*). This is done in the *Pre-processing* stage, see Section 3.2.1.

Later, when evaluating the SVF for any position inside the cell, the actual geometry associated with the cell is used, together with the environment map of the rest of the city, to compute the final SVF value. This introduces an error that can be controlled by adjusting both the cell size (C_{size}) and the number N of the $N \times N$ cells where to keep the geometry. This is done in the *SVF computation* stage. See Section 3.2.2.

When choosing between using a raster method or a vector-based method, classical studies have always observed in their results that raster methods gain in efficiency and computational cost, while vector-based methods often gain in precision. However, there are hybrid techniques and solutions between the two to arrive at a better balance between the two extremes, or even reduce the differences in results between the two different approaches (Wade et al., 2003). Our choice has been a ray tracing-based method, which belongs to the second kind, mainly based on their flexibility to accommodate any kind of geometry. As explained below, our technique is designed to be an adaptive tool for decision-making, allowing manual adjustment of the amount of geometry to be processed, and thus the precision and speed of the results obtained by the calculations. This option also allows us to work with 3D models from multiple sources, such as 3D cadastral data, geometry generated from LiDAR, or models generated procedurally from a real street map, to mention a few examples. Moreover, using a vector-based method allows us to perform vertical studies, for example on the façade of a building, to analyse the SVF at each point of the façade, something that a raster technique would not allow. Finally, our technique was designed to be very efficient for accurately computing a massive number of arbitrary observation points, while raster techniques are limited by their own discretisation: all samples that fall into the same discretised cell (i.e., texel) would obtain the same value, because of the intrinsic limitation in accuracy of raster maps. However, using a 3D city model instead of an image-based representation implies that there

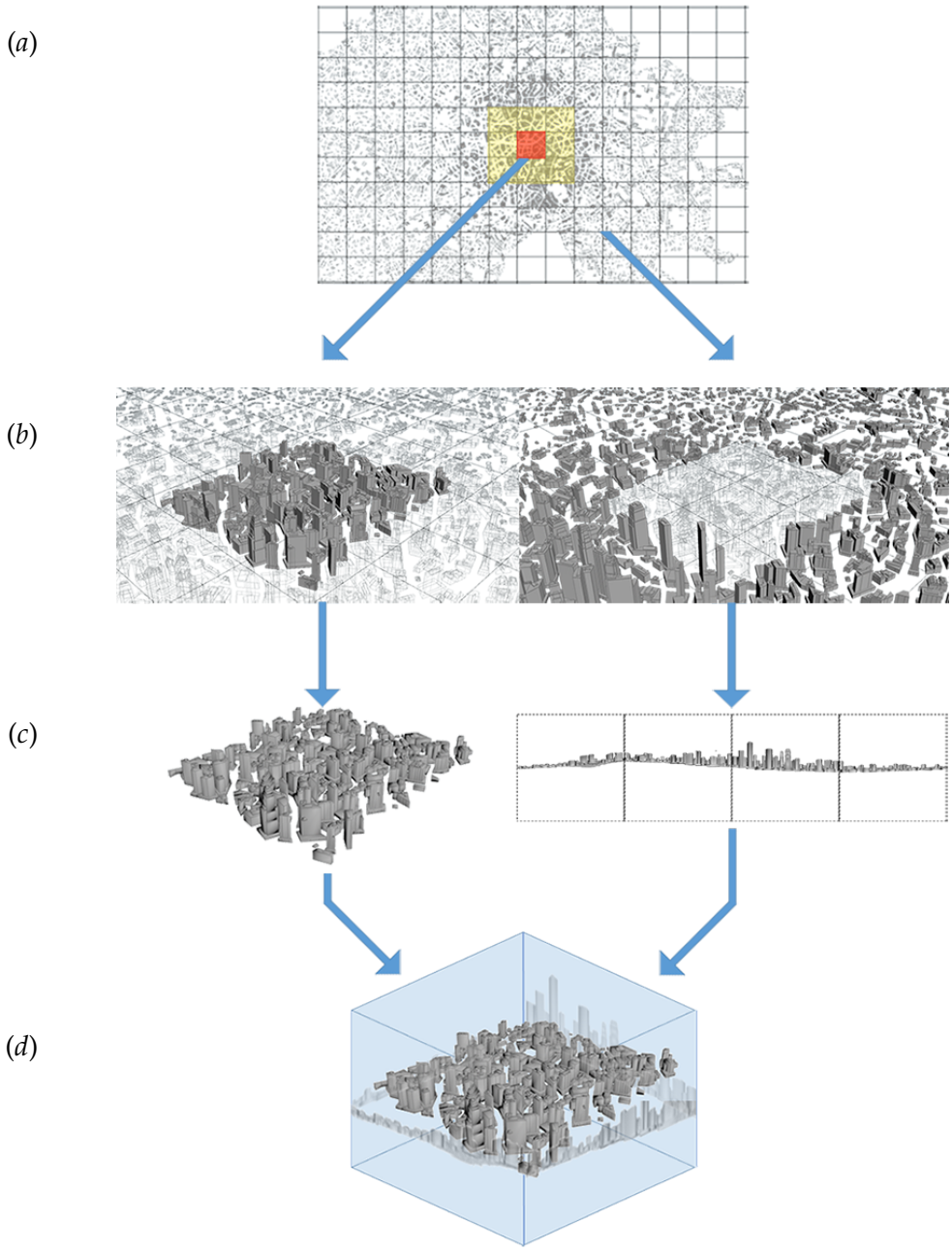

Figure 3.2. Overview of our method. Given a *viewcell* in a city (in red), we encode its surroundings in an environment map and compute the SVF from the geometry in the viewcell plus its corresponding environment map.

is no such discretisation, thus eliminating the limitations related to the dimensions and resolution of the scenario.

3.2.1 Preprocessing

Given a large city, we superimpose a regular grid, and we identify all the buildings inside each grid cell. Then, for each cell, we classify the whole city geometry into two sets: the geometry associated to the cell, and the rest of the other geometry in the city. See Figure 3.2(*b*). To improve the quality of the final results (see Section 3.3),

for each cell we actually select the geometry in the cell itself plus all the geometry in a subset of $N \times N$ cells centred in the currently selected cell.

In order to calculate the SVF from a specific point in a cell, the environment map corresponding to that cell must first be generated. Therefore, the first time that a cell is required to calculate the SVF from a point of its geometry, the environment map of that cell is generated and stored in memory for the successive SVF calculations that may require it, see Figure 3.2(*c*). The environment map is generated from a panoramic image of the surroundings of the cell, taken from its centre, thus obtaining an image that replaces the geometry far from this cell since it already appears in the panorama with an almost identical perspective. In a classic implementation, the environment (i.e., the buildings and other elements, such as the trees of our second set) is projected onto the six faces of a cube and stored as six square textures (or unfolded into six square regions of a single texture). However, as our interest is in computing the SVF, we can realize that the projections on the bottom and top sides are not needed: the bottom would result in fully occluded projection (i.e., the ground), while, if we remember that all the geometry in the selected cell and surrounding ones was deleted, the top projection will always return an image of the empty sky, see Figure 3.2(*d*). Taking all this into account, the environment map of a cell is generated by taking a panoramic screen capture from the centre of that cell and storing it in memory. As will be presented in the results of Section 3.3.3, the cost of this operation is very low.

It is important to note that an environment map is a projection onto a surface that is considered to be at a large distance of its centre of projection, or that the surface it is projected onto is large with respect to the size of the environment, which is consistent with our selection of the buildings at the farthest distance to be on the environment map, while closer ones are evaluated at the geometry level. This is an important point to understand the nature of our approximation and the error that can be obtained from it, see Section 3.3.

3.2.2 SVF computations

The SVF computation algorithm is described following the procedure presented in Algorithm 1. First, the geometric model of the urban environment is loaded from a file. This file can contain any type of urban element, because the presented technique only deals with its geometry, without discriminating its nature. Then, a grid appears over the top-view of the 3D model, allowing the user to adjust the cell size, and with this, its accuracy, as described in Section 3.3.3.

Next, a grid cell (the viewcell) must be chosen, determining in which region of the urban environment the SVF computations take place. Only the geometry of the designated viewcell plus the neighbouring $N \times N$ cells is kept, where N is also a parameter adjustable by the user. With all the geometry *not* selected in the previous step, an environment map composed by a panoramic photograph of the geometry beyond the designated $N \times N$ zone is generated. After these two elements are determined (i.e., the geometry to keep and the environment map), the method is ready to perform the SVF computations.

The SVF computation takes as input a sample distribution of points representing partitions of the sky dome (Beckers and Beckers, 2014) (rays), the geometry selected for a given cell (cellGeometry), and its corresponding environment map (cellEnvMap). This hemisphere has been meshed with a Monte Carlo probabilistic procedure looking for its maximum coverage, according to a target number of patches. In this projection, it is possible to read directly the azimuths of the cell

Algorithm 1 Function to compute the SVF for one singular observation point

```
function COMPUTESVF(rays, cellGeometry, cellEnvMap)
    local variables
        r, each ray
        hits, counter of occlusion hits
        t, intersected geometry reference
    end local variables
    hits ← 0
    for r in rays do
        t ← r.INTERSECT(cellGeometry)
        if t is an occluder then
            hits ← hits + 1
        else
            t ← r.INTERSECT(cellEnvMap)
            if t is an occluder then
                hits ← hits + 1
            end if
        end if
    end for
    return 1-(hits/LENGTH(rays))
end function
```

centres. Moreover, from the zenithal angles of the band limits, it is possible to deduce the angular positions of the cell centres. After that, a sky partition with cells whose inscribed circles have a diameter of 1° is introduced. In particular, for our technique, we work with an hemisphere of $10,000$ cells. The rays to be casted start from the centre of the hemisphere with one of the sampled directions, and end at the corresponding 3D collision point with the scene. The generated samples are centred around each projection point. Then, for each sample, we generate a ray from the projection point to the sample and evaluates its intersection with the city geometry.

If the ray does not hit the city geometry, we check the intersection against the projected geometry of the environment map. The face of the cubic environment map with which each ray is intersected is determined by the method by Voorhies and Foran (Voorhies and Foran, 1994). Again, any building or tree acts as an occluder, so any hit with a building or a tree in the geometry, or on the environment map, should be computed as an occlusion.

An important observation is that we actually do not use the full sphere of directions, but only the upper half, which represents the samples that are meaningful for the computation of the SVF. The reason why only the upper hemisphere of directions is required is that we only need to obtain the fraction of the sky that is visible for the given measuring point. Any direction coming from below the horizon will be blocked by the Earth itself. From the upper hemisphere, $\boldsymbol{M}$ rays are projected following a Monte Carlo distribution.

3.3 Results and Discussion

3.3.1 Case Studies

A set of tests has been made to test the performance and results of this technique. The first scenario for testing is a moderate 3D city model composed by about 700

buildings, generated procedurally, that are represented by more than 136K polygons. The extension of the city is $2,821\text{m} \times 3,726\text{m}$ and was set up to check the behaviour of the algorithm within a small setting. See Figure 3.3.

Figure 3.3. The model of the first scenario, composed by about 700 buildings.

A larger scenario was created to realize a more complex testing. We procedurally generated a 3D city model, which consists of more than 4,200 buildings (about 850K polygons). The extension of this largest city is $7,636\text{m} \times 6,805\text{m}$, see Figure 3.4. The topography of the test scenario simulates an European-like city with a large urban centre and smaller buildings in the suburbs. In addition, the entire city is located on an area with different slopes (variable ground heights), to be more realistic than the previous case of a city on a perfectly flat plane. In this case we observed a similar reduction in computation times.

Figure 3.5 shows the geometry hit from the projection point represented by a small hemisphere in the middle of the building geometry. As we can see, only a reduced set of polygons is actually selected for the SVF computations, while the rest of the rays either hit the geometry in the environment map or increase the sky view factor. This first tests backs our hypothesis, showing that only geometry from nearby buildings have a direct contribution on the SVF computation.

In our results, only less than 0.10% of the rays intersect the geometry projected in the environment map on average. This demonstrates that the farthest geometry of the scene has a much lower impact in comparison to the nearest one, showing that our Level-of-Detail technique is well suited to make the calculation of the SVF more efficiently. However, it is important to note that this average will vary depending on the height of the buildings and the overall layout of the city.

The tools resulting from this thesis, have been fully developed in the SideFX Houdini environment (SideFX, 2019), which among its many functions and features,

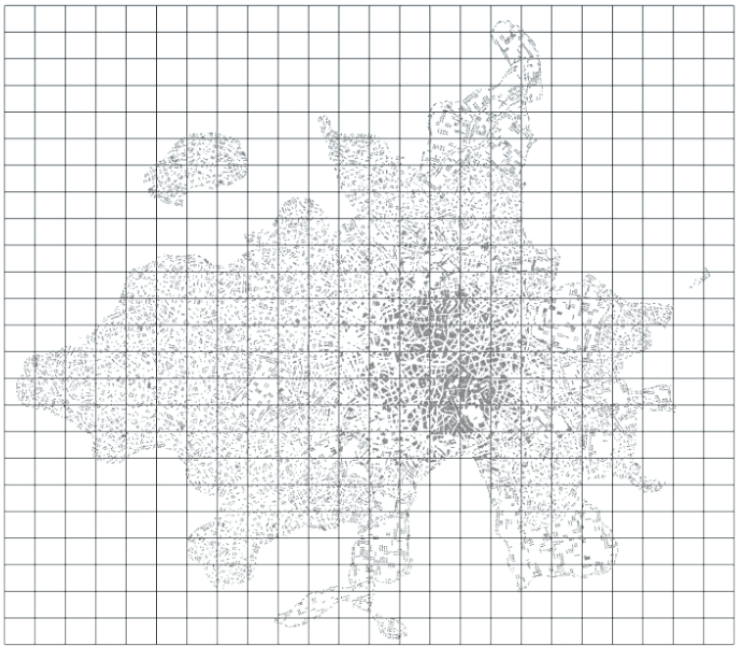

Figure 3.4. The model of the second scenario, composed by about 4,200 buildings.

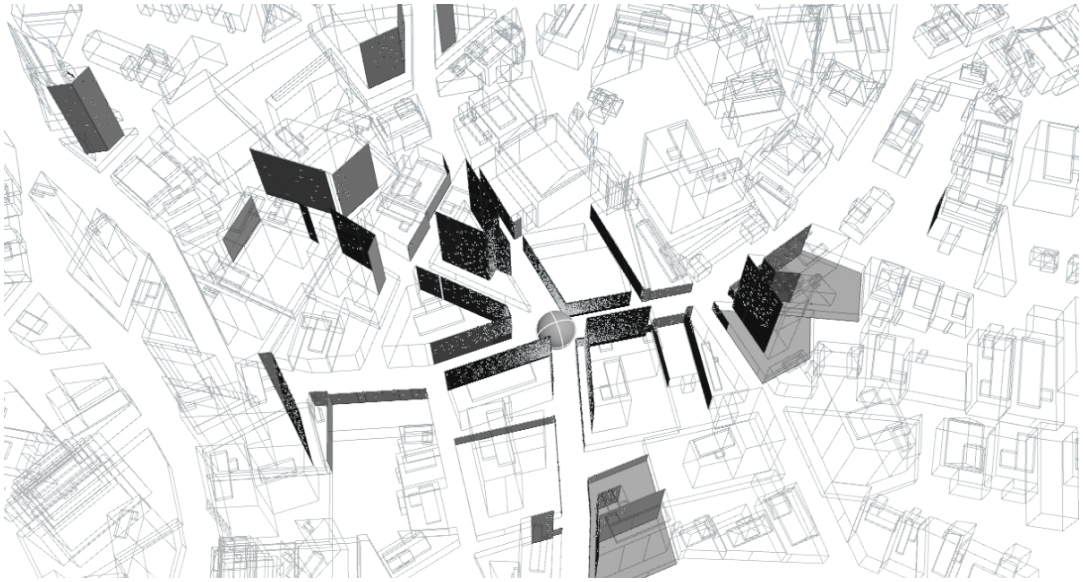

Figure 3.5. The actual geometry that is intersected from a projection point located inside a dense urban area. Observe that only a fraction of the actual geometry contributes to the final result.

allows working with 3D models procedurally and supports the execution of scripts in Python language. All the experiments were performed on a computer with an Intel Core i7-4790 CPU running at 3.60Ghz, 16GB of DDRAM3 memory and a GPU NVidia GeForce GTX 770Ti. The operating system used was Windows 10 Pro 64bits.

3.3.2 Analysis

We can study the time complexity of the algorithm by considering that the cost of tracing rays on a number R of objects (i.e., buildings) is $O(f(R))$, with f an arbitrary function that depends on the acceleration data structure used. In our case, this cost is limited to a subset of the city with a reduced number r of buildings, with $r < R$, thus resulting in a net result of $O(f(r))$, as evaluating the environment map requires a constant computational time ($O(1)$). This implies a strong reduction of the computational time with respect to a full ray-traced solution. However, it must be noted that the computational load in this case is transferred to memory consumption: The evaluation of several SVFs for a given cell requires a constant memory, proportional to the number of buildings associated to the cell, which we can assume roughly proportional to its size $C_{size}^2 \times N^2$, plus the memory needed for the environment map itself. For a full city, it must be taken into account that every cell requires to store r buildings on average, and its environment map, thus considerably increasing the associated memory costs. Fortunately, this is largely compensated when several SVFs are computed inside a reduced number of cells, which reduces storage costs to only those of these cells themselves.

Concerning the accuracy of our computations, in our first experiments, for $C_{size} = 50\text{m} \times 50\text{m} = 250\text{m}^2$ and $N = 3$, we have observed a maximum relative error below 1%. Also, increasing C_{size} to $100\text{m} \times 100\text{m}$ reduces this error to below 0.50%, which confirms our previous analysis. This is analysed further in our case study.

It is important to mention the error introduced by the use of the environment map in the approximations. As mentioned before, environment maps consist of an image, projected onto a given projection point, of a scene that is assumed to be very large with respect to the measuring area, in our case a cell. This corresponds to an approximation where two different rays, leaving two different positions but with the same directions, will end up hitting the same point on the environment map. This is the so called parallax error. In our case, this means that two identical samples computed from two different points will result in the same occlusion value. For projection points that coincide with the one used for the environment map construction, this error is null, and the only possible remaining error is the one of the finite-area pixels on the panoramic image, which we found to be negligible.

For SVF computations inside the cell but not on the projection point of the environment map, the parallax error will increase because of the mismatch between the projection point used and the one for the environment map. However, this error is controlled by defining the geometry associated with a given cell as the geometry of the cell itself plus its $N \times N$ neighbours. Also, this error is easy to control by the user by setting appropriate values for C_{size} and for N. Actually, in the limit of C_{size} going to 0, or when N is a large number, the associated error goes to 0: in the first case, the projection point will be the same as the one the environment map was taken from, and, in the second (i.e., N being very large), the geometry associated to the cell would become close to the full city itself, while the environment map would represent a smaller fraction of the outer city. In both cases, the net result is that the error becomes 0, at the expense of an increased computational cost.

One characteristic of our technique is storing, for each cell, its associated geometry and environment maps. However, according to our test, this increased storage cost is largely outweighed by the increase in speed for the computation of a large number of SVF. However, if only a single (or a reduced number of) calculation is required, it is clearly better to directly compute the SVF with the full city geometry.

3.3.3 Case Study Results

The technique we present in this chapter has been implemented in five different areas of the city, taking in each one fifty computations of the SVF in different random locations within the evaluation cell, recording the processing time and the relative error between the calculation with all the geometry and the calculation using our LoD technique. Also, the experiment has been repeated with three different cell sizes (50m, 100m and 200m) and different numbers of cells by side (1, 3, 5 and 7), varying the amount of geometry to keep in each case.

To evaluate the accuracy of the presented technique, each calculation was performed both with our technique and by considering all the geometry of the case study as a reference solution. With both values, we calculate the relative error introduced by our LoD technique. Figure 3.6 shows the result of the experiments adjusting three different cell sizes and their relative errors.

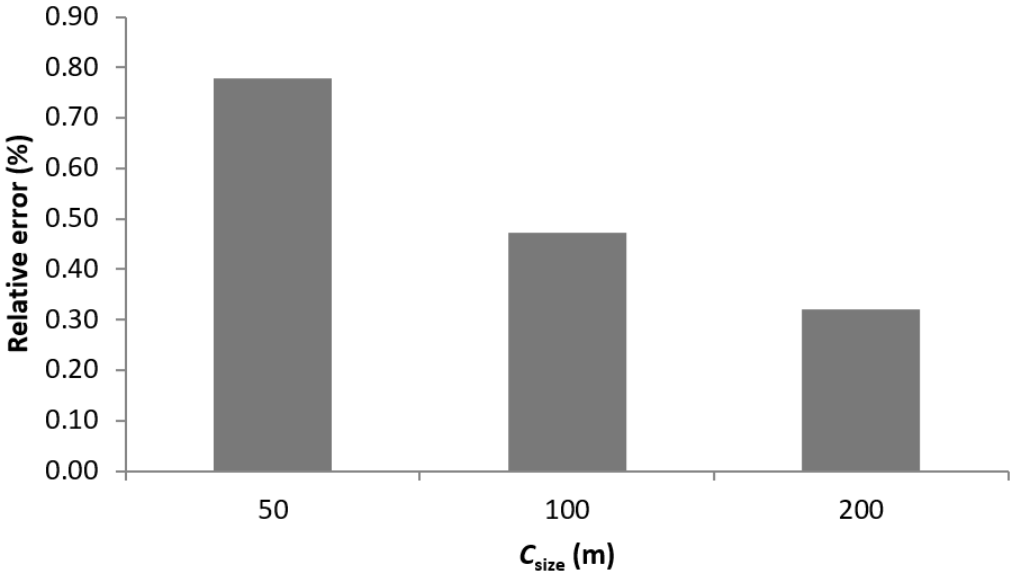

Figure 3.6. Error versus C_{size}. The bar graph shows how the relative error, when compared to the full-geometry calculation, decreases as we expand the size of the cells using $N = 3$.

More calculations could be performed increasing C_{size} to more than 200m in our scene, but the relative error would reduce, reaching a stable value related to the inherent noise of the sampling technique. The error is inversely proportional to C_{size} because the more the size of the cells we use increases, the more geometry is used in the calculations, thus reducing the effect of the imprecision introduced by the environment map. Thus, the methodology would be to always propose an error threshold, and iteratively increase C_{size} to reduce the error value until the threshold is reached.

On the other hand, Figure 3.7 shows the results of selecting three different numbers of cells per side ($N = 3, 5$ and 7) for the geometry to keep for the computations (all the rest would be represented in the environment map), and the relative error. Calculation has been performed with a single cell also to show that it is necessary to group adjacent $N \times N$ cells to prevent parallax error. The relative error decreases less when increasing from 5 to 7 cells per side, as it is already significantly low.

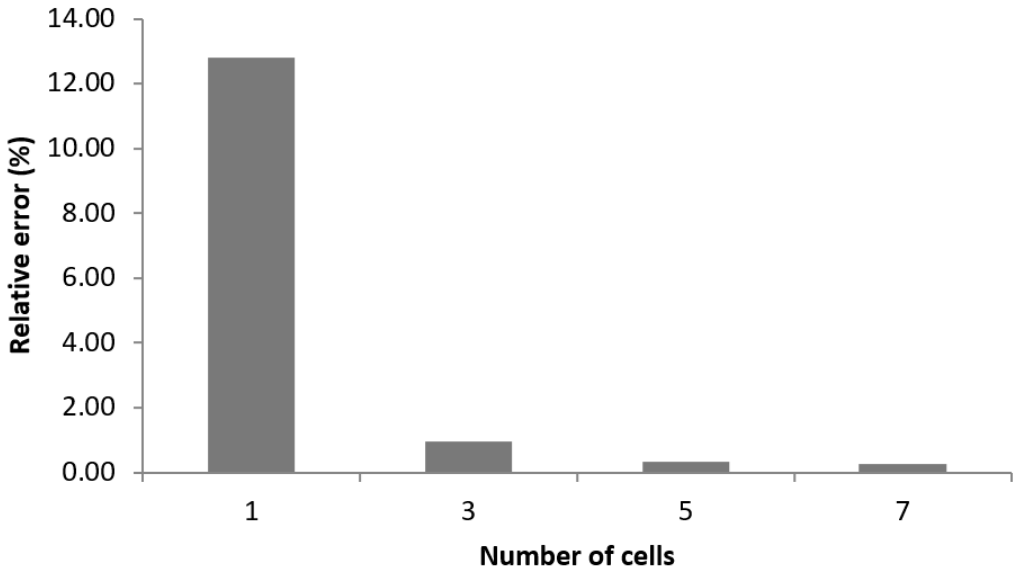

Figure 3.7. Error versus N. Bars show how the relative error decreases as we expand the number of cells using $(C_{\text{size}}) = 50$m.

After all the experiments, the optimum settings for the 3D model of our city were decided to be a C_{size} of 100m and $N = 3$ cells per side for the region of geometry to keep. In this scenario, the average relative error of the fifty SVF measurements is 0.47%, and the computational time is 27% that of the computational time required when using all the geometry of the 3D model.

Finally, a last experiment has been performed to see how the vertical displacement (the y-axis in our system) of the observation points affects the relative error due to the gap with the environment map. Figure 3.8 shows the error to observe the effect. The maximum relative error recorded is less than 10%, although it might rise above this in the case of a very high building surrounded by other high city buildings (our tallest buildings are around 100m on that area of the 3D city). If a greater accuracy is required, the solution is to take more environment maps at regular intervals in the y-axis, and using the corresponding one in the calculation of SVF. Also, we added another parameter for the vertical offset from which the environment map is generated and used. With that parameter it is possible to obtain an even better accuracy at the SVF calculations.

To visualize the SVF, we imposed a grid on the area to calculate the SVF. The result allows to evaluate the visible sky from the selected region, as can be seen in Figure 3.9. The computation of this representation takes about 9 minutes to complete. As we can see, SVF values in open areas have higher values than in crowded or closed areas. Also, we can observe the absence of values above 0.60, given that we are inside a dense urban area. This is due to the effect of the urban form irregularity, since the areas with more homogeneous distribution and height of the buildings have lower SVF values from the ground, while the more irregular areas have higher SVF values (Leung and Steemers, 2008).

The same approach can be applied to show the level of error of the technique with the same configuration as previously set. Naturally the error will grow as the grid points move away from the centre of the cell, because of the parallax error already mentioned. As we can see from Figure 3.10, except for a few points on the outer limits of the calculation area (closer to the environment map), most of the

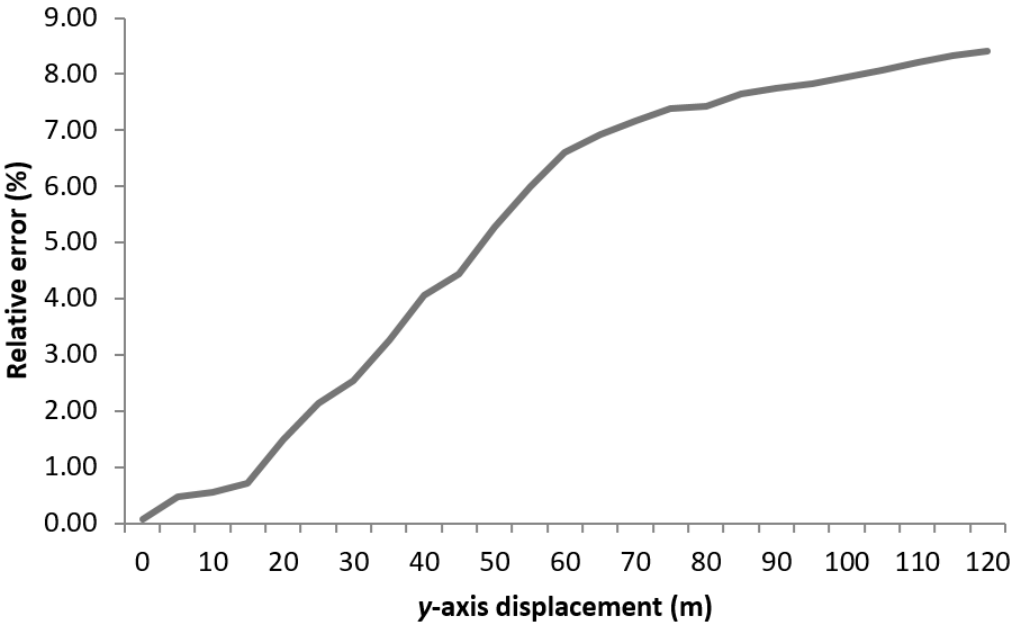

Figure 3.8. Error versus y-axis displacement. The line shows how the relative error increases as the observation point ascends vertically from the original position from where the panoramic image for the environment map was taken.

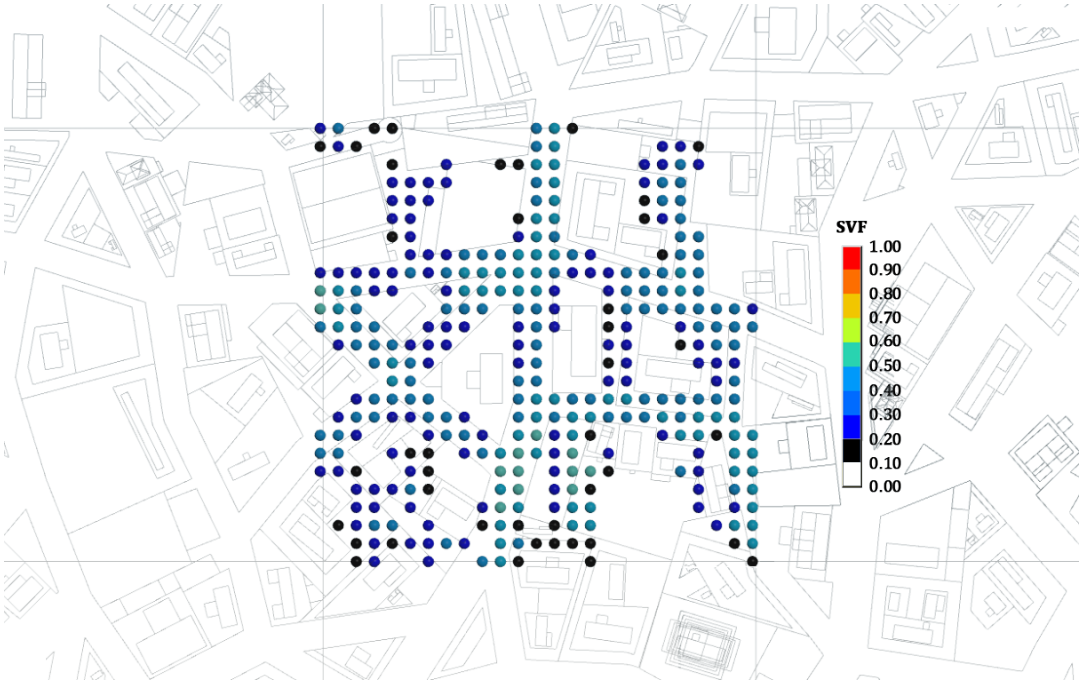

Figure 3.9. SVF at ground level, categorized into scale levels ranging from black to red. SVF values below 0.10 are transparent to make the figure clearer, avoiding cluttering the image with black points.

calculation points are not painted because of its low error level, showing a great concordance with the calculations done with more classic approaches. In any case, if the result is not accurate enough, the system allows the parameters to be adjusted

TABLE 3.1: Geometry reduction and timings for our two test cases. Timing to build up the environment map is not included in these figures.

Case Study	Original Geometry (Polygons)	Reduced Geometry (Polygons)	Geometry Reduction (%)	Average Time Full Geometry (s)	Average Time LoD Geometry (s)	Speedup (u)
Scen. 1	136,782	5,510	4.03	0.80	0.52	1.53
Scen. 2	856,440	6,386	0.75	2.81	0.51	5.53

again until a desired precision is achieved.

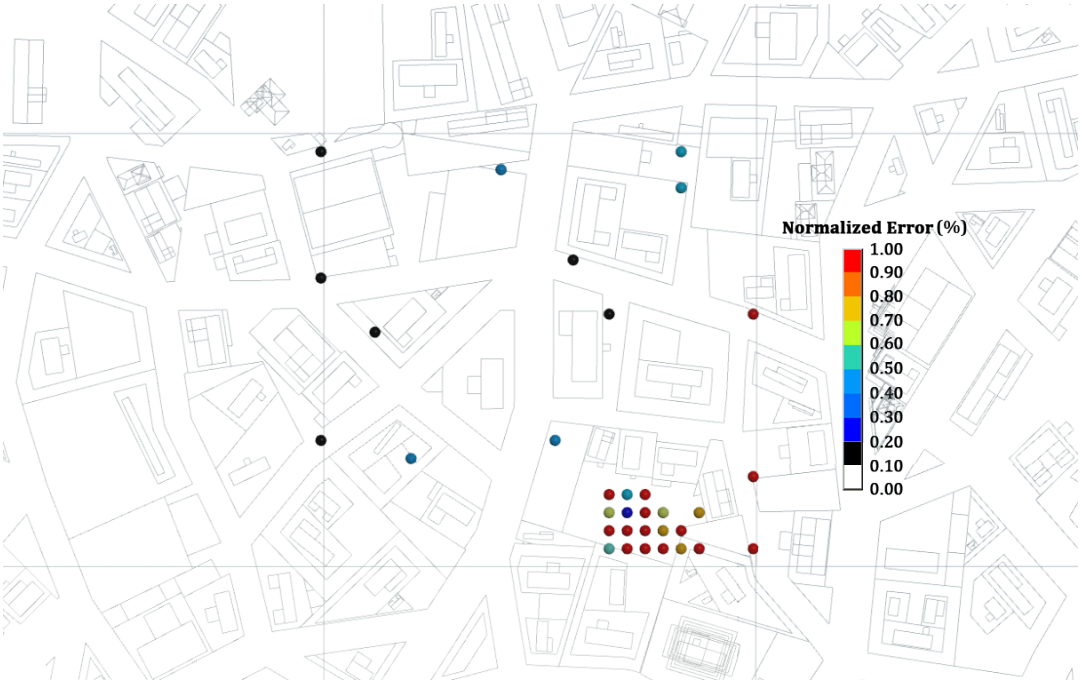

Figure 3.10. Relative error of the SVF, normalized from black to red. Note the increase in value when the measuring points approach the borders of the cell. Values with an error below 0.1 were made transparent to increase readability.

Concerning computational time, Table 3.1 presents the results for the two test scenarios with a C_{size} of 50m $\times$ 50m and $N = 3$ cells. As we can see, the time with our technique remains stable regardless of the scene complexity (we keep 4.03% of the geometry for the first scenario and 0.75% for the second), thus increasing the effectiveness of our proposed technique as the size of the city increases, and further amortizing the cost of the environment map setup and storage. Also, in absolute terms, the more SVFs we compute, the larger the benefit, as this environment map needs to be computed only once for each view cell where we compute SVFs, and is reused for any SVFs that need to be computed within that cell. The environment map set up required 0.30 seconds for both cases, as its computation is really small if we take advantage of the capabilities of modern GPUs, that can take four screenshots of 512 $\times$ 512 pixels to make up the panorama of an environment map in a fraction of a second.

To find the proper values of C_{size} and N in a case study, several iterations were performed on the case study by modifying both values until achieving the level of accuracy desired for the study.

It is important to note that our technique also allows massive measurements of SVF in vertical positions, something that would not be possible using a raster-based method. In this way it is possible to measure the SVF from the façade (and even the windows) of one or several buildings of the studied area, see Figure 3.11.

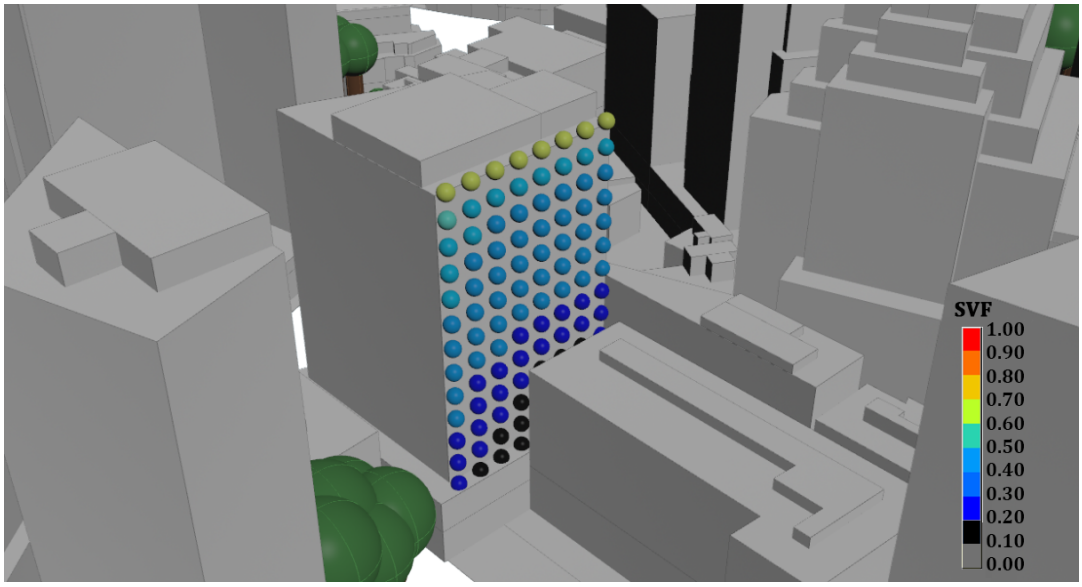

Figure 3.11. A vertical mesh measuring SVF through the façade of a building of the city shown in Figure 3.1.

Although one could think of computing the SVF without the environment map and working only with the geometry of a cell of specific size (e.g., 200m $\times$ 200m), there are situations, both natural and human-made, that show that it is not possible to do that without incurring in a serious precision error. An example of a natural situation would be the Sugarloaf Mountain, in Rio de Janeiro (Brazil), while a human-made example would be the Tour Bretagne, in the French city of Nantes. In both cases, an element of the distant environment can occlude further observation points. Using the environment map, our technique considers those elements while using only a restricted subset of the geometry can generate important errors if the occluders are out of the viewcell. Thus the environment map is necessary to keep the efficiency and accuracy in all kinds of scenarios.

Finally, it is also important to note that this technique allows working not only with synthetic models but also with real data as long as their geometry is available in a 3D file format. Thus, it is possible to study the SVF in the restitution of a 100% real environment. As an example, we measured of SVF along a street with 3D model of Paris, see Figure 3.12.

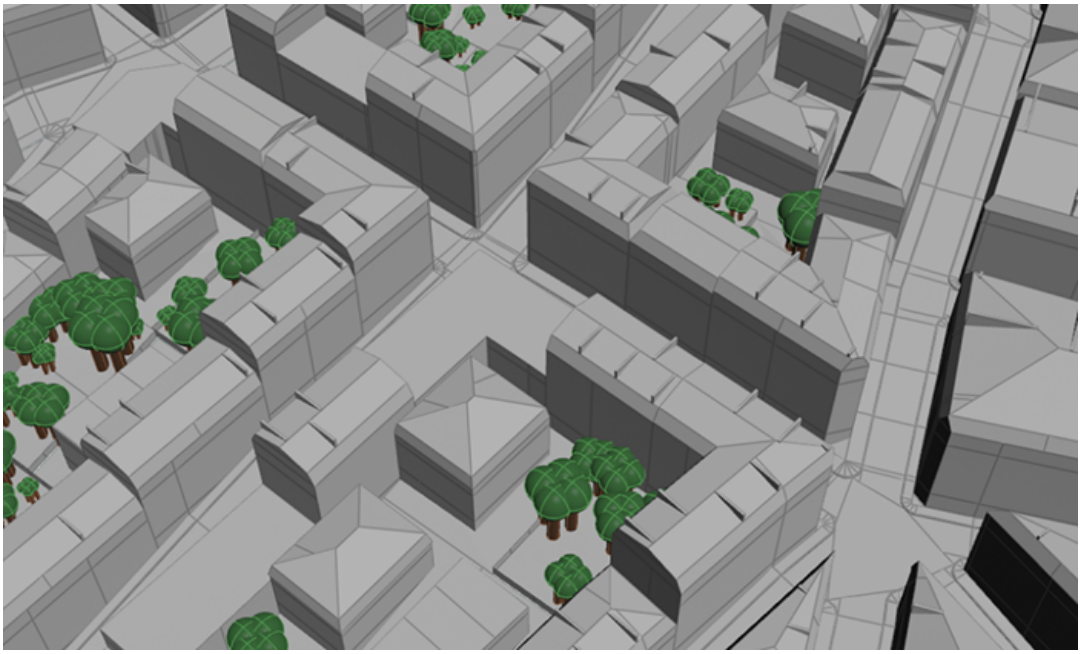

(*a*) 3D vision mode.

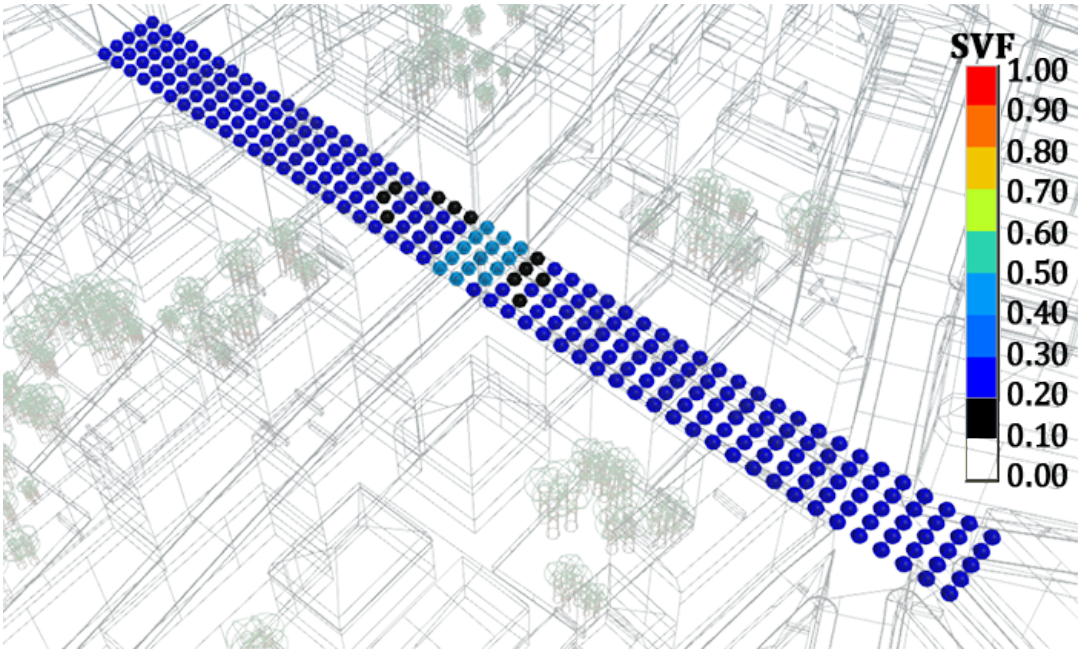

(*b*) SVF vision mode.

Figure 3.12. SVF measured along a street in Paris.

Chapter 4

A Procedural Technique for Thermal Simulation and Visualization in Urban Environments

4.1 Introduction

The concept of Urban Physics has flourished in recent years as a result of the global growth of cities and an accompanying improvement in computational tools. Urban Physics essentially provides a way to qualify and quantify the different energy flows, both natural and artificial, that occur in a city. The search for efficient simulation tools is an ongoing active line of research (Beckers, 2012). In particular, most of the tools available to simulate and analyse thermal behaviour have been conceived for a building scale (Crawley et al., 2001; ESRU, 2019), and less so for an urban (Masson, 2000; Martilli, Clappier, and Rotach, 2002; Salamanca and Martilli, 2010; Mauree, Blond, and Clappier, 2018) or district scale (Lindberg, Holmer, and Thorsson, 2008; Robinson, 2012; Mauree et al., 2017; Wang et al., 2018; CitySim, 2019).

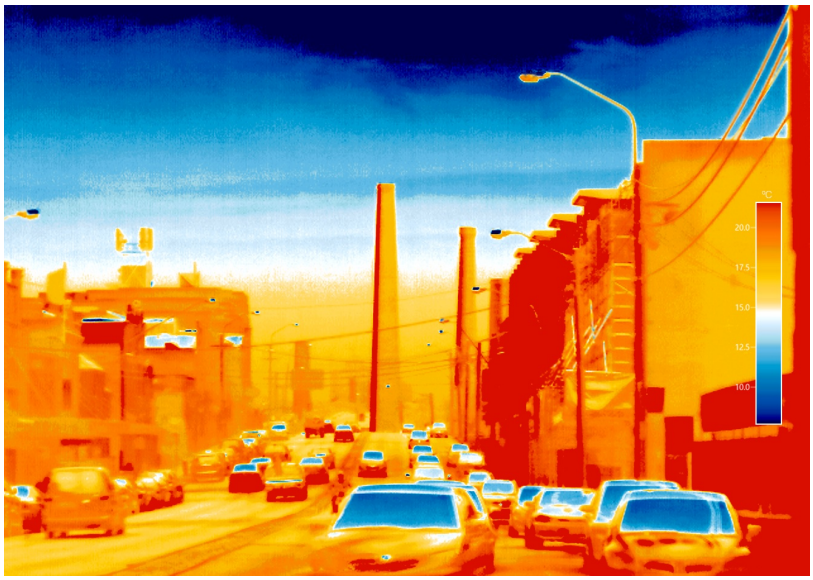

Figure 4.1. A thermographic capture of an urban environment (credit: Adam Sébire, PhD student at UNSW Faculty of Art & Design).

Computing a complete thermal simulation on an urban scale requires taking into

account both the thermal and the geometric models of the buildings involved. Most of the simplified thermal methods are based on an electrical analogy (Fraisse et al., 2002). By selecting nodes on a building model, a circuit network can be represented and solved to assess temperature. Setting the nodes, however, is generally done manually, which is not only error-prone, but also very complicated for a multi-storey building and even more so on an urban scale. Furthermore, to work on an urban scale, apart from taking into account the geometric and thermal models of the buildings that make up the urban environment, their environmental conditions such as the temperature of the air and the sky, solar radiation and even the heat exchange between buildings that are close to each other, must be considered.

In this chapter, we propose a method for procedurally generating the circuit network for all the buildings within an urban environment, as well as presenting a variation of temperatures in an urban environment over time. Given a geometric model and the corresponding physical construction parameters (i.e., the conductance and heat capacity of each material layer of the buildings) the system parses the model and generates a set of rules representing the interfaces for conductive heat transfer. From these rules, the technique procedurally generates an electrical circuit that simulates the conductive heat exchange at each step of the simulation. In addition to this conductive calculation, a radiative calculation is also performed simulating the heat exchange between the exterior surfaces of the buildings and its surrounding heat flows by using climatic data, a solar radiation calculation and a thermal exchange simulation between nearby buildings. As a result, we obtain a thermal calculation system that allows the temperature changes to be analysed over time. Our tests have shown promising results when we perform a validation with real world data, and we show, as a conceptual technique, that the parameters of the building model, such as the number of floors or the materials that make up the walls, can be changed to analyse temperature variations in the urban environment.

Our contributions are, namely the automatic generation of the circuit network, the resolution of the system in short simulation times and the visualisation of the temperature changes in the buildings. The potential benefit of our approach is that it could be used for testing optimal node configurations or analysing building parameter changes. We believe that this analysis could be a useful tool for urban planning, architecture and other related fields.

4.2 Fundamentals

In this section, we present all the physical concepts related to the methodology that we use to implement our thermal simulation technique for urban environments.

4.2.1 Shortwave Radiation

Shortwave radiation (SW) is radiant energy with wavelengths in the near-ultraviolet, the visible, and near-infrared spectra. Downward shortwave radiation is sensitive to solar zenith angle, cloud cover and surface albedo.

For our technique, it is necessary to calculate the shortwave radiations emitted from the sun that reach each surface, as well as its reflected component towards other nearby surfaces. The method selected was that of the extraterrestrial solar radiation equation (Lavery, 2007), which requires a whole set of physical, geometric and climatic variables. Some of these variables are global, such as the global solar constant

G_{sc} (1367 $W \cdot m^{-2}$), while others depend on the location of the case study and consider elements such as latitude angle (φ), climate (tropical, mid-latitude summer, subarctic summer or mid-latitude winter) or altitude (H). And finally, there is a set of variables that depend on the solar calendar as is the case of the angle of the Earth's declination (δ), the hour angle (ω) and the zenith angle (θ). The atmosphere must be taken into account as well, so two coefficients must be calculated to determine reflected and absorbed solar radiation. The first coefficient is beam radiation (G_{cb}), which is the ratio of the transmitted direct radiation to the total radiation incident at the top of atmosphere. The second one is the diffuse radiation (G_{cd}), the ratio of the transmitted diffuse radiation to the total radiation incident at the top of the atmosphere.

By putting this all together, Equation 4.1 is obtained for calculating the solar radiation that reaches the ground between two particular times (ω_1 and ω_2) for the n-th day of the year.

$$I_c = \frac{12 \cdot 3600}{\pi} \cdot G_{sc} \cdot \left(1 + 0.033 \cdot \cos \frac{360 \cdot n}{365}\right) \cdot \left(\cos \varphi \cdot \cos \delta \cdot (\sin \omega_2 - \sin \omega_1) + \frac{\pi \cdot (\omega_2 - \omega_1)}{180} \cdot \sin \varphi \cdot \sin \delta\right) \tag{4.1}$$

When solar radiation reaches a surface i, part of this radiation is reflected according to the albedo coefficient of that surface (r_i), and reaches other surfaces, visible from the first one, see Equation 4.2.

$$Q^i_{ref} = I_c \cdot r_i \tag{4.2}$$

Taking this into account, the form factors between all the surfaces in the scene must be calculated. In radiative heat transfer, the form factor between two surfaces (A and B) is expressed as $FF_{A \to B}$ and is the proportion of the radiation which leaves surface A and strikes surface B. Several methods are available for this purpose (Sillion and Puech, 1994). We use a projection method where we compute the visibility through a distribution of rays cast from each surface. The sun's radiation reflected by a surface i (Q^i_{ref}) is distributed among the visible surfaces, multiplied by its form factor, see Equation 4.3.

$$Q^i_{rec} = \sum_1^j Q^j_{ref} \cdot FF_{j \to i} \cdot (1 - r_i) \tag{4.3}$$

The solar radiation that is not reflected is absorbed by the surfaces, causing changes in the exterior temperature of the walls, see Equation 4.4.

$$Q^i_{abs} = I_c \cdot (1 - r_i) \cdot A_i \tag{4.4}$$

Thus, the total shortwave radiation that is absorbed by a surface i (Q^i_{sun}) is equivalent to the sum of the radiation absorbed by the sun (Q^i_{abs}) and the radiation reflected by other surfaces and reaching the surface (Q^i_{rec}), see Equation 4.5.

$$Q^i_{sun} = Q^i_{abs} + Q^i_{rec} \tag{4.5}$$

4.2.2 Long-wave Radiation

In an urban environment, a surface receives long-wave radiation from multiple sources, and its temperature is affected accordingly. An exterior surface of a building receives this type of radiation from the celestial vault (sky radiation) and other nearby surfaces in the urban environment (environmental radiation).

Sky Radiation

To calculate the sky radiation on an urban environment, it is first necessary to know the irradiance of the sky, which is calculated from the dew-point temperature. In our case studies, we assume a clear sky, so we use Clark and Allen's expression (Clark and Allen, 1978). Through the emissivity of the sky, it is possible to calculate the infra-red radiation of the sky on a horizontal plane, taking into account the exterior air temperature. With that infra-red radiation, the temperature of the sky is calculated by Equation 4.6. Temperatures are expressed in degrees Kelvin, so we must convert the sky temperature to degrees Celsius.

$$Sky_{Temperature} = \sqrt[4]{\left(\frac{Horizontal_{IR}}{\sigma}\right)} - 273.15 \tag{4.6}$$

By knowing the temperature of the sky at a given moment, it is possible to calculate the heat exchange between the celestial vault and an exterior surface i of a building by applying the Stefan-Boltzmann law, taking into account the SVF, the Stefan-Boltzmann's constant (σ) and the difference between sky and surface temperatures to the fourth power, see Equation 4.7. The epsilon coefficient for emissivity (ϵ) must be applied as well to represent the emission capacity of the surfaces.

$$Q^i_{sky} = SVF_i \cdot \epsilon \cdot \sigma \cdot (T_i^4 - T_{sky}^4) \tag{4.7}$$

The SVF is the ratio of radiation that is received by a specific point to that which would be received from the whole hemispheric radiant environment around that point. The SVF ranges between 0 and 1. Values close to 1 mean that almost the entire hemisphere is visible, which is the case of exposed features (planes and peaks), while values close to 0 are present in areas with high concentration of large buildings, especially those with narrow streets, from where almost no sky is visible.

Air Convection

Air temperature is another factor to which an urban environment is exposed. In order to calculate the heat flow between a surface i exposed to the air temperature (normally the external walls and roofs of the buildings), it is necessary to know the convective exchange coefficient of that surface (h^i_{cv}). The expression to calculate the heat flow is shown in Equation 4.8.

$$Q^i_{air} = h^i_{cv} \cdot (T_i - T_{air}) \tag{4.8}$$

Environmental Radiation

At each step of the simulation and for each exterior surface, we compute its thermal exchange with Stefan-Boltzmann's law. This is done by selecting all the surfaces in the scene with a non-null form factor with respect to the selected one. For each exterior surface, energy emitted to other visible surfaces is calculated by applying an

emissivity coefficient (ϵ). After that, for each exterior surface, the energy received from the other exterior surfaces is added and an absorbency coefficient (α) is applied, see Equations 4.9 and 4.10. Absorbency and emissivity coefficients are used considering surfaces as "grey bodies".

$$Q^{i-j}_{emitted} = \epsilon \cdot A_i \cdot F_{i \to j} \cdot \sigma \cdot (T_i^4 - T_j^4) \tag{4.9}$$

$$Q^{i-j}_{received} = \alpha \cdot Q^{i-j}_{emitted} \tag{4.10}$$

Thus, the heat exchange between a wall and its surroundings (Q_{sur}) is equivalent to the total radiation received ($Q_{received}$) from the environment minus the total radiation emitted into the environment ($Q_{emitted}$), see Equation 4.11.

$$Q^i_{sur} = \sum_1^j Q^{j-i}_{received} - \sum_1^j Q^{i-j}_{emitted} \tag{4.11}$$

Other factors

There are other factors that affect the thermal behaviour of an urban environment, especially in the interior of buildings such as population density, artificial lighting, the presence of household appliances and even the use of air conditioning devices. All these factors are introduced as one more heat flow in each surface i (Q^i_{other}), thus ensuring their effect is contributed as a constant variable throughout all the conductive steps of the simulation.

Total Radiation

Each one of the factors presented in this chapter must be taken into account when converting the energy received by a surface into variations of its temperature. To do this, Equation 4.12 presents the total heat flux received by a surface i within an urban environment (Q^i_{total}) at a given moment, taking into account the contribution of each heat radiation, in addition to the absorbency coefficient (α).

$$Q^i_{total} = \alpha \cdot Q^i_{sun} - Q^i_{sky} - Q^i_{air} + Q^i_{sur} + Q^i_{other} \tag{4.12}$$

4.3 Simulation

4.3.1 Overview

In this section we provide an overview of our technique, describe how the thermal model is generated and how the simulation over time is performed. Figure 3.2 provides an overview of the proposed method which is described with the procedure shown in Algorithm 2.

The method takes as its input a 3D urban model (already simplified into its basic geometric structure), with all material descriptions, the desired simulation time and the time step. The structure is determined by building geometries, that is, the dimensions of the walls and their interconnections. The materials are represented with a database that indicates the number of layers that form each wall, as well as the physical parameters of the material each layer is composed of. From this structure and these materials, the process generates the circuits using an electrical analogy. This step is explained in more detail in Section 4.3.2

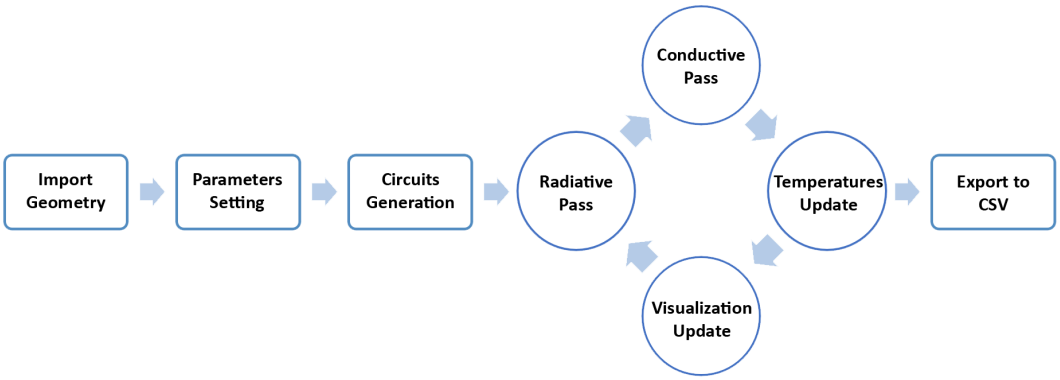

Figure 4.2. Overview of our method. The simulation takes a 3D urban model and a collection of parameters and provides output results for visualisation and analysis.

For the simulation, environmental and physical parameters should be established, such as the initial temperature of building surfaces, external temperatures and dynamic climate-based data for the specific location where the thermal behaviour it is intended to be simulated. This step is explained in more detail in Section 4.3.3

Once these adjustments have been made, the simulation starts, calculating a radiative pass and a conductive pass at each time step, updating the internal and external temperatures of the buildings and changing their representative colour to visualise their evolution over the period of time being simulated. The radiative calculations are described in greater detail in Section 4.2.

4.3.2 Urban 3D Model Processing

The first step of the procedure is to load and process the 3D model of the urban environment on which the thermal behaviour is to be simulated over the desired period of time. Once the urban model has been loaded, the system performs a geometric simplification and three pre-process stages that prepare the 3D model for the simulation. These stages are performed only for the first time that the model is used, thus it is not necessary to repeat its calculation in subsequent simulations of the same urban environment.

During the simplification of the model, the system takes the position of the buildings, their number of floors and their height to recreate them in a simpler schematic version, using procedural generation rules. This simplification is used to standardise the buildings, retaining their size, approximate volume and position such that the peculiarities of each individual building are not considered relevant for the simulations. In addition to being simplified, the 3D model divides its geometry into subdivisions of size l, this variable being the most important to control the precision of the technique.

The first pre-process stage consists of calculating the SVF for each primitive of the geometric model. In this technique, the SVF is required to calculate the energy that reaches each surface from the sky at each simulation time step. Calculating the SVF is done using a ray-casting technique (described in Chapter 3) applied to the observation points, in this case the centre of the primitives of the model. Since this technique works with a 3D geometric model and not with an image-based representation, there are no problems with spatial resolution.

The second pre-process stage consists of calculating the form factor between each primitive with respect to the rest of the primitives in the 3D model. In this technique,

Algorithm 2 Procedure to simulate thermal behaviour

```
procedure SIMULATE(urbanModel, simTime, timeStep)
    local variables
        circuits                    //circuits of the urban model
        t                           //current simulation time
    end local variables
    IMPORTGEOMETRY(urbanModel)
    CALCULATEVIEWFACTORS(urbanModel)
    PARAMETERSSETTING( )
    circuits ← CIRCUITSGENERATION(urbanModel, temperatures)
    t ← 0
    while t < simTime do
        RADIATIVEPASS(urbanModel)
        CONDUCTIVEPASS(circuits)
        TEMPERATURESUPDATE(circuits, urbanModel)
        VISUALIZATIONUPDATE(urbanModel)
        t ← t + timeStep
    end while
    EXPORTTOCSV( )
end procedure
```

the form factor (FF) is required to calculate the energy that is exchanged between surfaces at each time step of the simulation. The calculation of FF is also done by ray-casting, except that the hemisphere that casts the rays is placed perpendicularly to the centre of each primitive, instead of perpendicular to the ground. In this way, it is possible to calculate what percentage of visibility a primitive has of the elements in its environment.

The third pre-process stage consists of generating the procedural rules that generate the electrical circuit corresponding to each building in the urban environment to be simulated. These circuits are required to calculate, by solving them, the conductive step during the simulation. Circuit generation is explained in more detail in Section 4.3.5.

4.3.3 Parameters Setting

The next step of the procedure is to set all the parameters required for the simulation. We use three types of parameters: physical, environmental and simulation.

The physical parameters define constants such as density, thermal capacity and the infiltration of air and thermal conductivity and the glazing transmission factor of the windows. In this set of parameters, there is also the flow of heat induced by the other factors presented in Section 4.2.2. These parameters are general and do not depend on the environment or the buildings.

The environmental parameters define constants specific to the location to be simulated. Such parameters can be the latitude and longitude, the time zone, the altitude with respect to the sea-level or the climate data file of the area. These parameters will not be constant and will be changed for each case study located in a different part of the world.

The simulation parameters are those related to time, i.e. the start date and time of the simulation, its duration and the time step. Also included here are the initial

temperature parameters for the surfaces and interiors of the buildings that make up the urban environment.

4.3.4 Solar simulation

This procedural simulation technique calculates and represents the solar path at each time step. This is necessary because, although the morphology of the urban environment remains stable over time, the same does not occur with the position of the sun with respect to the Earth. This obviously implies that the amount and intensity of solar radiation received by the exterior surfaces of urban environments varies with time and that must be represented in the simulator.

Therefore, in our method, the sun is geometrically represented by a sphere and, by means of a ray-casting technique, our method detects at each moment which surfaces receive direct sunlight and which do not. The position relative to the urban environment that this sun must occupy in the 3D scenes of the case studies is calculated at each time step of the simulation from the measurement of the azimuth (γ_{sun}) and the altitude (α_{sun}) of the star, thus obtaining its directional vector, see Figure 4.3. It should be mentioned that the solar directional vector depends directly on three circumstantial variables that will be stipulated by the simulation parameters set for each case study: date, time and geographical coordinates of the area to be simulated.

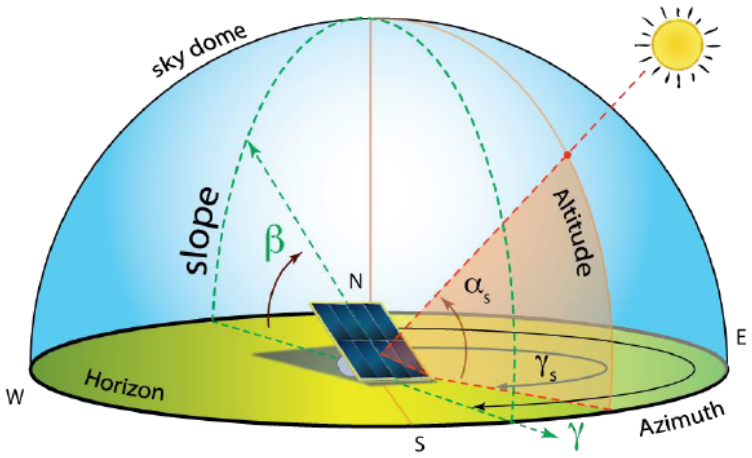

Figure 4.3. To obtain the directional vector of solar radiation, the altitude (α_{sun}) and azimuth (γ_{sun}) of the star are calculated at each time step (Credit: Jeffrey R. S. Brownson).

In this way, and following the formulation shown in Section 4.2, it is possible at each step of time to calculate the solar radiation emitted on a horizontal plane. This radiation must be separated into its two components, direct and diffuse, and must also multiply by a cosine for any surface that is not parallel to the horizontal plane. Table 4.1 shows an example of radiative calculation for an April day with a time step of one hour. The table shows for each hour their corresponding solar times and hour angles, the beam and diffuse radiation coefficients (τ_b and τ_d) and the beam and diffuse solar radiation (Q_{sun} and Q_{dif}).

It should be noted that for implementation and approximation, the simulation technique assumes that, if an exterior surface of the urban environment receives direct sunlight, the entire surface in question receives uniformly the total solar radiation corresponding to the current time step.

TABLE 4.1: Example of solar radiation calculation from 4:00 to 23:00, for an April day with tropical climate in Ecuador.

Time	Solar	ω_1 Time 0	Solar	ω_2 Time 1	τ_b	Q_{sun} ($W \cdot m^{-2}$)	τ_d	Q_{dif} ($W \cdot m^{-2}$)
4:00	2.03	-149.59	3.03	-134.59	0.00	0.00	0.27	0.00
5:00	3.03	-134.59	4.03	-119.59	0.00	0.00	0.27	0.00
6:00	4.03	-119.59	5.03	-104.59	0.00	0.00	0.27	0.00
7:00	5.03	-104.59	6.03	-89.59	0.00	0.00	0.27	0.95
8:00	6.03	-89.59	7.03	-74.59	0.18	24.60	0.22	29.58
9:00	7.03	-74.59	8.03	-59.59	0.36	134.86	0.17	62.73
10:00	8.03	-59.59	9.03	-44.59	0.47	278.92	0.13	79.04
11:00	9.03	-44.59	10.03	-29.59	0.53	412.05	0.11	87.64
12:00	10.03	-29.59	11.03	-14.59	0.57	512.08	0.10	91.82
13:00	11.03	-14.59	12.03	0.41	0.59	567.10	0.10	92.77
14:00	12.03	0.41	13.03	15.41	0.60	571.68	0.10	90.93
15:00	13.03	15.41	14.03	30.41	0.59	525.90	0.10	86.32
16:00	14.03	30.41	15.03	45.41	0.57	435.12	0.10	78.58
17:00	15.03	45.41	16.03	60.41	0.53	310.33	0.11	66.82
18:00	16.03	60.41	17.03	75.41	0.46	169.59	0.13	49.05
19:00	17.03	75.41	18.03	90.41	0.35	42.60	0.17	20.57
20:00	18.03	90.41	19.03	105.41	0.17	0.60	0.22	0.77
21:00	19.03	105.41	20.03	120.41	0.00	0.00	0.27	0.95
22:00	20.03	120.41	21.03	135.41	0.00	0.00	0.27	0.00
23:00	21.03	135.41	22.03	150.41	0.00	0.00	0.27	0.00

4.3.5 Circuits Generation

To simulate the conductive heat exchange inside a building, it is possible to use an electrical analogy where each wall is expressed as a circuit between the exterior temperature of the wall and the interior temperature of the floor (Kampf and Robinson, 2007). The main idea of the electrical analogy is to connect rooms (or floors) of a building by nodes that represent wall conductivity and capacitance. The walls and roofs may be represented by many layers and could also be linked to the outside temperature. By solving the circuit network constructed, dynamic temperatures over time could be provided. In the following, with very little loss of generality, we assume each floor of a building is a single room, since the difference of temperature between interior walls of a same floor is usually less than 2° Celsius when there is no presence of internal elements that alter the temperature of the rooms individually, and that difference can be omitted for simulation purposes at urban scale.

As the main problem of the electrical analogy is that traditionally the nodes that make up the circuit must be placed manually on the model of the building (Levine, 2015), we propose a procedural technique to solve this association automatically, given a set of modular rules.

Building Circuits

Circuits are created between the outside temperature and the interior temperature for each floor of each building. Figure 4.4 represents the circuit for a single storey. In these circuits, each line represents one of the walls that is interposed between the

outside temperature and the interior temperature. The resistors represent the resistance of the material and the insulation of the wall, while the capacitors represent its inertia. However, since the buildings often have several floors, the created circuits rapidly grow in complexity and become difficult to manage. See Figure 4.5.

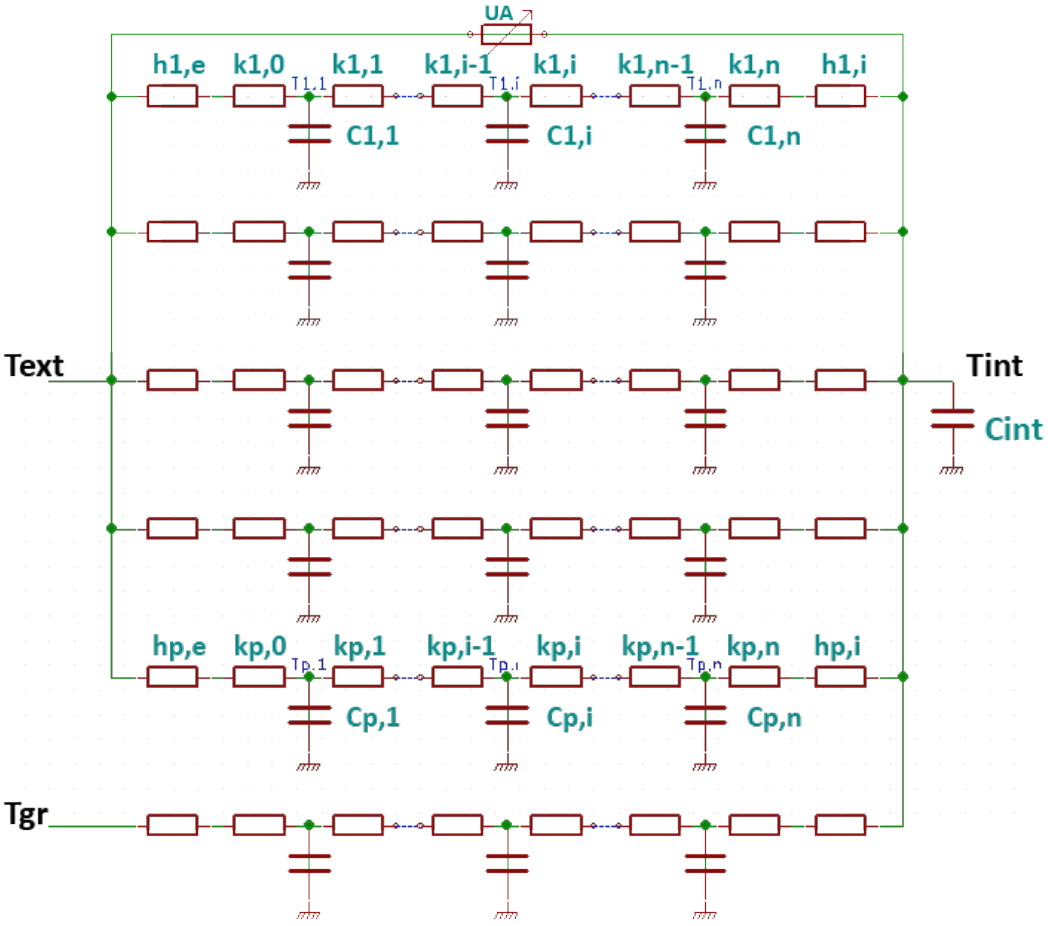

Figure 4.4. Circuit generated to represent the heat flow between outdoor and indoor temperatures in a single-storey building.

Procedural Rules

To reduce circuit complexity, we create simple modular rules to encapsulate redundant structures in the design. First, we declare the rule "wall", as shown in Figure 4.6, which consists of a series of resistances and capacitors located between the exterior temperature (T_{ext}) and the interior temperature of a building (T_{int}). In this way, the effect of conductive heat between the outside temperature and the interior temperature on the other side of the wall is simulated. It is important to mention that at each end of the circuit of the "wall" rule, specific thermal resistances (*he* and *hi*) are placed to simulate the convective effect of the heat when filtering through the wall. The "wall" rule determines the composition of the walls and allows us to alternate between several models of them according to the number of resistances and capacitors that are included in its design ($3R2C$, $2R1C$, etc.) (Fraisse et al., 2002). We have to take into account the three trivial cases for the rule "wall": The rule "wall" can represent a simple wall, but it can also be a ceiling or a floor of a storey.

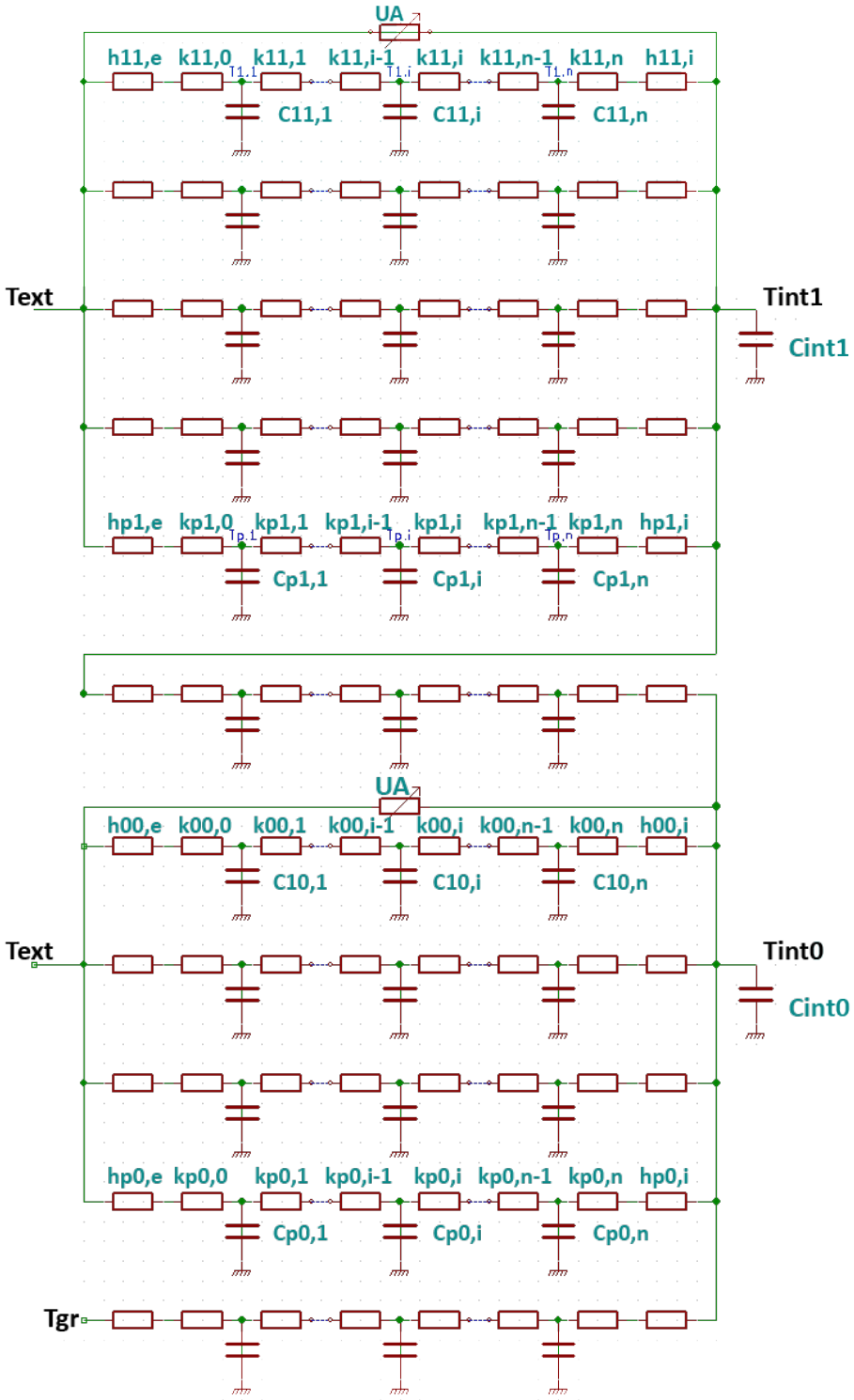

Figure 4.5. Circuit generated to represent the heat flow between outdoor and indoor temperatures in a two-storey building.

With the "wall" rule, it is now possible to create rooms. A room represents a floor, which could be a ground, top or intermediate floor, of a building. The difference is that the ground floor has its own ground, while the top floor will have the roof directly in contact with the outside. The intermediate floors will have the ground connected to the roof of the immediately inferior floor, and the same is true for the

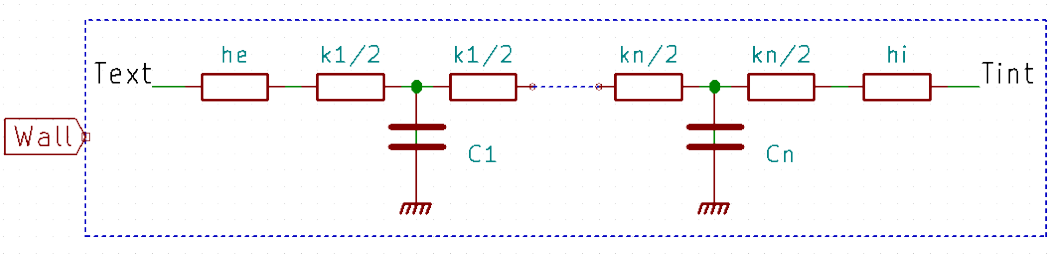

Figure 4.6. "Wall" design rule, which consist of a series of resistances and capacitors located between the exterior temperature (T_{ext}) and the interior temperature of a building (T_{int}), emulating the thermal properties of the physical materials that make up that wall.

ceiling, which will be connected directly to the immediately superior floor. Bearing all this in mind, we create another modular rule called "room", which represents the four walls of a floor with its translucent component, see Figure 4.7. In this way, the effect of conductive heat between the outside temperature (T_{ext}) and the interior temperature of the room (T_{int}) is simulated.

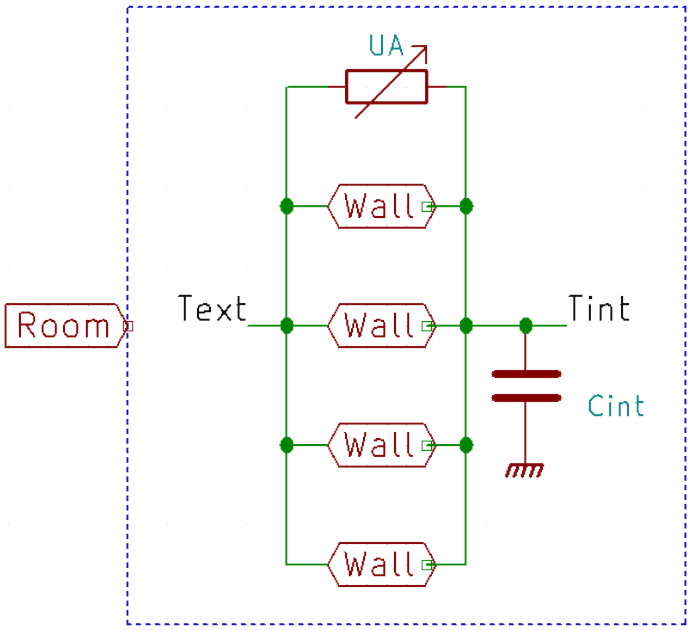

Figure 4.7. "Room" design rule, which consists of four walls located between the exterior temperature (T_{ext}) and the interior temperature of a room (T_{int}), omitting the floor and the ceiling, but taking into account the glazed part of the room as a variable resistance (UA).

With these two simple rules, it is possible to create any building. For example, a two-storey building would have, from a conceptual point of view, a much simpler design (see Figure 4.8) than the original two-storey building circuit (see Figure 4.5).

Circuit Formulation

While the electrical circuits for the buildings are generated by the procedural rules, the system must assign values to each resistance and capacitor. The resistance of a wall layer is calculated by dividing the layer thickness (e), in metres, by its thermal conductivity (λ), in $W \cdot m^{-1} \cdot K^{-1}$, and its area ($A$), in m^2, see Equation 4.13.

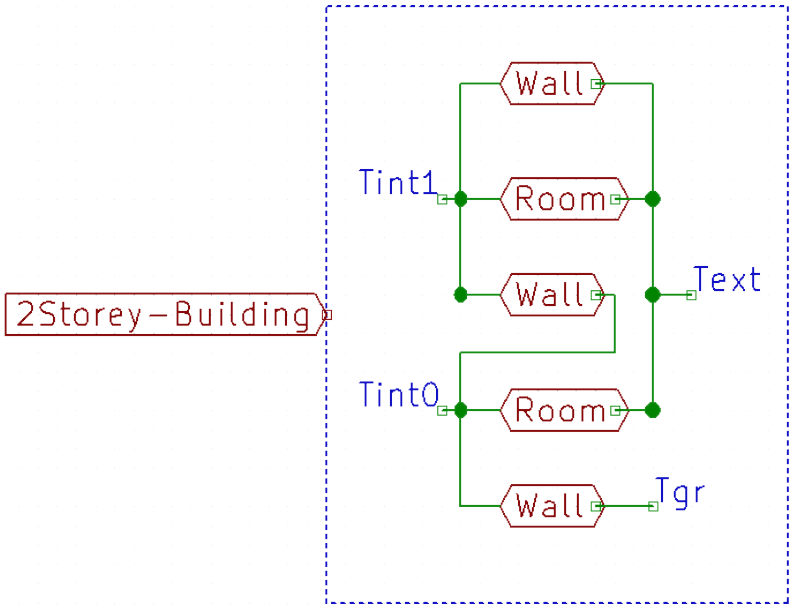

Figure 4.8. A two-storey building modelled using the "Room" and "Wall" rules. Using our procedural rules, the circuit generated from a building is much more understandable and the nodes are placed automatically, for later calculation..

$$k = \frac{e}{\lambda \cdot A} \tag{4.13}$$

The capacitance of a wall layer is calculated by multiplying the layer's mass (m) in kg by its thermal capacity (c_p) in $J \cdot kg^{-1} \cdot K^{-1}$, see Equation 4.14.

$$C = m \cdot c_p \tag{4.14}$$

In addition to assigning the resistances and capacitors of each wall, a heat flow must also be established between the outside temperature of the wall and the interior temperature of the floor. This is expressed as a potential difference between both points of the circuit. The heat flow (Q_{cond}) of a wall is calculated by dividing the difference between its outside and inside temperatures by its total resistance (R_{wall}). This total resistance of the wall is the sum of all the thermal resistances (k), see Equation 4.15.

$$Q_{cond} = \frac{T_1 - T_2}{R_{wall}} \tag{4.15}$$

The symbols that appear in the circuits are listed in the List of Symbols.

Converting Energy to Temperature

Once we have calculated all the radiation that reaches a surface i, either from the sun, the sky, other nearby surfaces or urban elements, see Equation 4.12, it is possible to obtain the temperature of that surface at any given moment with Equation 4.16, where Δt is the time step of the simulation, conveniently chosen so that the simulation converges, and l is the cell size of the subdivisions of the buildings. This heat flow becomes a change in the outside surfaces temperature, and will also have an

impact on the interior temperatures of the corresponding building after the conduction step.

$$T_i(t+\Delta t) = T_i(t) + \frac{\Delta t}{l \cdot c_p^i \cdot \rho_i} \cdot (\alpha \cdot Q_{sun}^i - Q_{sky}^i - Q_{air}^i + Q_{sur}^i + Q_{other}^i) \tag{4.16}$$

Circuit Resolution

The main algorithm is programmed in Python. First, the algorithm iterates over the planes that compose each building in the scene (each plane can be a wall, a floor or a ceiling) and, according to its position and its interconnection with the other floors of its building, detects whether it is a top, bottom or intermediate floor so as to assign each with the corresponding procedural rule that will represent it in the circuit. Then, the Python library *Ahkab* (Venturini, 2013) is used to create the circuit from the procedural rules previously assigned. Once the circuit is built, the library's solver is invoked and the intensity and potential of each point in the circuit are obtained, thus allowing the values required for the interior and exterior of each wall to be obtained. Finally, we iterate over the time step established and the calculations are carried out to update the temperatures accordingly.

4.4 Results and Discussion

In this section we present four case studies computed with our technique, each one designed with its own specific objective. The objective, data and models used for each case study are presented here, along with the procedure followed to obtain the corresponding results. We also present a study of the sensitivity of the procedural technique in response to the change of parameters and a discussion about the results where we list the strengths and weaknesses that this technique presents.

4.4.1 Case Study 1: Accuracy Validation

This first case study was developed to validate whether the entire design and formulation of the technique is able to achieve results close to real-case measures. As this case study was based on a real urban neighbourhood, we used real measurements and environment conditions as input data for our simulator.

We used a study carried out in the city of Bayonne (France), where thermal measurements on the exterior walls of the buildings had been taken on the Rue des Tonneliers (Beckers et al., 2017). In this study, measurements of air temperature were taken from 4:00 in the morning until 23:00 and, using thermal cameras, the exterior temperature of four different street walls was measured.

First, the real 3D scenario was modelled following the map data that accompanies the study, see Figure 4.9. The model consists of four blocks of buildings, each between four and five floors high located along an urban canyon, see Figure 4.10, *a*. As the study also details the properties of the materials that make up the walls of buildings, it was possible to adjust the capacitors and resistances of each layer of material so that they coincided with the real case. The walls were generated using the $3R2C$ wall rule and the list of materials and their properties can be seen in Table 4.2.

For this simulation, the parameters were adjusted manually to match the real ones that were measured during the study (Aguerre et al., 2019), on April 23, 2017

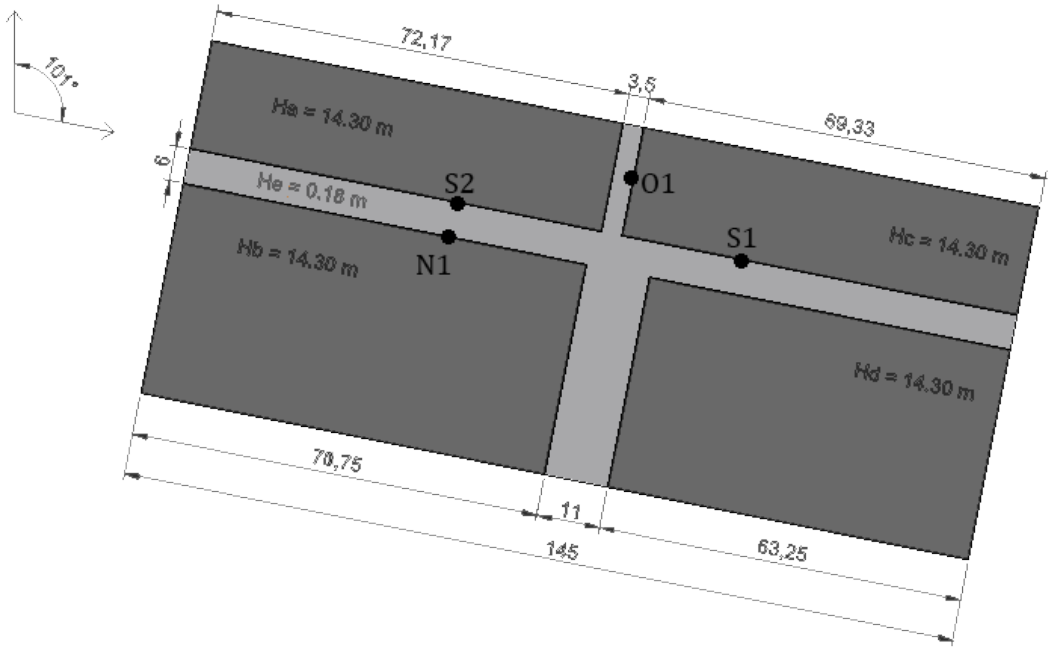

Figure 4.9. Map of the studied area in Bayonne.

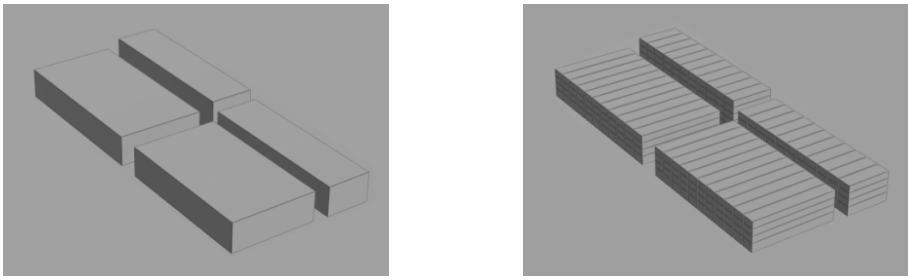

(*a*) Box model. (*b*) Subdiv. level 3 model.

Figure 4.10. 3D models procedurally recreated from the map of the Bayonne case study area, with different level of subdivisions.

from 4:00 to 23:59, every half hour. This data includes ambient air temperature and ground temperatures, in degrees Celsius, as well as the direct and diffuse radiation from the sun, in Wm^{-2}. Note that in this case study, the extraterrestrial solar radiation equation was not used because we had real measured data for the solar energy reaching the surfaces at each time step. Table 4.3 shows the physical parameters of the environment.

For this first case study, the evolution of the temperature of four specific walls was simulated, two facing south ($S1$ and $S2$), a third facing north ($N1$), and a fourth facing west ($O1$), see Figure 4.9. The simulation took 21.62 seconds to complete. Our initial simulated results were not very accurate compared to the actual measured data because, since the 3D model is so simple, the surfaces to be simulated are very large and that introduced an error due to the enormous size of the areas, and the large area represented by each SVF value.

To increase the level of accuracy, the model was improved by subdividing it increasingly into smaller primitives, simulating the case study at each iteration to verify its improvement. We observed that, the more we subdivided the model, the greater the accuracy obtained was. However, the computational cost also increased

TABLE 4.2: Material parameters for the simulation of the case study.

Material	Thermal conductivity (W/mK)	Thermal capacity (J/kgK)	Density (kg/m^3)	Thickness (m)
Concrete	1.75	920	2,200	0.2
Polyester	0.04	1,380	30	0.2
Plaster	0.35	800	1000	0.1

TABLE 4.3: Environmental parameters for the simulation of the case study.

Air density $(kg \cdot m^{-3})$	Air heat capacity $(J \cdot kg^{-1} \cdot K^{-1})$	Air infiltration $(vol \cdot h^{-1})$	Q_{other} $(W \cdot m^{-2})$
1.413	1,005	0.25	0.0

since there were more buildings in the scene and, therefore, also more circuits to be solved at each time step of the simulation. Figure 4.10, *b* shows the same 3D model but with the buildings partitioned so that they work with the same shape but with smaller surfaces. Figure 4.11 shows the results of this new simulation, compared with the real data. This simulation took 14.04 minutes to complete.

The model was progressively subdivided a total of four times. All the data related to each model used in this case study as well as their simulation times is presented in Table 4.4. From our analysis, we consider that "Subdivided level 3" is the most convenient model and, although "Subdivided level 4" is more accurate, we think that the little improvement in accuracy does not compensate the increase in simulation time. Accuracy has been computed by calculating the relative error accumulated over the four simulated temperatures throughout the calculation, with respect to the corresponding real measured temperatures. This results in a total error that, as observed, is inversely proportional to the number of subdivisions of the urban 3D model, see Figure 4.12. This error is also directly proportional to the subdivision size l used in the Import Geometry step presented in Section 4.3.2.

TABLE 4.4: Geometry, timings and total error for all the models in the Bayonne case study. The time to calculate the SVF and FF during the first run of each model is included in the pre-processing times.

3D Model	Number of Primitives	Pre-processing time (minutes)	Simulation time (minutes)	Total Error (%)
Box model	25	0.37	0.36	14.65
Subdiv. level 1	90	1.23	1.31	13.22
Subdiv. level 2	446	6.23	6.31	12.72
Subdiv. level 3	980	13.13	14.04	11.89
Subdiv. level 4	2,883	47.54	46.94	11.42

To evaluate the results graphically, Figure 4.13 shows three comparisons between the real and the simulated thermographies to demonstrate the accuracy of the simulation technique.

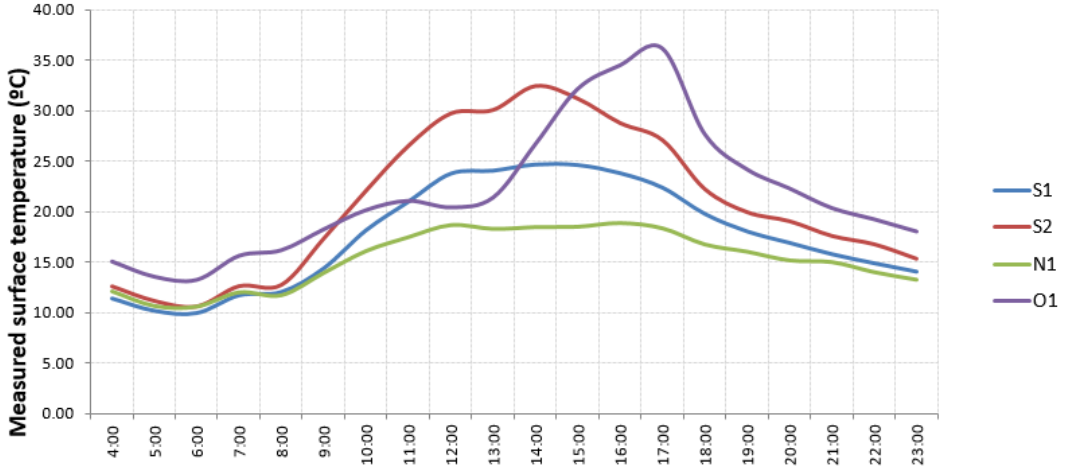

(*a*) Real data measured with thermal cameras on the four walls to be studied.

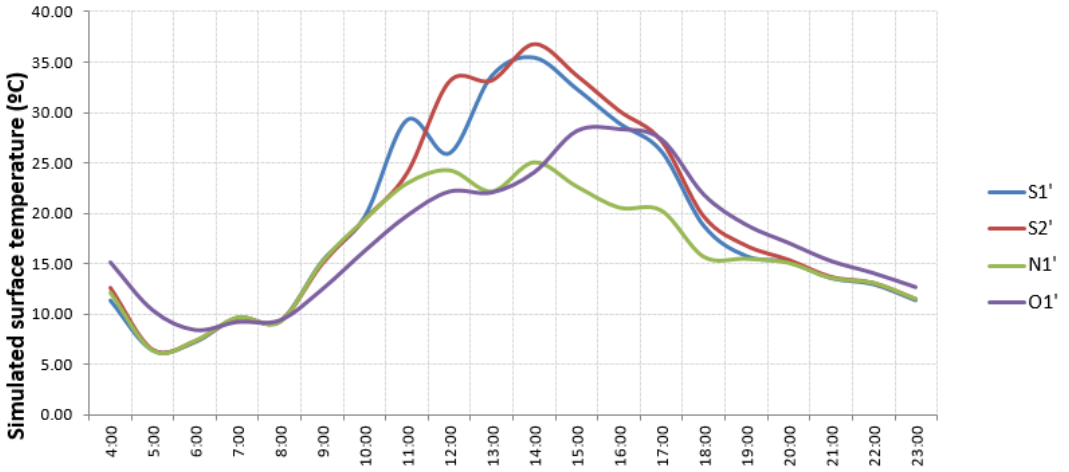

(*b*) Simulated data on the same four walls of the 3D model.

Figure 4.11. Results of the first simulation. On top, the real data measured with thermal cameras on the four walls to be studied. On bottom, the simulation on the same four walls with the new 3D model.

Over time, these differences fluctuate because of inaccuracies in the simulation caused by different factors. The first is that in the simulations, if the sun partially radiates a surface, the system considers that the surface is irradiated in all its extension. That said, this first imprecision can be corrected by increasing the subdivision size l in the 3D model and, therefore, having more primitives in the scene.

4.4.2 Case Study 2: Simulation with geometric and climatic data

This second case study was designed to use the simulation technique without the help of any real data.

The 3D model was procedurally generated from the map of a Barcelona neighbourhood, in Spain, obtained from the coordinates $41.40°N, 2.12°E$ in *OpenStreetMap* through the application *JOSM*. The area in question presents a group of buildings on Carrer Dalmases, see figure 4.14. The material configuration of the walls of the previous study case were maintained, whose properties can be seen in table 4.2. General physical parameters were maintained too and they are presented in table 4.3. About

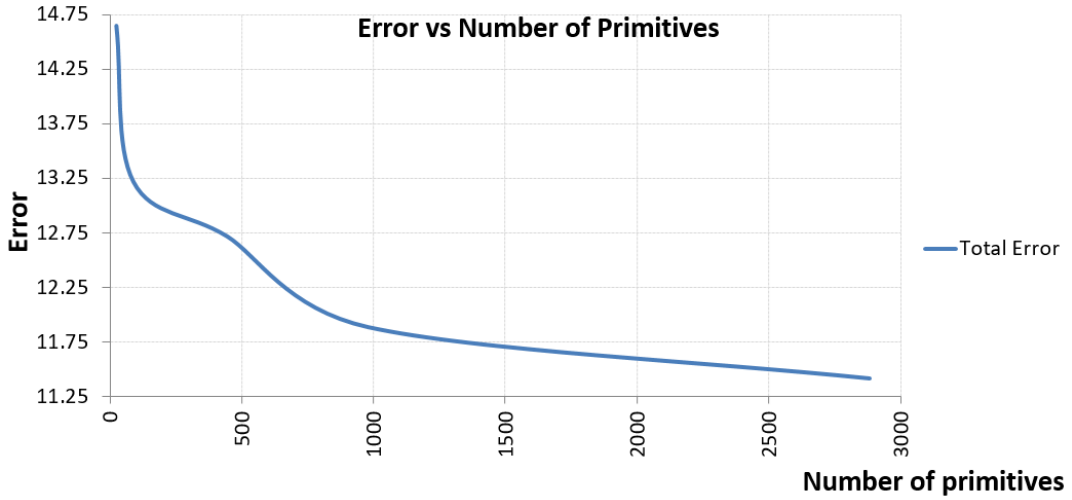

Figure 4.12. The total error of the simulation technique shows a relationship inversely proportional to the number of primitives.

the initial temperature of the buildings, the interior temperatures were initialized to 15° C and those of the exterior surfaces to 12° C. The temperatures of the air and the dew were obtained from a climatic data file of a weather station and the temperature of the ground was adjusted constant to the average of temperature of the air of the day plus 2° C. Note that in this case study, the solar path was calculated from the coordinates and the time zone of the study area ($UTC + 2$) in order to obtain, at each time step, the solar energy received by the exterior surfaces of the buildings.

The simulation was carried out by adjusting the initial date to April 23, 2018 between 4:00 and 23:59 and, as in the previous case study, several 3D models with different subdivision sizes were procedurally created. Table 4.5 shows these models properties.

TABLE 4.5: Geometry and timings for our all the models of the Barcelona case study. Timing to calculate SVF and FF the first run of each model is included in pre-processing time.

3D Model	Number of Primitives (buildings)	Pre-processing time (minutes)	Simulation time (minutes)
Box model	61	0.82	0.87
Subdiv. level 1	226	3.19	3.25
Subdiv. level 2	1,326	18.43	19.90

The model chosen as optimal was "Subdivided model 2" since the other models presented noise in their plots because their l value was too low and therefore the surfaces on which their buildings were divided were very large. Some captures of its thermal evolution are included in Figure 4.15 to observe the thermal behaviour of the buildings. The simulation took 19.90 minutes to complete.

4.4.3 Case Study 3: Scalability Demonstration

This third case study is designed to test our technique and its use by only using climatic data, geographic information and the physical properties of the materials

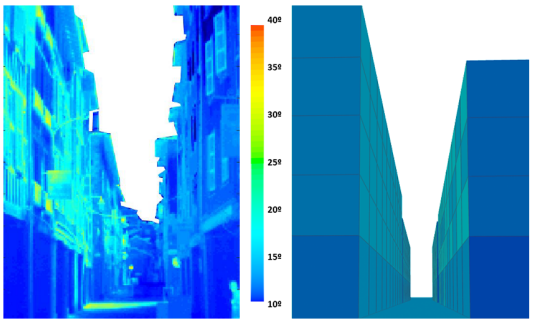

(*a*) Bayonne case study at 10:00

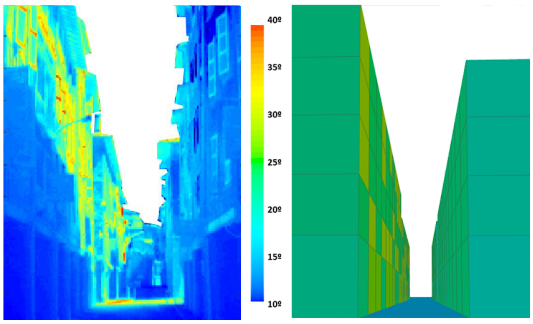

(*b*) Bayonne case study at 13:00

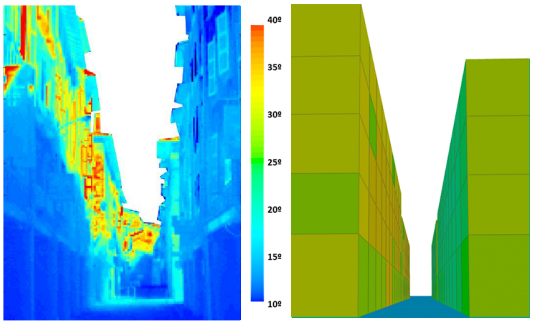

(*c*) Bayonne case study at 16:00

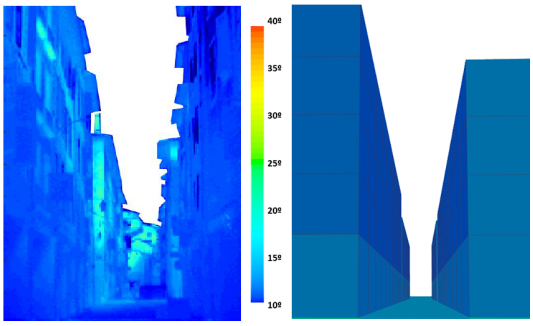

(*d*) Bayonne case study at 19:00

Figure 4.13. Graphical comparison at different times of the day of the real measurement from a thermal camera on the left and the simulated visualisation on the right.

that make up the buildings in the area to simulate. In addition, as we worked with an urban environment, the scalability of the procedural simulation technique is shown.

The 3D model used in this case study is an area of Vienna (Austria), see Figure 4.16. As we worked with a larger model, in this case study it was decided to only make a subdivision per building, so that each building was divided into a

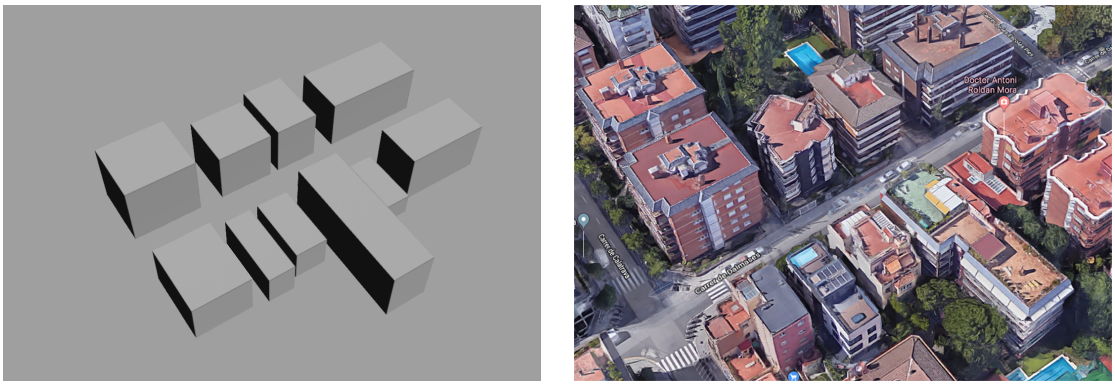

Figure 4.14. 3D model procedurally recreated from the map of the Barcelona case study area.

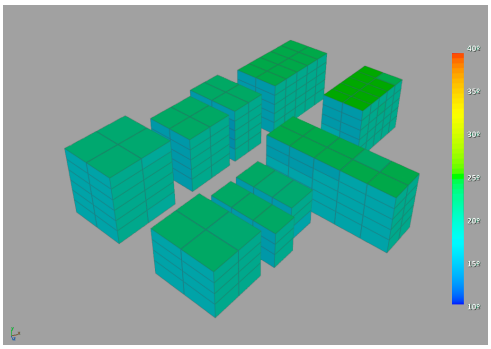

(*a*) Barcelona case study at 10:00

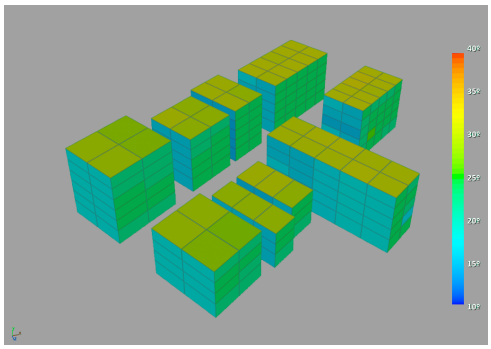

(*b*) Barcelona case study at 12:00

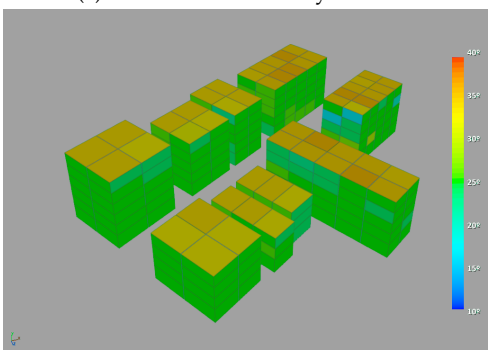

(*c*) Barcelona case study at 14:00

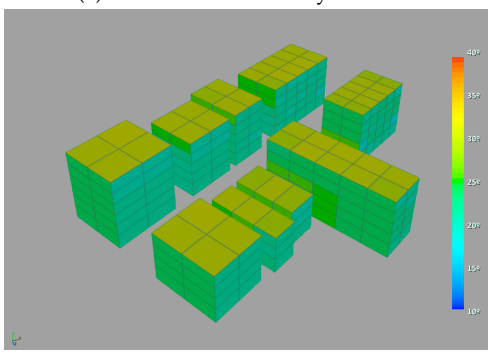

(*d*) Barcelona case study at 17:00

Figure 4.15. Visualizations of the Barcelona case study simulation.

given number of floors. The details of the models are shown in Table 4.6. A climate data file from Vienna was used and the simulation date was adjusted to August 16, 2018, from 04:00 to 23:59. The temperatures were initialised at 15° C for the interior temperatures and 12° C for the exterior surfaces, and the ground temperature was maintained at the average temperature of that day plus 2° C. The parameters of the materials (see Table 4.2) and the general physical parameters (see Table 4.3) were maintained from the previous case study. Finally, the coordinates were adjusted to $48.21°N, 16.36°E$ in the simulator interface.

Using this input data, the simulation took 24.79 minutes to complete and Figure 4.17 shows several visualisations of the thermal evolution of the buildings.

Performing simulations with large 3D models not only simulates the thermal

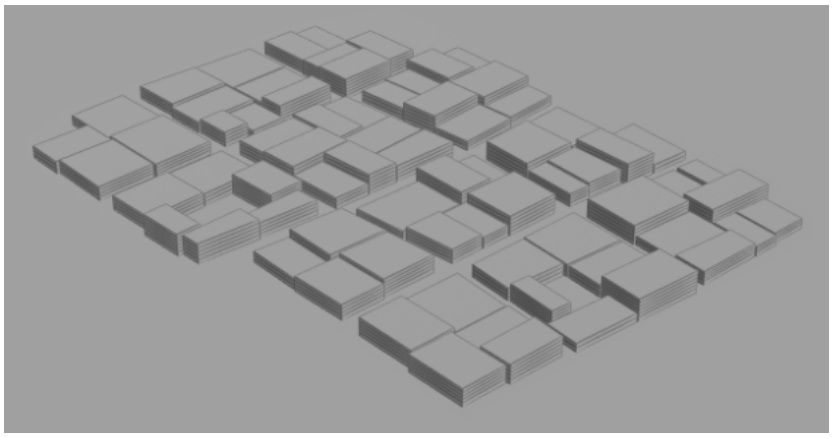

Figure 4.16. 3D model procedurally recreated from the map of the Vienna case study.

TABLE 4.6: Geometry and timings for the model from the Vienna case study. The time required to calculate the SVF and FF from the first run of the model is included in the pre-processing time.

3D Model	Number of Primitives	Pre-processing time (minutes)	Simulation time (minutes)
Subdiv. level 1	1,549	21.55	24.79

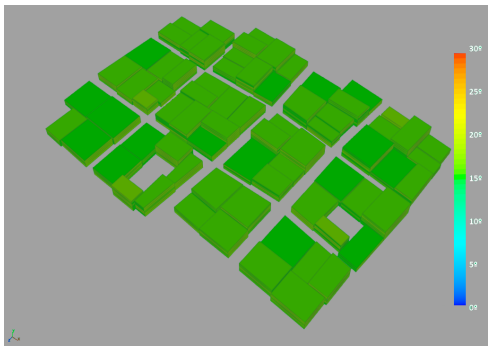

(*a*) Vienna case study at 10:00

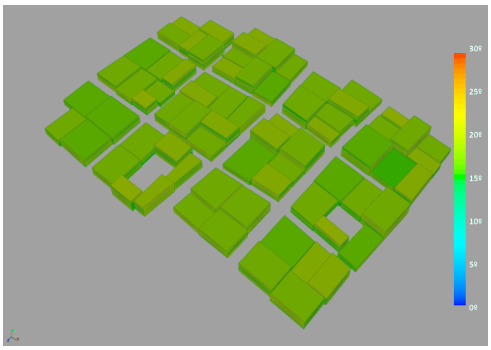

(*b*) Vienna case study at 12:00

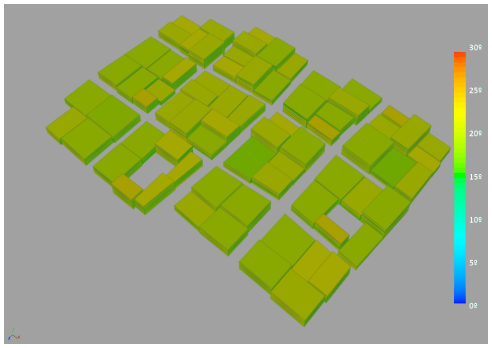

(*c*) Vienna case study at 14:00

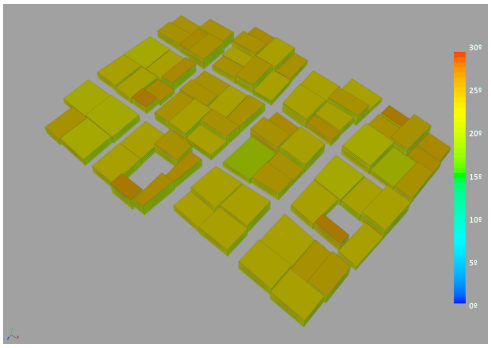

(*d*) Vienna case study at 17:00

Figure 4.17. Visualisations of the Vienna case study.

behaviour of an urban environment, but also makes it possible to analyse the behaviour of some buildings in particular and compare them with their environment.

Figure 4.18 shows the evolution of the average exterior temperature of the coldest and warmest building throughout the simulated period, as well as the average temperature of the entire urban environment at each time step.

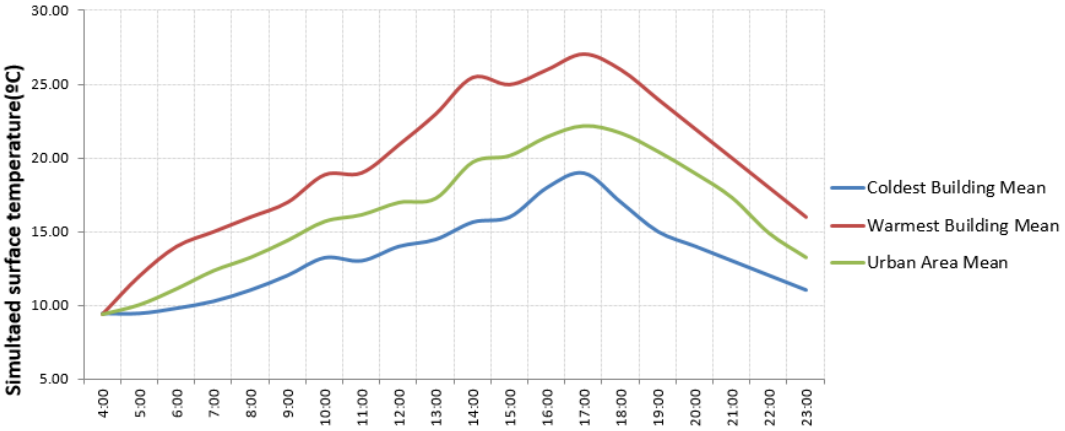

Figure 4.18. Evolution of mean exterior temperature of the warmest building, the coldest building and the entire urban environment.

4.4.4 Internal Temperatures and Procedural Rules Exploitation

This final case study was designed to show how, by playing with the procedural rules of the composition of the walls, successive simulations on the same 3D model are possible, as well as being able to study how the changes affect the thermal behaviour of several buildings. The 3D model used is simple, composed of only three small buildings located side by side in a line, see Figure 4.19. However, between simulations, parameters such as the height of the buildings, the width of the walls, the presence of gaps and windows in the façades and even the number of layers of material that make up the walls and their physical properties, were changed.

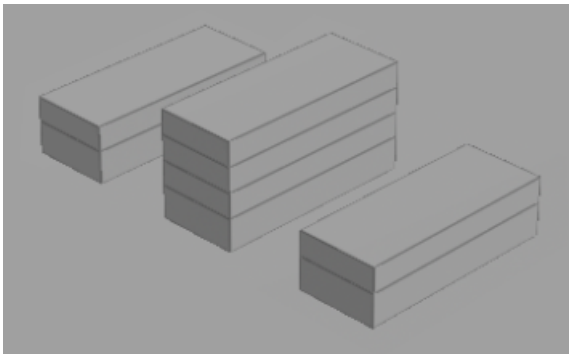

Figure 4.19. 3D model created to test the procedural rules of the technique, showing different parameters for the rules.

For this case study, the coordinates of the buildings are $41.40°N, 2.12°E$, and the climate type was set to "mid-latitude winter", with an altitude of 0 meters. The simulation period was adjusted to January 19, from 4:00 to 23:00. The material parameters were the same as those used in the previous case studies (the $3R2C$ wall rule), and can be seen in Table 4.2. Figure 4.20 shows the evolution of the interior temperatures of each floor of the three buildings over the simulated time period. The interior temperatures of the buildings have been initialised at 15° C, despite the fact that the

average air temperature is much lower. This initial setup is deliberate and aims to make the change in thermal behaviour more clearly visible for illustration purposes as a result of altering the procedural rules of the simulator.

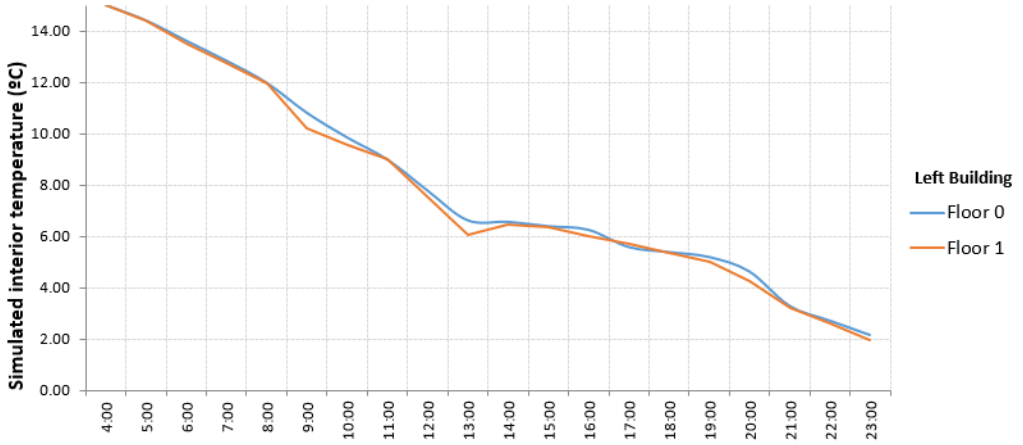

(*a*) Evolution of the interior temperature for the left building.

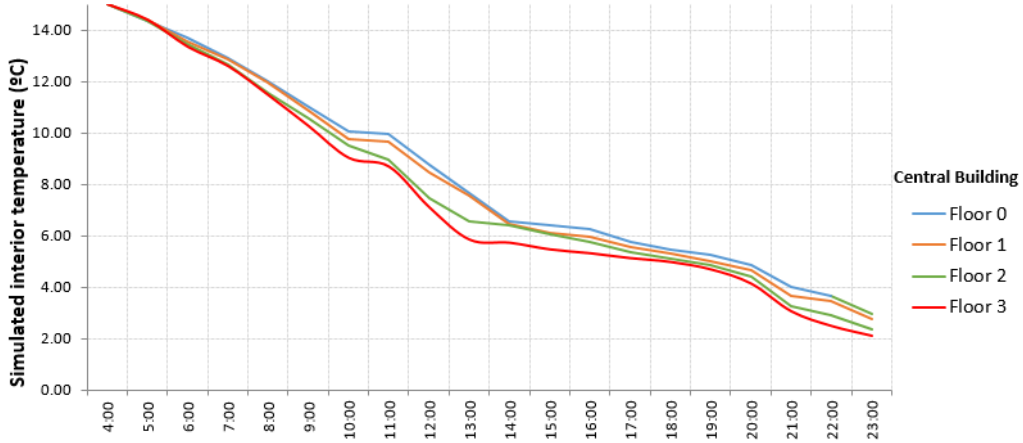

(*b*) Evolution of the interior temperature for the central building.

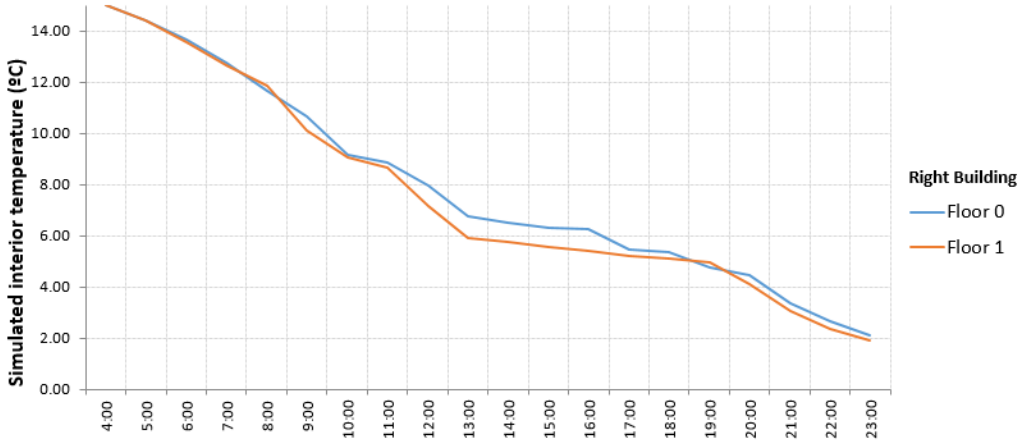

(*c*) Evolution of the interior temperature for the right building.

Figure 4.20. Results of the first simulation where the 3*R*2*C* wall rule was applied.

The same experiment was repeated with the same parameters, except for the wall rule used, where a $2R1C$ wall rule was applied (eliminating the concrete layer), and making the walls up with only two layers of material that isolate the interior temperature of the rooms from the temperature of the façade and the ambient temperature. In Figure 4.21 we can see how the interior temperatures of the buildings become significantly more sensitive to the outside temperatures, conserving less heat.

Later, the same experiment was repeated using the original parameters but this time procedurally changing the geometry of the 3D model. First, the number of floors in two of the buildings was increased to determine how this would affect the thermal behaviour of the urban environment, see Figure 4.22, *a*. As such, a slight difference in the internal temperatures of the buildings can be detected, see Figure 4.23.

To show how the thermal behaviour is affected by the glazing of the walls, a final experiment that maintained the parameters from the first simulation but used a slightly different 3D model with windows and openings on the exterior walls of the central building, was carried out, see Figure 4.22, *b*. The openings affect the variable resistance that simulates the heat transmittance in translucent surfaces and, therefore, the interior of the central building becomes more sensitive to sunlight and the outside temperature of the air, see Figure 4.24, whereas the other buildings present almost identical results to those in the first experiment.

4.4.5 Discussion

The case studies demonstrate a series of qualities this simulation and visualisation technique has. First, the case study presented in Section 4.4.1, through a balanced compromise between computational costs and the level of accuracy level of the calculations, shows that it is possible to perform a credible simulation of thermal behaviour in an urban environment based on climate data and geometry. This experiment refines the calculation system to achieve credible results when comparing the simulation with real measured data. In this way, the smaller the subdivision size l of the 3D model is, the more accurate the results are, but the simulation is also longer.

Second, the case study presented in Section 4.4.2 shows that it is possible to perform a simulation by recreating a real urban environment (generating the buildings procedurally) and its climatic data. The thermal evolution can be visualized thanks to the procedural technology that is responsible for processing the geometry and generating the circuits in the buildings to be used as the electrical analogy in the calculations. The case study presented in Section 4.4.3 demonstrates the applicability of our method to an urban scale.

Third, the case study presented in Section 4.4.4 shows that this technique allows the interior temperatures of each floor in an urban environment to be simulated and also visualised. This experiment presents another function of the technique and shows that it is possible to analyse the thermal behaviour of a building in relation to the number of layers of material in its walls and the physical properties of those materials.

As a result of these case studies and their analyses, we can list the following strengths derived from using our procedural simulation and visualisation technique:

- The technique allows the thermal behaviour of urban environments to be simulated and visualised.
- The pre-processing of the 3D model allows the technique to work with virtually any type of city, regardless of its topography, and is also able to simulate cities with different altitudes.

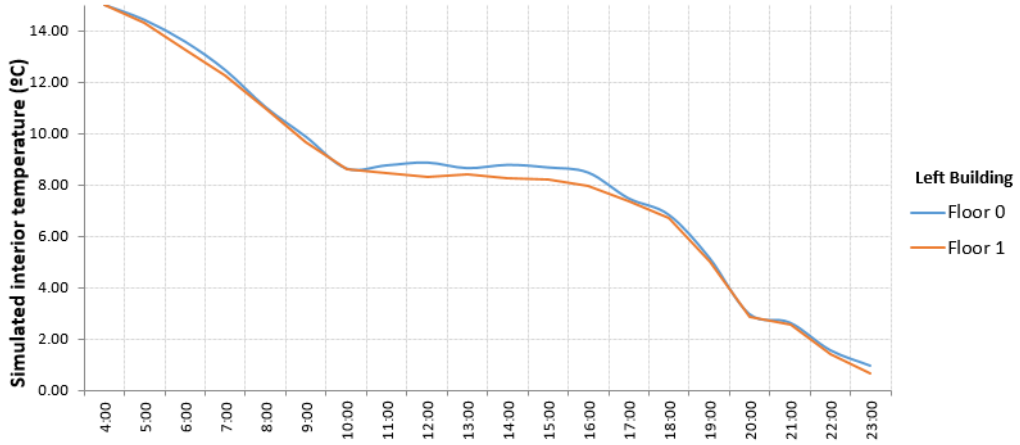

(*a*) Evolution of the interior temperature for the left building.

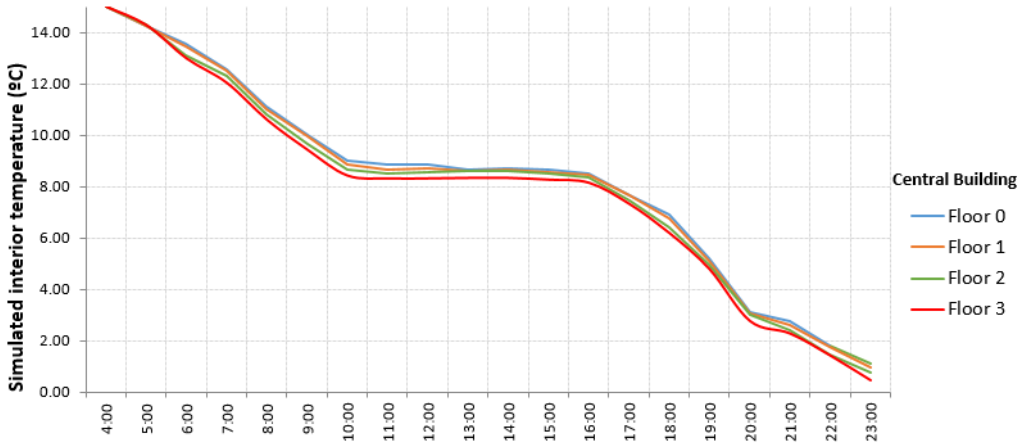

(*b*) Evolution of the interior temperature for the central building.

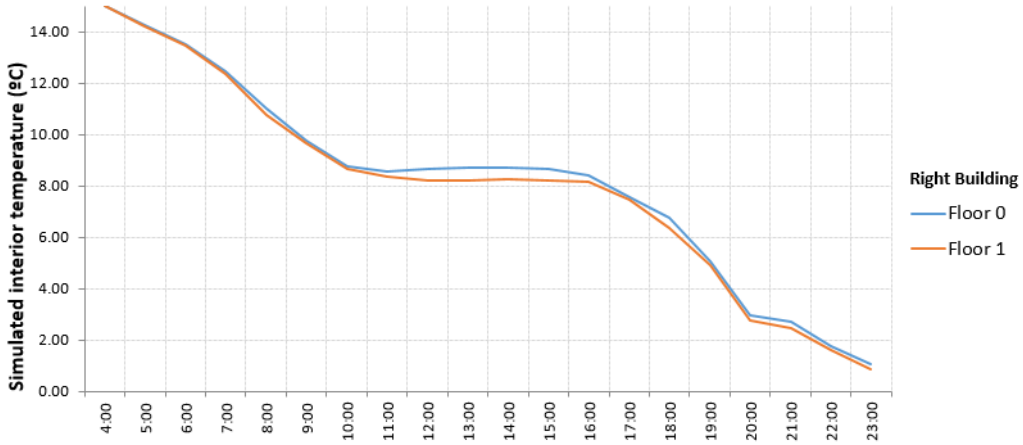

(*c*) Evolution of the interior temperature for the right building.

Figure 4.21. Results of the first simulation where the 2*R*1*C* wall rule was applied.

- The procedural technology allows buildings with different heights, wall composition and presence of windows, to be simulated simply by changing the corresponding parameters.

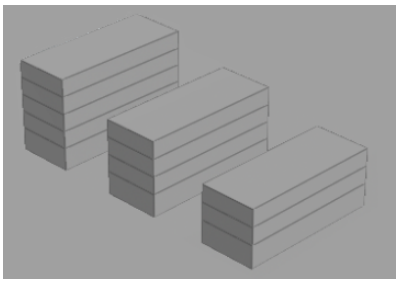

(*a*) Varying the height of the buildings.

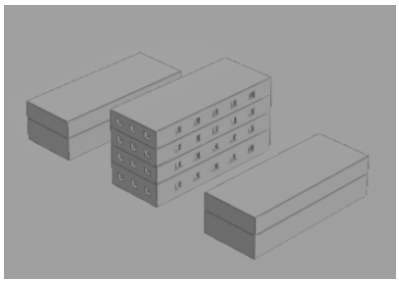

(*b*) Varying the presence of windows.

Figure 4.22. 3D models created to test the procedural rules of the technique, varying the height and the presence of windows in the buildings.

- The technique allows the evolution of the temperatures to be visually monitored by colouring the buildings at each step of the simulation.
- The technique allows the subdivision size of the model to be adjusted to achieve the desired balance between precision and computational time.

The weakness derived from using our procedural simulation and visualisation technique is that there are still not enough field studies with real measurements of interior temperatures of buildings to perform comparisons. At the moment, we can perform comparative experiments between different configurations of materials, but we do not have the degree of reliability the other aspects of the technique have.

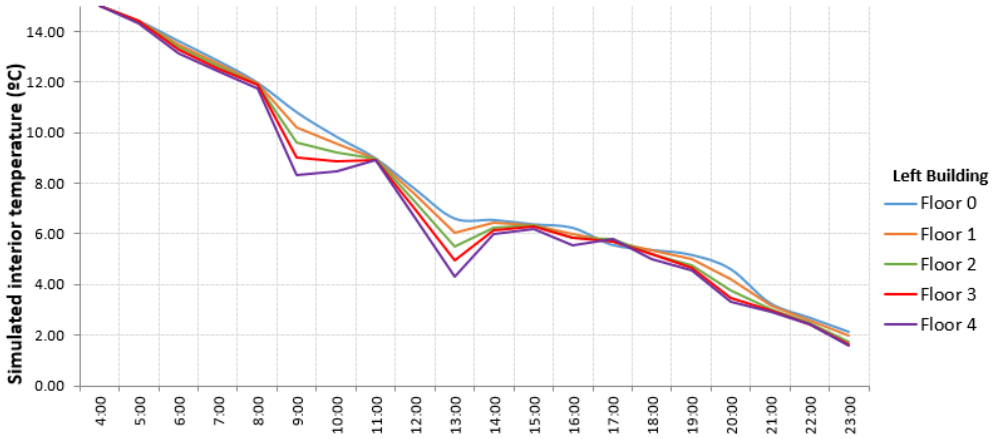

(*a*) Evolution of the interior temperature for the left building.

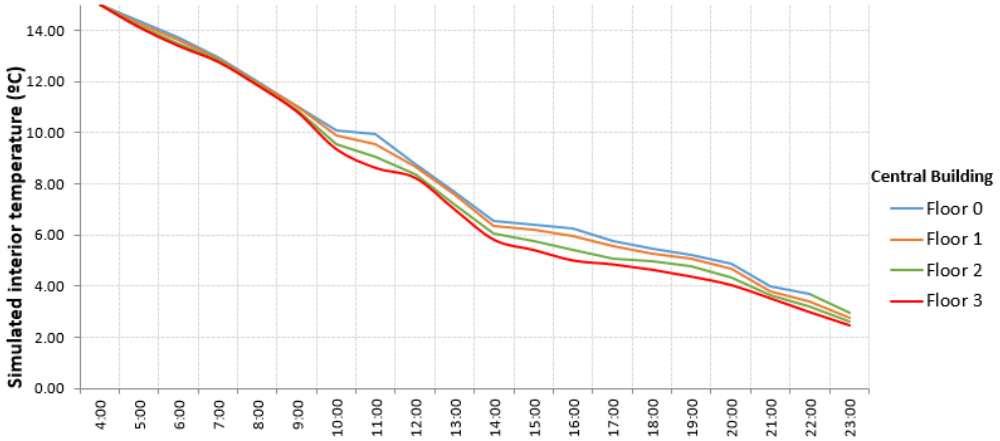

(*b*) Evolution of the interior temperature for the central building.

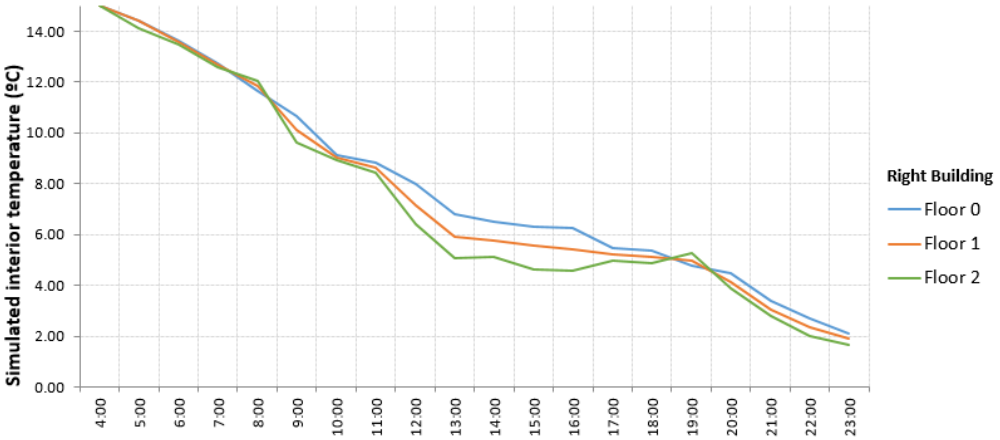

(*c*) Evolution of the interior temperature for the right building.

Figure 4.23. Results of the third simulation where the height of two buildings has been changed.

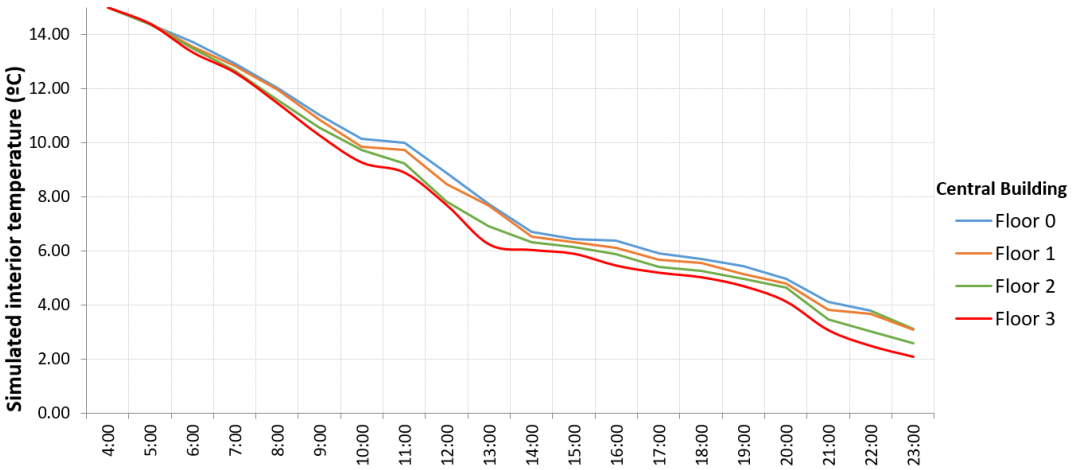

Figure 4.24. Results of the fourth simulation where the central building has more windows.

Chapter 5

A Level-of-Detail Technique for Urban Physics Calculations in Large Urban Environments

5.1 Introduction

The study of urban physics in order to explain physical behaviours of an entire city involves the compilation and treatment of large volumes of data. Nowadays it is possible to have access to a 3D model of a real urban area, or to generate it procedurally by reconstructing it geometrically from its physical 2D map. But only the complexity and the amount of geometry of this class of 3D models presents a difficulty when treating them in order to perform physical simulations and study their behaviour under certain phenomena or circumstances.

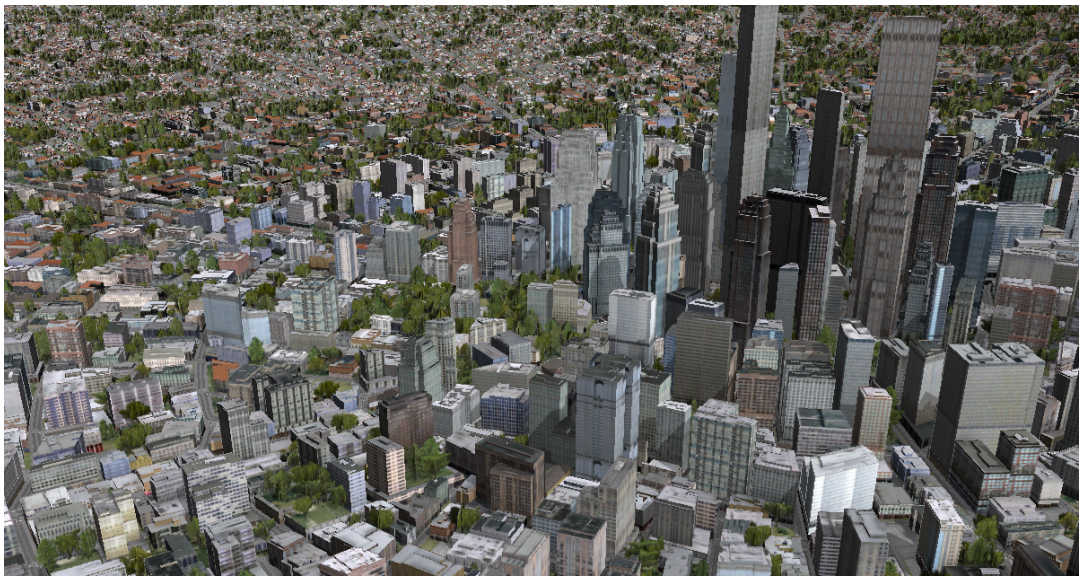

Figure 5.1. An example of a complex urban landscape where thermal simulation can be time consuming.

In Chapter 4, a procedural technique was presented to simulate the thermal behaviour on a large urban environment while keeping simplicity and accuracy. Users set the level of precision with which they want to work and the technique allows to simulate different case studies by changing the input parameters, both physical and structural. Besides, as can be seen in the results presented in Chapter 3, there is a direct relationship between the computational cost and the amount of geometry to

be processed in the 3D model with which we work. As a result of this direct relationship, if we want to perform a complex simulation in a very large urban environment, the cost in virtual memory and simulation time may be unsustainable at some point. Thus, this chapter presents a solution to this unsustainability.

The first time the problem of the amount of geometry to be processed was confronted, in Chapter 3, it was decided to implement a Level-of-Detail technique that decoupled an entire 3D city into smaller subsets named "viewcells", in order to be able to treat them more efficiently. In that case, the decoupling was performed to massively measure the amount of visible sky in areas of an urban environment without processing all the geometry present in each calculation. This technique was based on the fact that, to calculate the sky view factor in an urban environment, it would rarely be necessary to process the enormous amount of geometry that makes up a complex 3D model of a large city. The same principle can be applied to the problem of thermal simulation. In a large 3D city, simulating the thermal behaviour at a specific point of the model will have a greater contribution of the surrounding geometry than the furthest one. So our proposal is to approach the problem in the same way as in Chapter 3, decoupling the large urban environment into smaller viewcells and using a LoD technique with impostors to replace the geometry that will be omitted in each simulation.

5.2 Material and Methods

The main objective is to reduce the computational cost when we need to simulate, with a certain degree of accuracy, the thermal behaviour of a specific area within a large urban environment. To achieve this objective, as in the original technique presented in Chapter 3, given a large city, we superimpose a regular grid, and we identify all the buildings inside each grid cell. Then, for each cell, we classify the whole city geometry into three sets: the geometry associated to the cell, the geometry next to that cell and the rest of the other geometry in the city.

The electrical analogy is used and the circuits are generated in each buildings present in the urban environment. The circuits corresponding to buildings within the current viewcell are generated in a standard way, while the circuits of the most distant buildings are simplified versions to reduce the computational cost of the simulation. This is explained in detail in Section 5.2.2.

The impostor method presented in Chapter 3 is used, so that when ray casting is used to calculate the SVF, the FF or the solar radiation from a specific position in the city, the rays must collide first against the geometry and then against the environment map in order to take into account all the original geometry of the scene.

5.2.1 Thermal simulations

The changes generated by joining the two techniques involve a profound modification of the original thermal calculation algorithm. The new algorithm is described following the procedure presented in Algorithm 3. First, the geometric model of the urban environment is loaded from a file. This file can contain any type of urban element, because the presented technique only deals with its geometry, without discriminating its nature. Then, a grid appears over the top-view of the 3D model, allowing the user to adjust the cell size, and with this, its accuracy.

Next, a grid cell (the viewcell) must be chosen, thus determining in which region of the urban environment the thermal simulation takes place. Only the geometry

Algorithm 3 Procedure to simulate the thermal behaviour

```
procedure SIMULATE(cellGeo, farGeo, cellEnvMap, simTime, timeStep)
    local variables
        circuitsIn                  //circuits inside the viewcell
        circuitsOut                 //circuits outside the viewcell
        t                           //current simulation time
    end local variables
    IMPORTGEOMETRY(cellGeo)
    CALCULATEVIEWFACTORS(cellGeo, cellEnvMap)
    circuitsIn ← CIRCUITSGENERATION(cellGeo, temperatures)
    circuitsOut ← CIRCUITSGENERATION(farGeo, temperatures)
    PARAMETERSSETTING( )
    t ← 0
    while t < simTime do
        RADIATIVEPASS(cellGeo)
        CONDUCTIVEPASS(circuitsIn, circuitsOut)
        TEMPERATURESUPDATE(circuitsIn, circuitsOut, cellGeo)
        VISUALIZATIONUPDATE(cellGeo)
        t ← t + timeStep
    end while
    EXPORTTOCSV( )
end procedure
```

of the designated viewcell plus the neighbouring $N \times N$ cells is kept, where N is also a parameter adjustable by the user. With all the unselected geometry in the previous step, an environment map composed by a panoramic photograph of the geometry beyond the designated $N \times N$ zone is generated. After these two elements are determined (i.e., the geometry to keep and the environment map), the method is ready to perform the thermal simulation.

The thermal simulation takes as input the geometry selected for a given cell (cellGeo), its corresponding environment map (cellEnvMap), the geometry unselected for the given cell (farGeo), the simulation time (simTime) and the time step of the simulation (timeStep).

When a ray casting technique is used to determine visibilities between the geometry of the urban environment, if the ray does not hit the city geometry, we check the intersection against the projected geometry of the environment map. In this way, the impostor technique is applied to the calculations of SVF, FF and solar radiance.

5.2.2 Model simplification

As we showed in Chapter 3, the simplification of the model is implemented through the use of the impostor technique. However, the LoD technique we consider in this chapter not only consists of replacing the far geometry to the observation point with an environment map that represents it in its place. Unlike when we used the impostor to massively measure SVF from a single area of a large urban environment, simulating the thermal behaviour involves calculating the interactions between all the buildings of the city at each time step, updating their temperatures. For this, once the partitioning of the urban environment has been done, each building is associated with a data structure that identifies it and that stores a global temperature. In this way, all the buildings of the current viewcell generate their circuits with the

standard procedure presented in Chapter 4, while their neighbouring buildings use simplified circuits, simulating buildings of a single floor, see Figure 5.2. However, for every building whose geometry is replaced by the impostor technique, it is represented with the lowest LoD, a simple "wall" rule with a single resistance and capacitor between its exterior and interior temperatures.

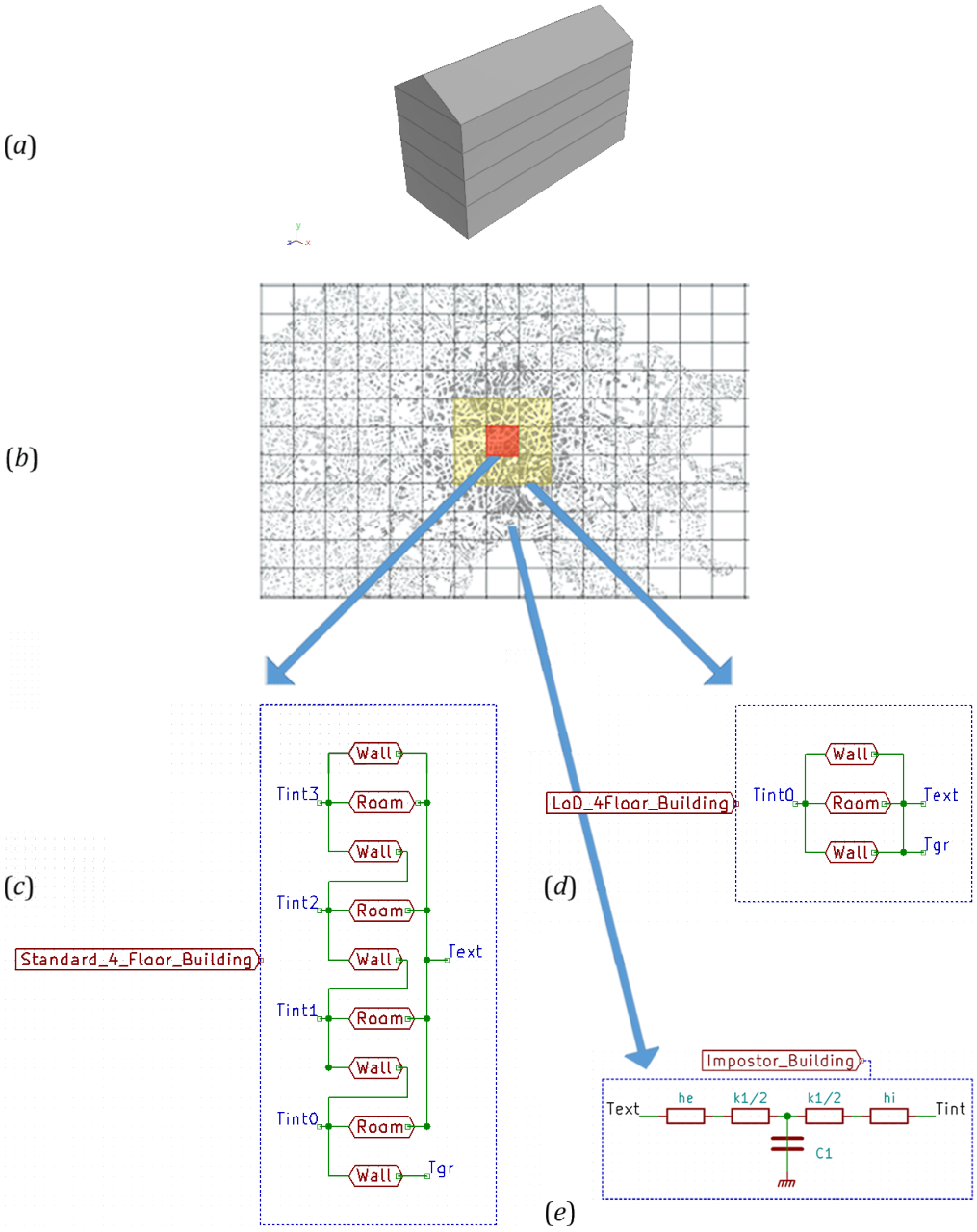

Figure 5.2. Overview of our method. If a building (a) is inside the studied viewcell (in red) its circuit will be generated in a standard way (c), while if it is in a neighbouring viewcell (in yellow), its circuit will be generated in a simplified way (d). If the building is beyond the buildings neighbourhood, the viewcell (outside the yellow area) will be replaced by an impostor and represented by a circuit consisting of a single wall of one material layer (e).

It is important to note that, for the impostor to function correctly, it must be possible to identify each building of the urban environment both at the geometry level and at the environment map level. To do this, each building is assigned a unique identifier number and a corresponding unique RGB colour code. At the moment of partitioning the city and creating the data set and the environment map corresponding to the viewcell, the distant buildings are coloured so that they can also be identified in the environment map when the calculation of radiative heat is made in the simulation. In this way, it is possible to use the impostor instead of the geometry to calculate the radiative pass by identifying the buildings that exchange heat between them by means of the RGB colours of the environment map and using the global average temperature of each one instead of having to count all temperatures of the exterior surfaces of the buildings.

5.3 Results and Discussion

5.3.1 Case Study

To test this new hybrid technique, a case study was designed from Vienna's urban 3D model, which was used in Chapter 4. The 3D model is an area of Vienna (Austria), see Figure 5.3. The climate data file from Vienna was used and the simulation date was adjusted to August 16, 2018, from 04:00 to 23:59. The temperatures were initialised at 15° C for the interior temperatures and 12° C for the exterior surfaces, and the ground temperature was maintained at the average temperature of that day plus 2° C. The parameters of the materials are presented in Table 5.1 and the general physical parameters are presented in Table 5.2. Finally, the coordinates were adjusted to $48.21°N, 16.36°E$ in the simulator interface.

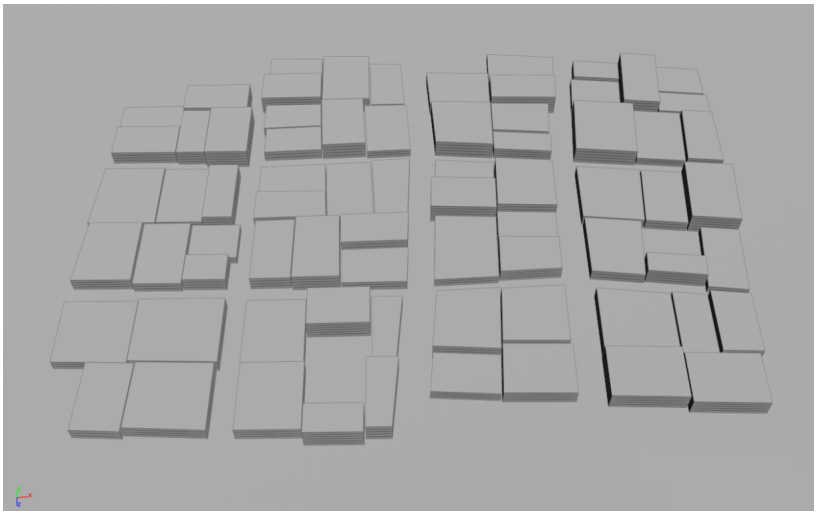

Figure 5.3. 3D model procedurally recreated from the map of the Vienna case study.

In this case study a subset of buildings was selected, determining the viewcell to be studied. Another subset of buildings neighbouring the chosen viewcell was also selected. The rest of the buildings were replaced by an environment map and an associated data structure, using the imposter technique, see Figure 5.4(*a*). As a result of this selection of buildings, the ones belonging to the viewcell maintain their original LoD, while the buildings belonging to the set of neighbouring buildings reduce their LoD using the procedural rules of single-story buildings. The buildings that do

TABLE 5.1: Material parameters for the simulation of the case study.

Material	Thermal conductivity (W/mK)	Thermal capacity (J/kgK)	Density (kg/m^3)	Thickness (m)
Concrete	1.75	920	2,200	0.2
Polyester	0.04	1,380	30	0.2
Plaster	0.35	800	1000	0.1

TABLE 5.2: Environmental parameters for the simulation of the case study.

Air density $(kg \cdot m^{-3})$	Air heat capacity $(J \cdot kg^{-1} \cdot K^{-1})$	Air infiltration $(vol \cdot h^{-1})$	Q_{other} $(W \cdot m^{-2})$
1.413	1,005	0.25	0.0

not belong to the viewcell or its neighbouring buildings, replace its geometry with the environment map and an associated data structure. See Figure 5.4(*b*). Once the LoD technique is applied, the simulation is carried out following the Algorithm 3.

5.3.2 Analysis

We can study the time complexity of the algorithm by considering that the cost of solving the thermal circuit of a building of a number R of floors is $O(f(R))$, with f an arbitrary function that depends on the acceleration data structure used. Using this hybrid technique, this cost will be different depending on whether the building is located inside, next to or far from the limits of the selected viewcell. In this way, there will be three sets of buildings: a large one with a computational cost of $O(1)$, since the technique will treat distant buildings as if they were from a single wall, a smaller one with a computational cost $O(f(r))$, where $r < R$, that treat buildings as if they were a single floor and a very small one with a computational cost $O(f(R))$ to treat all the floors of the buildings on which no LoD has been applied. This implies a strong reduction of the computational time with respect to a full geometry solution.

However, it must be noted that the computational load in this case is transferred to memory consumption: As seen in Chapter 3, the evaluation of several SVFs for a given cell requires a constant memory, proportional to the number of buildings associated to the cell, which we can assume roughly proportional to its size $C^2_{size} \times N^2$, plus the memory needed for the environment map itself. Nevertheless, this new hybrid technique also reduces the consumption of virtual memory with respect to the technique presented in Chapter 4 by not having to generate the complete circuits of all buildings in the urban environment when only a subset of them is needed. In the same way, the calculation time of radiative and convective steps in buildings is also reduced. The conductive calculations of buildings far from the viewcell under study are very fast, although less accurate, since far buildings use the electrical analogy over simplified circuits. Radiative calculations, on the other hand, will be very accurate between the viewcell and the buildings immediately surrounding it, and less accurate between the viewcell and much more distant buildings.

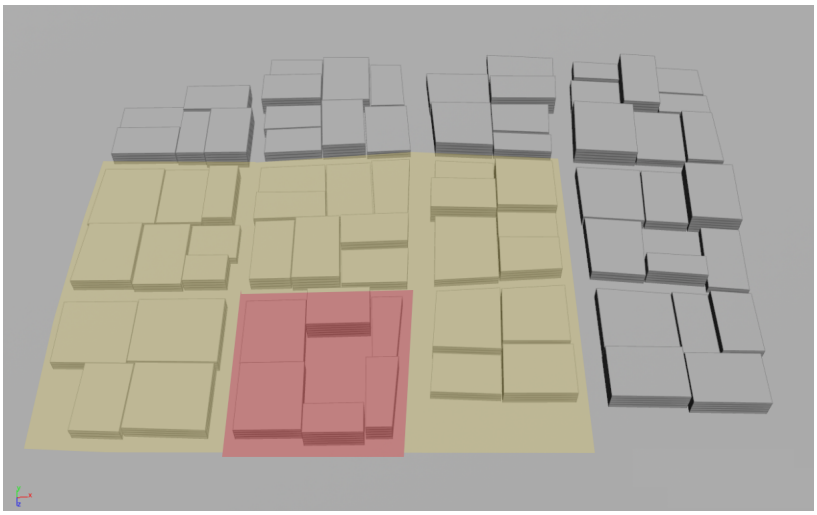

(*a*) In red the viewcell, in yellow the buildings neighbouring the viewcell and without colour the buildings distant to the viewcell.

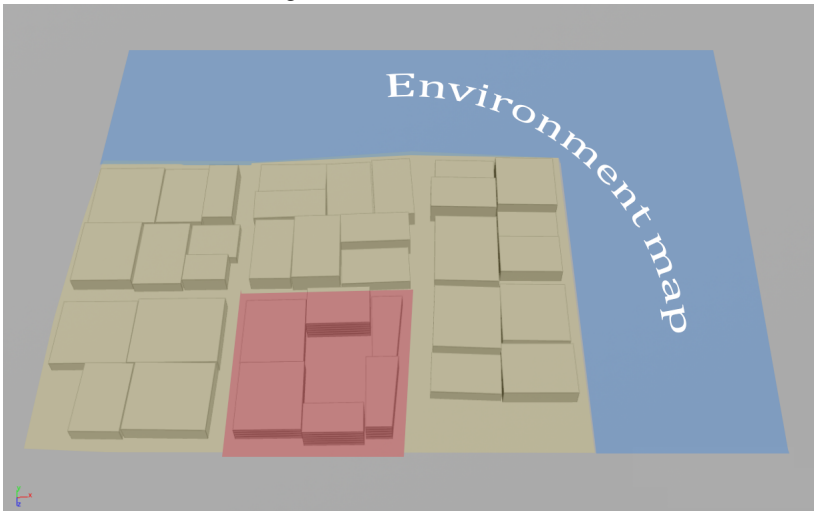

(*b*) The buildings in the red zone maintain their original LoD, while the buildings in the yellow zone use the procedural rule for single-floor buildings. The buildings beyond the yellow zone replace their geometry with an environment map and their associated data structure.

Figure 5.4. Three subsets of buildings are created on the 3D urban model, according to their distance from the viewcell.

5.3.3 Case Study Results

After performing the simulation twice for this case study, the first time using all the geometry and the second time using the LoD technique, it is easy to compare the results qualitatively (visually) and quantitatively (hour by hour), focusing on the previously chosen area of interest. See Figure 5.5. Visually, it is possible to appreciate how, despite having eliminated part of the geometry and simplifying another part, the results of the area to be studied do not differ much with respect to the results using all the geometry of the urban environment.

Table 5.3 presents a comparison of the computational time gain when using the imposter technique. By drastically reducing the amount of geometry present in the calculations, the simulation time decreases markedly. However, the impostor introduces an error that decreases the accuracy when simulating the thermal exchange between buildings in an urban environment. To analyse the error introduced by the

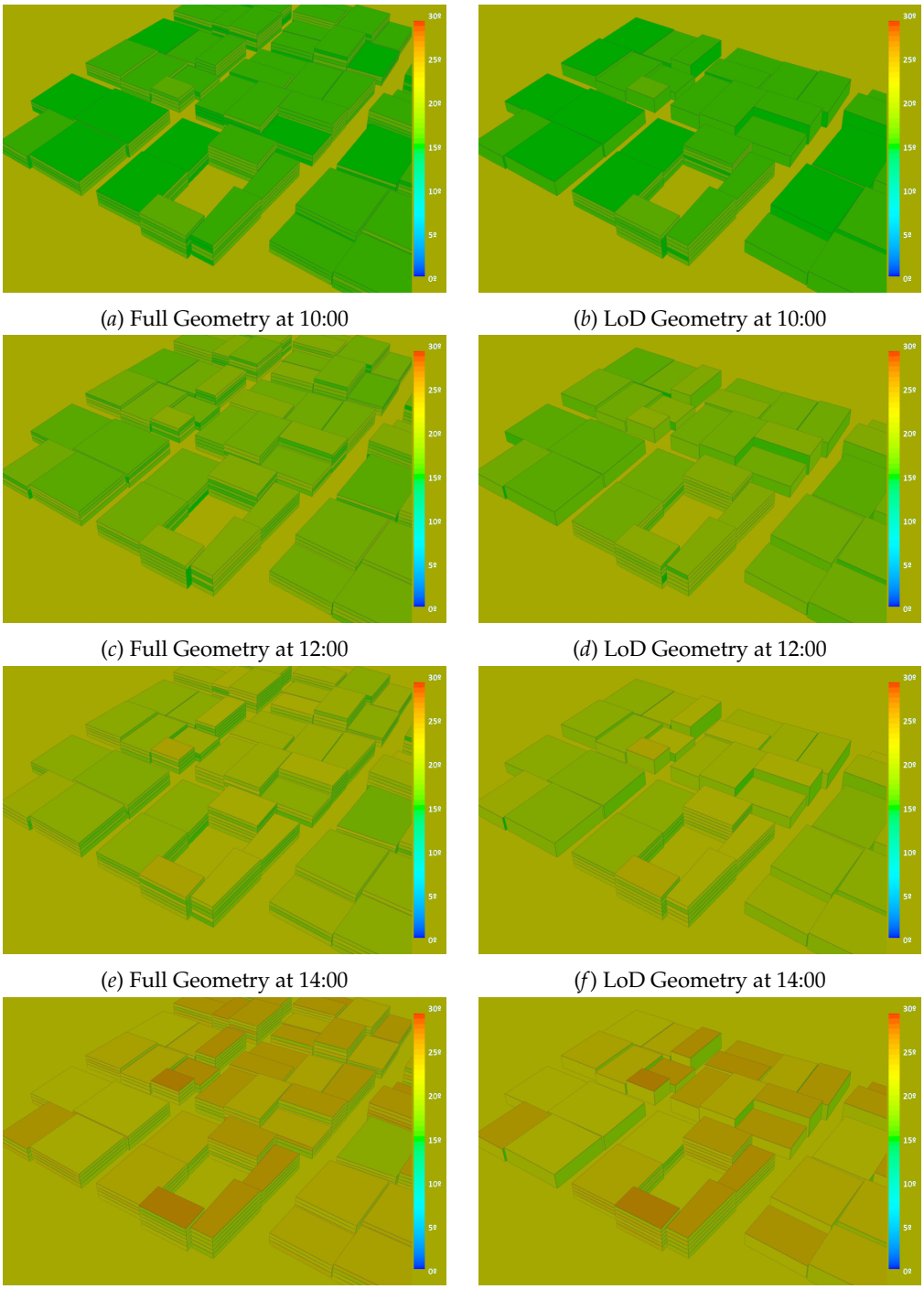

(*a*) Full Geometry at 10:00 (*b*) LoD Geometry at 10:00

(*c*) Full Geometry at 12:00 (*d*) LoD Geometry at 12:00

(*e*) Full Geometry at 14:00 (*f*) LoD Geometry at 14:00

(*g*) Full Geometry at 17:00 (*h*) LoD Geometry at 17:00

Figure 5.5. Visualisations of the Vienna case study. using all the geometry in the images on the left and using the LoD technique in the images on the right.

use of the impostor, three specific surfaces of the scene have been chosen and its heat flow emitted to a building visible from them and belonging to the viewcell has been measured. Of the three chosen surfaces, the first one belongs to the viewcell, the second one to the buildings neighbouring the viewcell and the third one to the area where the impostor technique has been applied. With these three surfaces it is possible to compare the energy that they contribute to the studied surface, both

using all the geometry of the scene and applying the LoD technique to reduce the computational cost, see Figure 5.6. It was observed that in the viewcell area, the difference between using the LoD technique is negligible, since in both cases the buildings maintain all their geometry and the differences in the calculations are the result of slight variations in temperatures, due to the changes between the simplified 3D model and the original. When measuring in the area neighbouring the viewcell, the difference is greater, since the buildings in the neighbouring area are treated as large one-story buildings when using the LoD technique. Finally, when measuring in the impostor area, the difference between using the LoD technique or not using it is much clearer, but its effect is diminished due to the distance and the low view factor with respect to the viewcell. With these results, it is observed that the farther away the surface that emits the heat flow to the building to study is, the less important the error will be, since the view factor between these two surfaces reduces its impact. Therefore, it does not matter if the error is significant in the area of the impostor, although it is recommended to try to keep it controlled in the area neighbouring the viewcell. To keep the error controlled, it is best to enlarge the size of the viewcell and the neighbouring area to the viewcell, in order to ensure that the error in the results is not significant until the building is at an adequate distance from the study area and its impact is minor.

TABLE 5.3: Geometry and timings for the model from the Vienna case study. The time required to calculate the SVF and FF from the first run of the model is included in the pre-processing time.

3D Model	Number of Primitives	Pre-processing time (minutes)	Simulation time (minutes)
Full Geometry	1,549	21.42	24.56
LoD Geometry	326	4.50	5.09

This type of techniques serve as tools designed to examine case studies by changing the parameters in order to observe how the thermal behaviour changes, thus letting the user decide which combination of parameters is the most optimal to get the desired thermal behaviour.

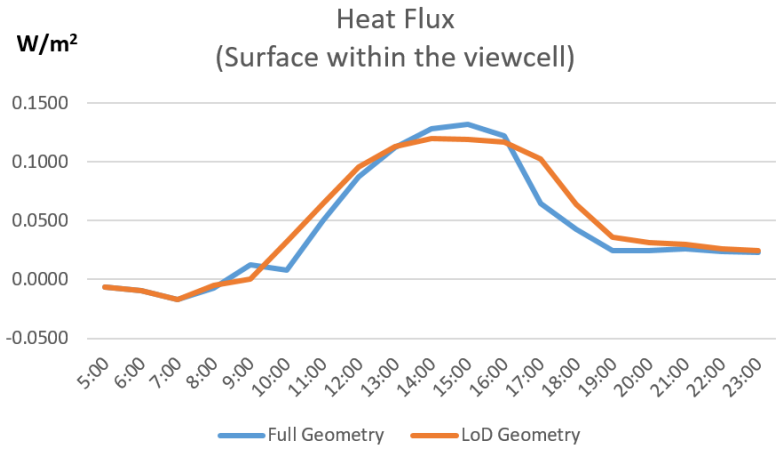

(*a*) Evolution of the heat flux added to the studied surface from the buildings in the viewcell area.

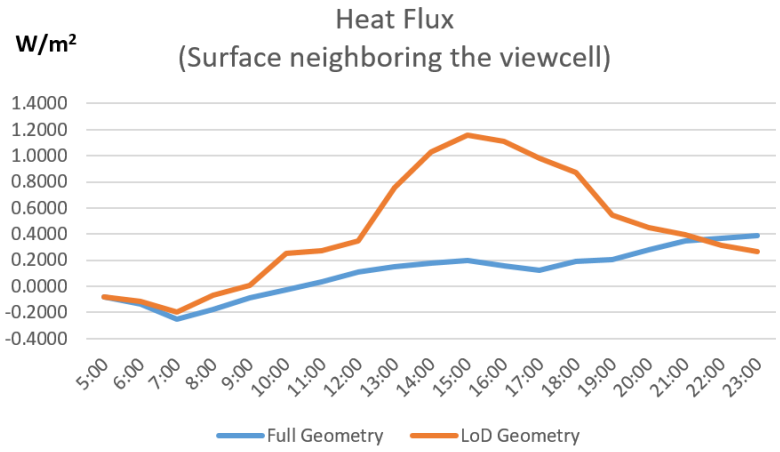

(*b*) Evolution of the heat flux added to the studied surface from the buildings in the area neighbouring the viewcell.

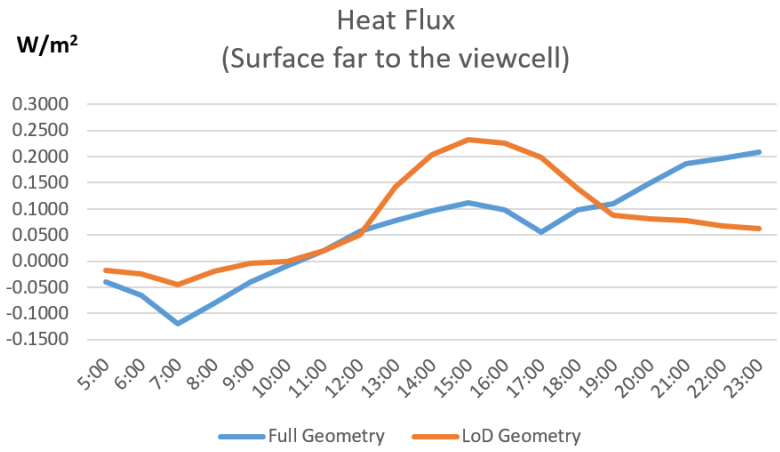

(*c*) Evolution of the heat flux added to the studied surface from the buildings in the impostor area.

Figure 5.6. Comparison of results when using the LoD vs Full technique to measure the heat flow contributed to a specific surface within the viewcell.

Chapter 6

Conclusions and Future Work

6.1 Conclusions

In Chapter 3 we have presented a method to approximate, within a user specified accuracy, the SVF in a large complex urban landscape. This is accomplished by embedding the city into a regular grid, and approximating the areas of the city far from the SVF computation area with an environment map associated with the cell. In our approximation, the user has an effective control of the error by selecting the cell size and the number of cells surrounding it, and keeping their geometry for accurate computations while replacing all the other farther geometry by an environment map centred in the selected cell. This allows the user to find the appropriate balance between speed of computation and accuracy of the results.

We have presented the results of several experiments to test the use of this technique, analysing the accuracy of the calculations and exposing several ways to manually adjust such accuracy as needed. With these results, it has been possible to measure the savings in computation time with respect to the standard calculations using the whole geometry of the city. Furthermore, we have shown some examples of the advantages of using our vector-based technique compared to a raster methods (Ratti and Richens, 2004; Gál, Lindberg, and Unger, 2009; Zakšek, Oštir, and Kokalj, 2011) and how treating all urban elements as simple geometry, instead of discriminating by type of urban element as in other techniques (Gál, Lindberg, and Unger, 2009; Lindberg and Grimmond, 2010; Lindberg and Grimmond, 2011; Gál and Unger, 2014), allows working in any kind of situation, even allowing the performance of calculations with verticality, and with no loss of accuracy because there is no discretisation.

We have also presented in Chapter 4 a procedural technique to simulate the radiative, conductive and convective heat in an urban environment, together with the heat exchanges between its buildings, by automatically generating and solving the electrical circuits that emulate the conductive heat exchange between the interior temperatures of a building and the outdoor air temperature and simulating the solar path and its radiation, as well as recreating the variations of air and sky temperature at each time step of the simulation. Our technique is capable of simulating all these calculations from a 3D model of the urban environment and a set of physical and simulation parameters that directly affect the thermal behaviour of the model. In addition, the technique does not require manual interaction with the 3D model, unlike other techniques that also use the electrical analogy (Levine, 2015), and the computation time is reasonable.

We provide a way to simulate different case studies by changing procedural and simulation parameters. The first case study demonstrates that it is possible to obtain realistic results in a reasonable simulation time if working with sufficiently small

subdivisions. This technique also allows the user to experiment with a variety of situations and to study the changes in the thermal behaviour of the model, according to the altered parameters. The data resulting from these simulations can be visualised dynamically either during or after the simulation. Thus, the main contribution of this work is the design and development of a tool capable of simulating and visualising the thermal behaviour of an urban model in 3D efficiently and with a low level of interaction by the user apart from introducing the elementary parameters and the properties of the terrestrial zone to recreate in the case studies. The originality of this technique lies in having been designed from a geometric, rather than a physical, point of view, in addition to using procedural technology to solve the most tedious part of the problem: generating the circuits to be used for the electrical analogy.

The two techniques allow to work with other simulations in large cities as well. The final element of our study was the proposal of combining the Level-of-Detail technique with the procedural simulation, with the objective of simulating the thermal behaviour in a very huge urban area, reducing computational complexity by avoiding rendering geometry not very relevant for calculations, while retaining accurate enough results. The resulting has been presented in Chapter 5, explaining the changes and implications of the combination of techniques. In this way, it is possible to have two techniques to simulate and visualize the thermal behaviour of buildings, according to the size of the 3D model to be used as a case study. If we work up to a scale and density similar to those of the Vienna case study in Section 4.4.3, with the standard procedural technique is sufficient. But if one wants to work with a larger environment, the impostor technique may reduce the computational cost drastically, although losing some precision in the results, as shown in Section 5.3.3.

6.2 Future work

One of the most promising avenues for future work is finding ways to take advantage of the observation that only a limited number of geometric elements surrounding a projection point actually have any influence on the computations in a large urban environment. This would require a computation of the involved geometry, which can be a complex task for highly detailed city models.

In addition to this, as there are more factors that affect the thermal behaviour of an urban environment, especially in the interior of buildings, it would be interesting to improve the rules of generation of procedural circuits to take into account factors such as population density, artificial lighting, the presence of household appliances and even the use of air conditioning devices. All this factors could be introduced as one more heat flow within the circuit, contributing its effect during the conductive step of the simulation.

On the other hand, an accurate error metric should be developed in order to automatically determine N and C_{size} depending on the maximum allowable error. The automation of the partitioning parameters of large urban environments would be a first step so that, by means of the simulation of an enormous quantity of case studies, rules of categorization of 3D cities would be created and stored in a learning database. In the same way, experiments could be carried out to analyse the weight of these two variables according to the type of scenario in which they are applied. This would allow the system itself to recommend and even adjust the sizes of the "view-cells" of an urban 3D model, detecting its patterns when imported and comparing them with those of the learning database.

Another interesting line for work is to upgrade these techniques by improving their accuracy by simulating more 3D models of urban environments with real measurements (and if possible with measurements of indoor temperatures), as they become available. Also, the calculations and the data structures should be optimised to reduce the simulation time even further; although compared with the techniques that use finite elements, the relationship between computational cost and accuracy is quite positive.

Beyond these optimizations and improvements, the tools presented in this thesis could be used in the near future to simulate and study other phenomena at an urban scale. In Chapter 1 some of these phenomena and their importance in the field of Urban Physics were mentioned, for example the decreased long-wave radiative heat losses due to reduced sky view factors or the increased storage of sensible heat in the construction materials in buildings. It would be interesting, for example, since this tool proposes a solution to the study of thermal behaviour, creating a new one that, in combination with ours, allows to study wind.

Bibliography

Aguerre, José Pedro et al. (2019). "A street in perspective: Thermography simulated by the finite element method". In: *Building and Environment* 148, pp. 225–239.

Ahmad, Tanveer and Huanxin Chen (2018). "Short and medium-term forecasting of cooling and heating load demand in building environment with data-mining based approaches". In: *Energy and Buildings* 166, pp. 460–476.

Alados, Inmaculada, I. Foyo-Moreno, and Lucas Alados-Arboledas (2012). "Estimation of downwelling longwave irradiance under all-sky conditions". In: *International Journal of Climatology* 32.5, pp. 781–793.

Anders, Karl-Heinrich (2005). "Level of Detail Generation of 3D Building Groups by Aggregation and Typification". In: *In: Proceedings of the XXII International Cartographic Conference, La Coruna*.

Beckers, Benoit, ed. (2012). *Solar Energy at Urban Scale*. Wiley.

Beckers, Benoit and Pierre Beckers (Nov. 2014). "Sky vault partition for computing daylight availability and shortwave energy budget on an urban scale". In: *Lightning Research and Technology* 46.6, pp. 716–728.

Beckers, Benoit et al. (2017). "Visualizing the Infrared Response of an Urban Canyon Throughout a Sunny Day". In: *Sustainable Building for a Cleaner Environment*. Springer, pp. 277–284.

Besuievsky, Gonzalo and Gustavo Patow (2013a). "Customizable LoD for Procedural Architecture". In: *Computer Graphics Forum* 32.8, pp. 26–34.

— (2013b). "Customizable LoD for Procedural Architecture". In: *Computer Graphics Forum* 32.8, pp. 26–34.

— (2013c). "The skylineEngine System". In: *XXIII Congreso Español De Informática Gráfica, CEIG2013*. Madrid, Spain, pp. 29–36.

Brown, M.J., S. Grimmond, and C. Ratti (2001). "Comparison of methodologies for computing sky view factor in urban environments". In: *International Society of Environmental Hydraulics Conference*.

Busato, F., R.M. Lazzarin, and M. Noro (2014). "Three years of study of the Urban Heat Island in Padua: Experimental results". In: *Sustainable Cities and Society* 10, pp. 251–258.

Chen, Shenchangeric Eric et al. (1991). "A progressive multi-pass method for global illumination". In: *Computer Graphics*, pp. 165–174.

CitySim (2019). *CitySim software*. URL: http://citysim.epfl.ch/.

Clark, Gene and Chester Allen (1978). "The estimation of atmospheric radiation for clear and cloudy skies". In: *Proc. 2nd National Passive Solar Conference (AS/ISES)*, pp. 675–678.

Clarke, J.A. et al. (1991). "'ESP-R A building and plant energy simulation research environment". In: *Energy Simulation Research Unit, ESRU Manual U* 91.

Clarke, Joe (2001). *Energy Simulation in Building Design (Second Edition)*. Second Edition. Oxford: Butterworth-Heinemann.

Cohen, Barney (2015). "Urbanization, City growth, and the New United Nations development agenda". In: *Cornerstone* 3, pp. 4–7.

Crawley, Drury B. et al. (2001). "EnergyPlus: creating a new-generation building energy simulation program". In: *Energy and buildings* 33.4, pp. 319–331.

Décoret, Xavier et al. (1999). "Multi-layered impostors for accelerated rendering." In: *Comput. Graph. Forum* 18.3, pp. 61–73.

DOE, LBNL (1982). "engineer manual–version 2.1 A". In: *Berkeley, USA: University of California*.

Douglas, Ian and Ted Munn (2002). *Causes and consequences of global environmental change*. Wiley.

Eisemann, Elmar and Xavier Décoret (2007). "On Exact Error Bounds for View - Dependent Simplification". In: *Computer Graphics Forum* 26.2, pp. 202–213.

Elwy, Ibrahim et al. (2018). "Outdoor microclimatic validation for hybrid simulation workflow in hot arid climates against ENVI-met and field measurements". In: *Energy Procedia* 153, pp. 29–34.

EnergySoft (2016). *User's Manual Energy Pro 5*.

ESRU (2019). *ESP-r*. URL: http://www.esru.strath.ac.uk/Programs/ESP-r.htm.

Evangelisti, Luca, Claudia Guattari, and Francesco Asdrubali (2018). "On the sky temperature models and their influence on buildings energy performance: a critical review". In: *Energy and Buildings*.

Evyatar, Erell, David Pearlmutter, and Terry Williamson (2011). *Urban Microclimate: Designing the Spaces Between Buildings*.

Fairey, Philip et al. (2002). "EnergyGauge USA: A residential building energy simulation design tool". In:

Fraisse, G. et al. (2002). "Development of a simplified and accurate building model based on electrical analogy". In: *Energy & Buildings* 34.10, pp. 1017–1031.

Gál, T., F. Lindberg, and J. Unger (2009). "Computing continuous sky view factors using 3D urban raster and vector databases: comparison and application to urban climate". In: *Theoretical and applied climatology* 95.1-2, pp. 111–123.

Gál, T. and J. Unger (2014). "A new software tool for SVF calculations using building and tree-crown databases". In: *Urban Climate* 10, pp. 594–606.

Green Design Tools (2001). "VisualDOE 3.0 Program Documentation". In: *Eley Associates, San Francisco*.

Greene, Ned (Nov. 1986). "Environment Mapping and Other Applications of World Projections". In: *IEEE Comput. Graph. Appl.* 6.11, pp. 21–29.

Grimmond, C. S. B. et al. (2001). "Rapid methods to estimate sky-view factors applied to urban areas". In: *International Journal of Climatology* 21.7, pp. 903–913.

Harish, VSKV and Arun Kumar (2016). "A review on modeling and simulation of building energy systems". In: *Renewable and Sustainable Energy Reviews* 56, pp. 1272–1292.

Hénon, Aurélien et al. (2011). "High resolution thermo-radiative modeling of an urban fragment in Marseilles city center during the UBL-ESCOMPTE campaign". In: *Building and Environment* 46.9, pp. 1747–1764.

Hirsch, James et al. (2010). "eQUEST: Introductory tutorial, version 3.63". In: *Camarillo, CA*.

Holmer, B., U. Postgård, and M. Eriksson (2001). "Sky view factors in forest canopies calculated with IDRISI". English. In: *Theoretical and Applied Climatology* 68.1-2, pp. 33–40.

Jeschke, Stefan and Michael Wimmer (Feb. 2002). *An Error Metric for Layered Environment Map Impostors*. Tech. rep. TR-186-2-02-04. human contact: technical-report@cg.tuwien.ac.at. Favoritenstrasse 9-11 / 186, A-1040 Vienna, Austria: Institute of Computer Graphics and Algorithms, Vienna University of Technology.

Jeschke, Stefan, Michael Wimmer, and Heidrun Schumann (May 2002). "Layered Environment-Map Impostors for Arbitrary Scenes". In: *Proceedings of Graphics Interface 2002*. Ed. by Wolfgang St"urzlinger and Michael McCool. Calgary, CA: AK Peters Ltd., pp. 1–8.

Kampf, Jerome Henri and Darren Robinson (2007). "A simplified thermal model to support analysis of urban resource flows". In: *Energy & Buildings* 39.4, pp. 445–453.

Kaushika, N.D., Anuradha Mishra, and Anil K. Rai (2018). "Solar Radiation Characteristics". In: *Solar Photovoltaics*. Springer, pp. 15–26.

Khan, Basit et al. (2018). "Development and Application of an Online Coupled Chemistry Urban Microscale Model PALM-4U". In: *EGU General Assembly Conference Abstracts*. Vol. 20, p. 7501.

Kidd, C. and L. Chapman (2012). "Derivation of sky-view factors from lidar data." In: *International journal of remote sensing* 33.11, pp. 3640–3652.

Kong, Qiongxiang, Xiao He, and Yaolin Jiang (2017). "Fast simulation of dynamic heat transfer through building envelope via model order reduction". In: *Building Simulation* 10.3, pp. 419–429.

Krüger, E.L. and David Pearlmutter (2008). "The effect of urban evaporation on building energy demand in an arid environment". In: *Energy and buildings* 40.11, pp. 2090–2098.

Landsberg, Helmut E. (1981). *The urban climate*. Vol. 28. Academic press.

Lavery, N.P. (2007). "Mathematical framework for predicting solar thermal build-up of spectrally selective coatings at the Earth's surface". In: *Applied mathematical modelling* 31.8, pp. 1635–1651.

Leung, Kam Shing and Koen Steemers (2008). "193: Estimating Average Sky View Factors of Urban Surfaces with Simple Geometric Parameters". In: Citeseer.

Levine, Steven (2015). *Temperature Simulation in Residential Building By Use of Electrical Circuits*. Tech. rep. B.S. in Systems Science and Engineering. Washington University in St. Louis.

Lewis, Roland W., Perumal Nithiarasu, and Kankanhalli N. Seetharamu (2004). *Fundamentals of the finite element method for heat and fluid flow*. John Wiley & Sons.

Lin, Tzu-Ping, Andreas Matzarakis, and Ruey-Lung Hwang (2010). "Shading effect on long-term outdoor thermal comfort". In: *Building and Environment* 45.1. International Symposium on the Interaction between Human and Building Environment Special Issue Section, pp. 213 –221.

Lindberg, F. and C. Grimmond (2011). "The influence of vegetation and building morphology on shadow patterns and mean radiant temperature in urban areas: model development and evaluation". In: *Theoretical and Applied Climatology* 105.3-4, pp. 311–323.

Lindberg, F. and C. S. B. Grimmond (2010). "Continuous sky view factor maps from high resolution urban digital elevation models". In: *Climate Research* 42.3, pp. 177–183.

Lindberg, F. and C.S.B. Grimmond (2018). *SOLWEIG*. URL: https://umep-docs.readthedocs.io/en/latest/OtherManuals/SOLWEIG.html.

Lindberg, Fredrik, Björn Holmer, and Sofia Thorsson (2008). "SOLWEIG 1.0 - Modelling spatial variations of 3D radiant fluxes and mean radiant temperature in complex urban settings". In: *International journal of biometeorology* 52.7, pp. 697–713.

Martilli, Alberto, Alain Clappier, and Mathias W Rotach (2002). "An urban surface exchange parameterisation for mesoscale models". In: *Boundary-layer meteorology* 104.2, pp. 261–304.

Masson, Valéry (2000). "A physically-based scheme for the urban energy budget in atmospheric models". In: *Boundary-layer meteorology* 94.3, pp. 357–397.

Matzarakis, A. and O. Matuschek (2010). *SkyHelios*. URL: https://www.urbanclimate.net/skyhelios/description.htm.

— (2017). *RayMan*. URL: https://www.urbanclimate.net/rayman/.

Matzarakis, Andreas et al. (2015). "Developments and applications of thermal indices in urban structures by RayMan and SkyHelios model". In: *ICUC9 9th international conference on the urban climate jointly with the 12th symposium on the urban environment*.

Mauree, Dasaraden, Nadège Blond, and Alain Clappier (2018). "Multi-scale modeling of the urban meteorology: Integration of a new canopy model in the WRF model". In: *Urban climate* 26, pp. 60–75.

Mauree, Dasaraden et al. (2017). "Multi-scale modelling to evaluate building energy consumption at the neighbourhood scale". In: *PloS one* 12.9, e0183437.

Mohajerani, Abbas, Jason Bakaric, and Tristan Jeffrey-Bailey (2017). "The urban heat island effect, its causes, and mitigation, with reference to the thermal properties of asphalt concrete". In: *Journal of Environmental Management* 197, pp. 522–538.

Moonen, Peter et al. (2012). "Urban Physics: Effect of the micro-climate on comfort, health and energy demand". In: *Frontiers of Architectural Research* 1.3, pp. 197–228.

Nahon, Raphaël (2017). "Modélisation des échanges radiatifs à l'échelle urbaine pour un urbanisme bioclimatique". PhD thesis. Lille 1.

Nuruzzaman, Md (2015). "Urban heat island: causes, effects and mitigation measures-a review". In: *International Journal of Environmental Monitoring and Analysis* 3.2, pp. 67–73.

Oke, TR (1995). "The heat island of the urban boundary layer: characteristics, causes and effects". In: *Wind climate in cities*. Springer, pp. 81–107.

Pardo-García, S. and M. Mérida-Rodríguez (2017). "Measurement of visual parameters of landscape using projections of photographs in GIS". In: *Computers, Environment and Urban Systems* 61, pp. 56–65.

Ratti, Carlo and Paul Richens (2004). "Raster analysis of urban form". In: *Environment and Planning B: Planning and Design* 31.2, pp. 297–309.

Rau, Jiann-Yeou et al. (2006). "LOD Generation for 3D Polyhedral Building Model". In: *Advances in Image and Video Technology*. Ed. by Long-Wen Chang and Wen-Nung Lie. Vol. 4319. Lecture Notes in Computer Science. Springer Berlin / Heidelberg, pp. 44–53.

Remund, J. et al. (2010). "The use of Meteonorm weather generator for climate change studies". In: *10th EMS Annual Meeting, 10th European Conference on Applications of Meteorology (ECAM) Abstracts, Sept. 13-17, 2010 in Zürich, Switzerland*.

Robinson, Darren (2012). *Computer modelling for sustainable urban design: Physical principles, methods and applications*. Routledge.

Salamanca, Francisco and Alberto Martilli (2010). "A new Building Energy Model coupled with an Urban Canopy Parameterization for urban climate simulations-part II. Validation with one dimension off-line simulations". In: *Theoretical and Applied Climatology* 99.3-4, p. 345.

Santamouris, Matheos (2013). *Energy and climate in the urban built environment*. Routledge.

— (2014). "On the energy impact of urban heat island and global warming on buildings". In: *Energy and Buildings* 82, pp. 100–113.

Shade, Jonathan et al. (1996). "Hierarchical image caching for accelerated walkthroughs of complex environments". In: *Proceedings of the 23rd annual conference on Computer graphics and interactive techniques*. ACM, pp. 75–82.

SideFX (2019). *Houdini 17*. URL: http://www.sidefx.com.

Sillion, F.X. and C. Puech (1994). *Radiosity and Global Illumination*. Eurographics technical report series. Morgan Kaufmann Publishers.

Solomon, Susan et al. (2007). *Climate change 2007-the physical science basis: Working group I contribution to the fourth assessment report of the IPCC*. Vol. 4. Cambridge university press.

Sparrow, Ephraim M. (2018). *Radiation Heat Transfer, Augmented Edition*. Routledge.

Stocker, Thomas (2014). *Climate change 2013: the physical science basis: Working Group I contribution to the Fifth assessment report of the Intergovernmental Panel on Climate Change*. Cambridge University Press.

Svensson, M. K. (2004). "Sky view factor analysis-implications for urban air temperature differences". In: *Meteorological applications* 11.03, pp. 201–211.

UN (2014). *World Urbanization Prospects: The 2014 Revision-Highlights*. UN.

Unger, J. (2004). "Intra-urban relationship between surface geometry and urban heat island: review and new approach". In: *Climate Research* 27.3, pp. 253–264.

— (2008). "Connection between urban heat island and sky view factor approximated by a software tool on a 3D urban database". In: *International Journal of Environment and Pollution* 36.1-3, pp. 59–80.

Venturini, Giuseppe (2013). *Ahkab, a SPICE-like electronic circuit simulator written in Python*. URL: https://ahkab.github.io/ahkab/.

Voorhies, Douglas and Jim Foran (1994). "Reflection Vector Shading Hardware". In: *Proceedings of the 21st Annual Conference on Computer Graphics and Interactive Techniques*. SIGGRAPH '94. New York, NY, USA: ACM, pp. 163–166.

Wade, T. G. et al. (2003). "A comparison of vector and raster GIS methods for calculating landscape metrics used in environmental assessments". In: *Photogrammetric Engineering and Remote Sensing* 69.12, pp. 1399–1405.

Wang, Danhong et al. (2018). "CESAR: A bottom-up building stock modelling tool for Switzerland to address sustainable energy transformation strategies". In: *Energy and Buildings* 169, pp. 9–26.

Yan, Da et al. (2008). "DeST—An integrated building simulation toolkit Part I: Fundamentals". In: *Building Simulation*. Vol. 1. 2. Springer, pp. 95–110.

Zakšek, K., K. Oštir, and Ž. Kokalj (2011). "Sky-view factor as a relief visualization technique". In: *Remote Sensing* 3.2, pp. 398–415.

Zhu, Dandan et al. (2013). "A detailed loads comparison of three building energy modeling programs: EnergyPlus, DeST and DOE-2.1 E". In: *Building Simulation* 6.3, pp. 323–335.